DUT

DURBAN UNIVERSITY OF TECHNOLOGY

INYUVESI YASETHEKWINI YEZOBUCHWEPHESHE

Evaluation of chitosan–coated magnetic nanoparticle-immobilized thermostable hemicellulases for enhanced saccharification and production of bioethanol

Sibongile Patience Mdlaka

Submitted in complete fulfilment for the Degree of Master of Applied Sciences in Biotechnology in the Department of Biotechnology and Food Technology, Faculty of Applied Sciences, Durban University of Technology, Durban, South Africa.

13 Sep 2022

Supervisor:
Prof. S. Singh (Ph. D)

Date

13-09-2022

Co Supervisor:
Dr. A. K. Puri (Ph. D)

Date

DECLARATION

I hereby declare that this dissertation is my own, unaided work. It is being submitted for the Degree of Master of Applied Sciences in Biotechnology, to the Durban University of Technology, Department of Biotechnology and Food Technology, Durban, South Africa. It has not been submitted before for any degree or dissertation to any other institution.

Sibongile Patience Mdlaka

2022

CONTENTS

ACKNOWLEDGEMENTS

I would like to offer my deepest gratitude and heartfelt thanks to the following people and organisations to have in one way or another contributed to my degree:

To Prof S. Singh and Prof K. Permaul for allowing me to be a part of the Enzyme Technology Research Group and for their guidance, support, and suggestions.

To Dr Adarsh K. Puri, for encouraging my research, your teachings and for allowing me to grow as a research scientist. Your advice, assistance and suggestions have been invaluable, through you I have significantly grown in research.

To my very best friend Celumusa Manqele for your unconditional love and unwavering support for without you I would not have made it.

To the National Research Foundation (NRF) and National Student fund (NSF) for providing financial support to make this work possible.

Finally, I thank God and my anscestors for letting me get through all difficulties to finally finish my degree.

DEDICATION

Above all, this work is highly dedicated to my late mother, the only parent I ever had Nelisiwe Perm Mdlaka who passed on to heaven on the 16 March 2005. Losing you was a bitter wrench, the pain cut to my core. It broke my heart to lose you, but you did not go alone for part of me went with you the day God took you home. I cried until my tears dried out. I know we can't be together but you will forever live safely in my heart. I know you are always with me spiritually and happy to see me doing good as you always wished.

LIST OF FIGURES

LIST OF TABLES

LIST OF ABBREVIATIONS

APTES	Aminoproply triethoxysilane
CCMNP	Chitosan-coated nanoparticles
CO_2	Carbon dioxide
CO	Carbon monoxide
DEAE	Diethylaminoethyl
DNS	Dinitrosalicylic acid
DSC	Differential scanning calorimetry
ELSD	Evaporative light scattering detector
EU	European union
FTIR	Fourier-transform infrared spectroscopy
GA	Glutaraldehyde
GC	Gas chromatography
HIV	Human immunodeficiency virus
HPLC	High performance liquid chromatography
HRTEM	High resolution transmission electron microscope
kDa	Kilodalton
NP	Nanoparticles
OA	Oleic acid
PAGE	Polyacrylamide gel electrophoresis
PDA	Potato dextrose agar
RSM	Response surface methodology
SEM	Scanning electron microscope
SCB	Sugarcane bagasse
SDS	Sodium dodecyl sulfate
SDS	Soluble solids
SSCF	Simultaneous saccharification and co-fermentation
TGA	Thermogravimetric analysis
TEM	Transmission electron microscope

TLC	Thin layer chromatography
U	Units
US	United states
UHC	Unburned hydrocarbons
XOS	Xyloologosaccharides
YPD	Yeast extraction-peptone dextrose

ABSTRACT

Enhancing the efficiency of saccharification of pentose and hexose sugars present in lignocellulosic biomass is a major bottleneck for industrial bioethanol production. This problem can be addressed by a concerted effort combining nanotechnology, enzymology and fermentation technology. Functionalized chitosan-coated magnetic nanoparticles (CCMNPs) were prepared and used for co-immobilization of purified xylan hydrolysing xylanase and xylosidase from the thermophilic fungus *Thermomyces lanuginosus* SSBP for the release of xylose. Stability studies revealed that immobilized enzymes were more stable than free enzymes over a wide range of pH (4.0 – 7.0) and temperature (40 – 90 °C) for xylanase and 30 – 80 °C for xylosidase. The optimum activity of the co-immobilized enzymes shifted slightly as compared to the free enzymes, with co-immobilized xylanase and xylosidase showing optimum activity at pH 6.5 and 6.0, respectively. The study showed sustained production of xylose as the major fermentable sugar under repeated batch and fed-batch saccharification of lignocellulosic biomass. Statistical optimization of saccharification of 1% xylan using response surface methodology indicated the enhanced release of xylose at 50 °C, pH 7.0 and enzyme dose of 60 U/mL xylanase and 30 U/mL xylosidase. Finally, liberated xylose was fermented with *Scheffersomyces stipitis* to yield bioethanol.

CHAPTER 1: INTRODUCTION AND LITERATURE REVIEW

The overdependence on fossil fuels for energy is not sustainable due to its gradual depletion, increasing cost and contribution to global warming. There is a pressing issue worldwide to explore alternative and renewable sources of energy and South Africa is no exception. The Department of Energy (DoE), South Africa was determined to achieve 42% renewable energy by 2020 (www.sanedi.org.za, 2020), and the country has committed to attaining substantial reductions in CO_2 emissions by 2025. Lignocellulosic waste is cost-effective and well suited to address existing energy and environmental concerns (Moodley, Sewsynker-Sukai and Kana 2020). Bioethanol production using lignocellulosic waste is a promising alternative with the potential to ameliorate the global energy crisis. Transportation contributes to more than 19% and 70% of global carbon dioxide (CO_2) and carbon monoxide (CO) emissions, respectively. Bioethanol produced by lignocellulosic biomass may reduce CO emissions by up to 30%, with a significant reduction in atmospheric CO_2. South Africa produces more than 65 million tons of wet sugarcane annually, mostly in the province of KwaZulu-Natal. In general, South Africa is among the top ten sugar exporters worldwide, exporting more than 75% of its sugar production. Therefore, the use of lignocellulosic biomass in South Africa as a natural renewable source is extremely feasible.

The constantly increasing world population (presently 7.7 billion) and industrialization (Leridon 2020) necessitate the promotion of renewable fuels to meet the escalating global demand (Balasubramanian and Chowdhury 2021). Oil prices started increasing in 2006 globally, According to the Energy Information Administration (EIA), U.S. crude oil production will fall to 10.0 million barrels a day in 2021 in order to mitigate COVID-19, which is now 42 cents per barrel (Zhongming *et al*. 2020).

More increases in the price are expected due to COVID-19 related economic disturbances worldwide. A reduction in oil prices is critically dependent on the development and adoption of effective fuel alternatives. Hirsch *et al.* (2005) argue that if alternatives are not forthcoming, the oil products will become scarce and expensive. Furthermore, this will affect the living standards of people in developing and developed countries leading to social unrest and global economic collapse Compeán and Polenske 2011).

Fermentative production of bioethanol using lignocellulosic biomass is primarily based on the efficient conversion of biomass into fermentable sugars. Glucose (C6) and xylose (C5) are the predominant biomass sugars which contribute above 90% fermentable sugars. Presently enzymatic hydrolysis is the most common and environmentally friendly method for converting renewable biomasses to carbohydrates and further to bioethanol or biohydrogen. It uses cellulases, such as endoglucanase (EC 3.2.1.4), exoglucanase (cellobiohydrolase, CBH; EC 3.2.1.91) and β-glucosidase (EC 3.2.1.21) to hydrolzse cellulose into glucose, while hydrolysis of xylan, the major hemicellulose, needs efficient hydrolysis using xylanase (EC 3.2.1.8) and β-xylosidase (EC 3.2.1.37). Industrial production of bioethanol and biofuel needs efficient and thermostable enzymes that can be used over repeated cycles. In industrial applications, thermostable enzymes provide high rates of reaction, high yields of product, increased stability, reduced contamination issues, and reduced viscosity.

The Enzyme Technology Research Group at the Durban University of Technology, sequenced the complete genome of the thermophilic xylanase super producer *Thermomyces lanuginosus* SSBP (Mchunu *et al*. 2013). This has enabled the identification, isolation, and exploration of robust enzymes out of a total of 5.105 protein-coding genes. This includes many industrially relevant enzymes including the above-mentioned enzymes for hydrolysis of lignocellulosic biomass. The group has also cloned, expressed, and engineered these enzymes for enhanced pH and thermostability.

Thermostable enzymes are well known for their significance and applications in industries. Most of the reported thermozymes are produced in mesophilic hosts by the cloning and expression of thermophilic genes host. This greatly increases the exploitation of thermophilic organisms in biotechnology. Enzymatic complexes, endo-β-xylosidase and β-xylanase are required for the degradation of xylan, which is a type of hemicellulose having a linear polymer of β-D-xylopyranosyl units which are linked by 1.4 glycosidic bonds.

These important enzymes are excreted from different microorganisms and macro organisms, for example, bacteria, fungi, yeast, marine algae, protozoans, crustaceans, insects, snails and seeds (Polizeli *et al*. 2005). However, the filamentous fungus *Thermomyces lanuginosus* is the principal source of xylanolytic enzymes in this study. The Enzyme Technology Research Group at the Durban University Technology produced extremely high levels of xylanase from this thermophilic

fungi. *T. lanuginosus* is interesting because it secretes xylosidase and xylanase into a medium with higher reported titres of xylanase than any other microbial source. Xylosidase from *T. lanuginosus* was expressed in *P.pastoris* to improve production (Gramany *et al*. 2016).

During the last few years, nanotechnology has revolutionized research in enzyme technology. In this project, we envisage including the potential of nanotechnology. Although there is a plethora of information on the preparation, functionalization, and immobilization of enzymes on nanoparticles. There is no report, to date on co-immobilization of thermostable xylanase and xylosidase on chitosan coated magnetic nanoparticles for repeated batch and fed-batch saccharification of lignocellulosic biomass. Previously, the preparation, characterization, and application of chitosan-alginate nanoparticles for immobilization of phytase was reported by the Enzyme Technology Research Group.

This investigation focuses on using nanoparticles as support matrices for co-immobilization of thermostable hemicellulolytic enzymes for enhanced saccharification of xylan as one of the most promising pentose sugars, which will be further fermented to bioethanol using appropriate yeast cultures.

1.1 Global energy demand

The world's population is increasing and is expected to double by the middle of the 21st century (Fanzo *et al*. 2022). Economic development will almost certainly continue growing as well. Energy security and global warming are analysed based on the 21st century threats due to the world's increasing population (Nel and Cooper 2009). The energy demand is expected to increase by 1.5 – 3 times (Dincer 2000). In South Africa, 109 out of every 1000 people are car owners. These numbers are quite high when compared to 15 per 1000 in Lagos and 50 per 1000 in Nairobi (Akinboade, Ziramba and Kumo 2008). Oil remains one of the main contributors to the world's energy demand and South Africa is no exception. The main energy indicators for South Africa are contained in Table 1.1.

Table 1. 1: Oil indicator for South Africa (Akinboade, Ziramba and Kumo 2008

	1975	1980	1985	1990	1995	2000	2005
Gasoline consumption (thousand barrels per day)	96.4	88.6	109.3	146.1	188.5	178.7	191.5
Oil supply/ GDP (toe per thousand 2000 US $)	0.129	0.111	0.093	0.095	0.099	0.088	0.098
Oil supply/population (toe per capita)	0.429	0.383	0.304	0.301	0.293	0.266	0.332
Net oil imports/GDP (toe per thousand 2000 US $)	0.164	0.158	0.123	0.102	0.112	0.101	0.105

This infers that South Africa is quickly shifting to a primary gasoline consumer due to the fast depletion of fossil fuels. Therefore, precautionary measures are being taken and South Africa is adapting the concept of blending gasoline with ethanol.

South Africa is motivated by success stories and political decisions on bio-ethanol blending by the United States of America (US), Brazil and many other countries (Bacovsky *et al*. 2010). The US uses the National Energy Modeling System (NEMS) to regulate energy production, consumption, and price trends for a 25-year period. With biomass being one of the technologies within NEMS playing role in several scenarios. The National Energy Modeling System consists of four biomass sources including forestry residues, agricultural residues, urban wood wastes/mill residues and energy crops (Haq and Easterly 2006).

The world's production of bio-based ethanol is constantly increasing. The price of bioethanol is dependent on the price of fossil fuel oil, which is constantly increasing. Therefore, there is a growing need to improve the security of fuel supplies (Sims *et al*. 2010). This necessitates research on alternative energy from bio-based sources such as bioethanol produced by microbial fermentation. Agricultural substitutes or wastes can be and have been used. Current attention is on the use of lignocellulosic biomass as an ideal renewable source to produce fuel ethanol. Yeast *Saccharomyces cerevisiae* has been the most widely used microorganism for the production of various products including the industrial production of ethanol (Khoshkho *et al*. 2022).

The technology of producing renewable energy sources such as ethanol, methane and hydrogen from biomass holds the potential of creating in-house energy resources while lowering the emission of greenhouse gases (Olguin-Maciel *et al*. 2020; Ahmad, Ali and Abd Rahim 2021). Large-scale implementation of biofuels in the transportation sector will demand that lignocellulosic biomass, which is found in a surplus throughout the world is used as raw material in the production process (Panchuk *et al*. 2020).

Annual global sugarcane production of 1,889,268,880 tones, South Africa is amongst top 15 producers globally out of approximately 120 countries. Sugarcane in South Africa grows over a range of agronomic and socio-economic conditions. South Africa is the leading producer of sugarcane in Sub-Saharan African (SSA) countries with 14 sugarcane milling companies (Hess *et al*. 2016). More than 45 000 farmers grow commercial sugarcane in South Africa with the milling season stretching from April to December (Bezuidenhout and Singels 2007). Out of 14 sugarcane millersin SA, KwaZulu – Natal (KZN) have twelve mills. The province of KZN has the largest supply area with mostly rain-fed sugarcane (75%), while 25% of the sugarcane plantations are produced under irrigation (Shikwambana *et al*. 2021). This makes sugarcane bagasse (SCB) an ideal sourcefor second-generation bioethanol production.

1.2 Lignocellulosic biomass, waste, and bioethanol

Lignocellulosic biomass is the most abundant biopolymer on earth comprising about 50% of the world's biomass with an annual production of 10 – 50 billion tons. Biomass energy currently contributes 9 – 13% of the global energy demand equivalent to 45± 10 EJ per year (Kim and Dale 2005). Many lignocellulosic materials have been tested and reported for bioethanol production as indicated in Table 1.2 below.

Table 1. 2: Composition of crops based on dry mass (Kim and Dale 2004)

	Residues/ Crop ratio	Dry matter (%)	Lignin	Carbohydrates	Ethanol yield (L/kg of dry biomass
Sugarcane		26.0		67	0.50
SCB	0.6	71.0	14.5	67.15	0.28
Corn	1	86.2	0.60	73.70	0.46
Corn stover		78.5	18.69	58.29	0.29
Oat	1.3	89.1	4.00	65.60	0.41
Oat straw		90.1	13.75	59.10	0.26
Rice	1.4	88.6		87.50	0.48
Rice straw		88.0	7.13	49.33	0.28
Sorghum	1.3	89.0	1.40	71.60	0.44
Sorghum straw		88.0	15.00	61.00	0.27
Wheat	1.3	89.0		35.85	0.40
Wheat straw		90.1	16.00	54.00	0.29
Barley	1.2	88.7	2.90	67.10	0.41
Barley straw		81.0	9.00	70.00	0.31

Lignocellulosic waste represents a promising option as feedstock for ethanol production considering its output/input energy ratio and global availability at low cost. Additionally, it can be processed in different ways for the production of any other bioenergy products such as synthetic gas, methanol, hydrogen and electricity. One of the advantages of lignocellulosic waste is that it does not compete with food and fertile cultivable land (Sanchez and Cardona 2008). The choice of technology to process biomass varies depending on the chemical composition of the biomass structure.

Ethanol from lignocellulosic material has already been introduced on a large scale in countries like Brazil, where sugarcane is used for ethanol production; in the US and in other European countries,

starch is used. Bioethanol is expected to dominate renewable biofuels in transportation. However, the raw material is also used for animal feed and human needs and therefore to meet the increasing demand for ethanol. Therefore, there is an urgent need to exploit lignocellulose feedstocks such as agricultural residues as well as dedicated crops for ethanol production (Hahn-Hägerdal *et al*. 2006).

Lignocellulosic raw materials particularly hardwood and agricultural raw materials may contain 5 – 20% pentose sugars (xylose and arabinose) which are not fermentable to ethanol by mostly used microorganisms including S. *cerevisiae*. The natural xylose-fermenting yeast *Pichia stipitis* CBS 6054 was reported to ferment xylose to ethanol with reasonable yield and productivity. However, these strains are inhibited by compounds generated during pre-treatment and hydrolysis of the lignocellulose material. Although filamentous fungi can tolerate inhibitors these are slow for competitive industrial processes. Therefore, recombinant bacterial and yeast strains are selected to meet industrial requirements/demands (Hahn-Hägerdal *et al*. 2006).

1.2.1 Sugarcane and sugarcane waste

Sugarcane (*Saccharum officinarum*) is a tall perennial grass of the genus Saccharum (family Poaceae, tribe Andropogoneae). Sugarcane is commonly grown in many tropical countries for several industrial applications, especially in the sugar and alcohol industries. It is favourable in warm temperatures commonly in regions like Brazil, Africa, India and the Asian Pacific region. Its general morphology is shown in Figure 1.1. Sugarcane is composed of a stem, which is the material that is removed before the milling of cane to juice for sucrose sugar or alcohol, and straw/trash, which is composed of fresh leaves, dry leaves and tops available before harvesting (Neto *et al*. 2005).

Major parts are extracted from the sugarcane stem and the dry pulp residue left after sugarcane stalks are crushed results in SCB. A ton of sugarcane produces around 250 kg of bagasse, whose combustion produces 6 kg of ash (Khaleghipour *et al*. 2021). Sugarcane is employed for ethanol production (first generation). However, Ferreira-Leitão and Bon (2014) predicted that SCB along with soluble solids (SS) can be used for second-generation ethanol production. This deployment in Brazil is highly favoured because the production process can be annexed to sugar/ethanol, and therefore requires low investment, infrastructure, logistics, and energy supply Corrales *et al*. (2012).

Significant applications of leaves are fuel for direct combustion, raw material for conversion by pyrolysis to char, oil and gas, as raw material for conversion by gasification and synthesis to methanol (Triana *et al*. 1990). Approximately 50% of the sugarcane residues are burnt to generate heat and power to operate sugar mills, ethanol, and distillery plants. The remaining is usually stockpiled, which constitutes a serious environmental problem (Micheal and Moussa 2021).

Sugarcane bagasse represents a great morphological heterogeneity consisting of fibre bundles and other structural elements such as parenchyma, vessels and epithelial cells (Sanjuan *et al*. 2001). It consists of about 40 –50% cellulose which is a polymer for glucose. Hemicellulose constitutes the second-largest component of SCB, which is an amorphous polymer that is made up of xylose and a small amount of lignin (Konde *et al*. 2021). Table 1.3 shows the chemical composition of sugarcane and different feedstocks.

Figure 1. 1: Sugarcane bagasse from sugarcane processing (Shah et al. 2022)

Table 1. 3: Percentage compositions of typical biomass feedstocks including sugarcane bagasse (Zhao et al. 2012)

Feedstock	Cellulose	Xylan	Galactan	Araban	Lignin	Mannan	Extractive	Ash
Woody biomass	45 –55	8 –25	0.3 –1.1	0.3 –3	18 –35	0.5 –6	2–7	0.2 – 1.1
Hybrid poplar	48.6	14.6	0.3	0.3	21.8	0.5	NA	0.7
Poplar	49.9	17.4	1.2	1.8	18.1	4.7	NA	0.5
White oak	43.6	18.0	0.4	2.4	23.2	2.9	NA	0.6
Red oak	43.4	18.9	NA	1.9	25.8	2.7	NA	NA
Walnut	46.2	16.5	NA	1.8	21.9	2.6	NA	NA
Maple	44.9	17.3	NA	2.8	20.7	2.9	NA	0.4
Grass biomass	25 –50	20 –50	0.55 –1	1.8 –3	10 –30	0.2 –0.6	4 –25	2 –7
Corn cob	36.4	18.0	1.0	3.0	16.6	0.6	7.3	9.7
Corn stover	40.9	21.5	1.0	1.8	16.7	NA	NA	6.3
Sugarcane bagasse	**40.2**	**21.1**	**0.5**	**1.9**	**25.2**	**0.3**	**4.4**	**4.0**
Wheat straw	38.2	21.2	0.7	2.5	23.4	0.3	13.0	10.3
Rice straw	34.2	24.5	NA	NA	11.9	NA	17.9	16.1
Switchgrass	31.0	20.4	0.9	2.8	17.6	0.3	17.0	5.8

*NA-Data not available

1.3 Xylan as a substrate

Xylan is the second most abundant polysaccharide which is present in dicot wood as the major hemicellulose constituent. Xylan serves as a major substrate for bioethanol production (Lee *et al*. 2011). Xylan is a linear chain of β-,4-linked xylosyl residue with around 120 degrees of polymerization (Jacobs and Dahlman 2001). Some of the xylosyl residues in the xylan backbone are substituted by a-1,2-linked 4-O-methyl glucuronic acid residues and acetylated at C-2 or C-3 **(**Timell, 1967**)**. As in other woody species, the reducing end of xylan generally contains a unique tetrasaccharide sequence consisting of b-D-Xylp-(1/3)-a-L-Rhap-(1/2)-a-DGalpA-(1/4)-D-Xylp (Lee *et al*. 2011). Xylose units in xylan are difficult to isolate and normally have 4 - 24 different sugar monomers (Bastawde 1992). Xylose accounts for almost one-third of the total sugar

contained in SCB. Therefore, microorganisms able to ferment both glucose and xylose are required for an efficient conversion of bagasse to ethanol (Martín *et al*. 2002).

1.4 Xylanolytice enzymes

Hydrolysis of xylan requires the action of endo-β-1-4 xylanase, β-xylosidase and a series of other xylanolytic enzymes (Fig.1.2) that cleave the side chain groups (Hebraud and Fevre 1990). The important xylanolytic enzymes can be produced from yeasts, fungi, marine algae, bacteria, snails, protozoans, seeds, insects, and crustaceans. Thermophilic microorganisms producing xylanolytic enzymes are of great potential for industrial applications due to suitability under harsh processing conditions (Kambourova *et al*. 2007). Efficient hydrolysis of the lignocellulosic structure requires pre-treatment, which involves loosening of the structure followed by hydrolysis of cellulose and xylose fractions in which lignin remains a solid by-product (Olsson and Hahn-Hägerdal 1996).

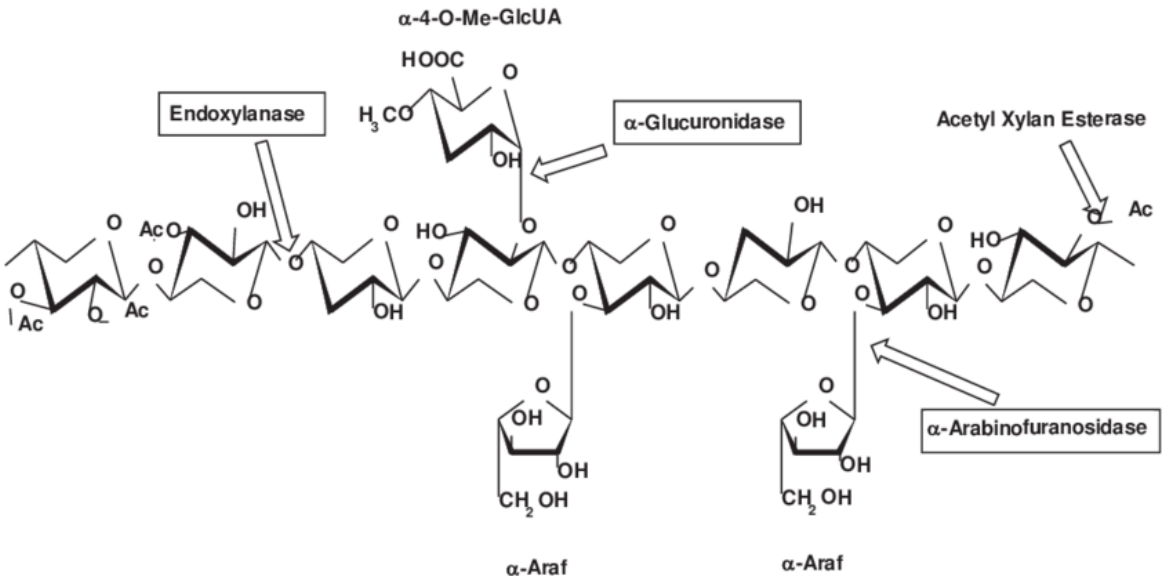

Figure 1. 2: Xylan structure with site of action for xylanolytic enzymes (Motta, Andrade and Santana 2013)

1.4.1 Xylanases

These are the most important xylanolytic enzymes of major industrial importance that hydrolyze insoluble xylan backbone into shorter, soluble xylooligosaccharides such as xylobiose and xylose (Fig 1.3) (Knob, Terrasan and Carmona 2010). Xylanases are frequently used in several industrial applications including the paper and pulp industry (Mah *et al*. 2021), biofuel production (Chaudhary *et al*. 2021), while Singh *et al*. (2021) outlined xylanase usage in detergents, food, and

pharmaceutical industries. Microorganisms are a rich source of xylanases produced by diverse genera and species of bacteria, actinomycetes and fungi. Several bacterial species like bacilli and filamentous fungi such as *T. lanuginosus* SSBP (Singh *et al*. 2000) are rich sources of xylanase, producing high titres of extracellular xylanase that hydrolyze xylan are active at high temperature and alkaline conditions, which are of great potential in industrial processes (Sharma and Kumar 2013). Xylanases have various industrial applications such as bleaching of paper and brightening of pulp in the paper and pulp industry. They are also used to improve food digestion and clarification of juices.

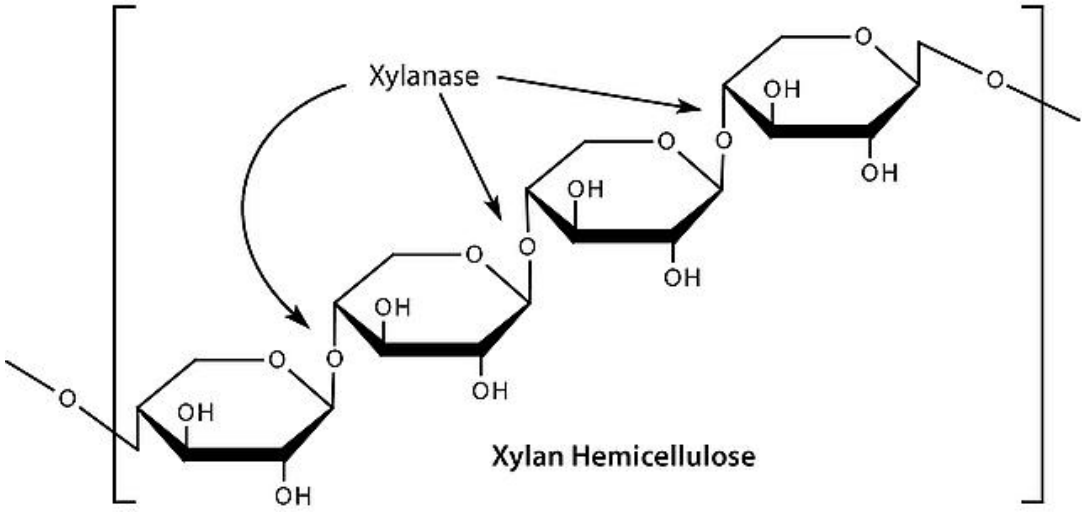

Figure 1. 3: Xylanase acting on xylan structure (Knob, Terrasan and Carmona 2010, SIGMA (https://www.sigmaaldrich.com/ZA/en/product/SIAL/95595)

1.4.2 Xylosidases

β-xylosidases hydrolyze soluble short xylooligosaccharides and xylobiose from the non-reducing end to liberate xylose and play an important role in minimizing the end-product inhibition of endoxylanases (Fig.1.4).

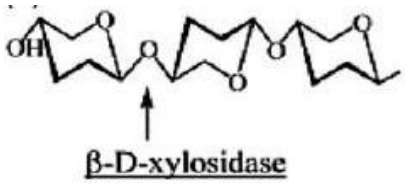

Figure 1. 4: Hydrolysis of a xylooligosaccharide by β-xylosidase (Knob, Terrasan et.al 2010)

Sunna and Antranikian (1997) described xylosidases as key xylanolytic enzymes possessing massive biotechnological applications, especially in food, bioconversion, pulp and paper industries. Furthermore, xylosidases play a significant role in transglycosylation reactions whereby monosaccharides or alcohols get attached or cleaved from xylose (Sunna and Antranikian 1997).

1.5 Microbial sources of β-xylanase and β-xylosidase

1.5.1 Microbial sources of xylanase

Xylanase can be produced by a variety of microorganisms such as filamentous fungi, yeasts and bacteria (Kumar, Dangi and Shukla 2018). Filamentous fungi are widely reported to be the most promising candidates for commercial production due to exceptionally high levels of xylanase production compared to bacteria and yeast (Kumar, Marin-Navarro and Shukla 2016). There is a huge demand for microbial xylanase to meet the global industrial demand. Large scale production also requires the application of genetic engineering (Uday *et al*. 2016).

1.5.1.1 Production of fungal xylanase

Filamentous fungi are the principal source of xylanase for industrial production. Fungal xylanases are routinely used to satisfy the increasing industrial demand in paper manufacturing (Patel *et al*., 2021), textile, food, feed, beverage, and biofuels production (Pathak, Bhardwaj and Singh 2014). Pathak *et al*. (2014) produced xylanase and cellulase from *Trichoderma harzianum* for efficient de-inking of photocopier waste papers.

The ability to improve fungal strains by genetic engineering makes fungi advantageous (Jin *et al*., 2021). Xylanases can be produced from mesophilic strains of such as *Aspergillus and Trichoderma* and thermophiles such as *Thermomyces*, which are known for high levels of xylanase production (Kumar, Marin-Navarro and Shukla 2016). In search of a super xylanase producer, Sharma *et al*.

(2015) isolated 90 fungal strains and 15 of them showed xylanolytic activity. Fungal strain 9 (*Aspergillus* s.p.S9) and fungal strain 20 (*Aspergillus* s.p.S20) showed highest activity of 59.5 U/mL and 49.75 U/mL, respectively. Singh *et al*. (2000) isolated *T. lanuginosus* SSBP as a hyper producer which produced 3400 U/mL xylanase.

1.5.1.2 Production of xylanase from yeasts

Xylanases have been detected in several yeasts belonging to *Kloeckera, Candida, Debaryomyces, Rhodotorula, Pichia, Zygosaccharomyces, Hanseniaspora and Kluyveromyces* isolated from grapes in South African vineyards and clarified grape juice. Other than xylanase; extracellular proteases, pectinases, β-glucanases, cellulases, lichenases, g-glucosidasess, sulphite reductase and amylases were also produced. Amadi *et al*. (2020) reported a simultaneous enzyme production of xylanase, cellulase and ligninase from *S. cerevisiae* SCPW 17 under solid-state fermentation.

Morais *et al*. (2013a) isolated and screened a total of 321 yeast strains for xylanase production and the ability to hydrolyze D-xylose. *Xylanicola*, *Spencermartinsiella* sp.1 and *Tremella* sp were identified as the best xylanase producers. Surprisingly, most isolates belonged to *Xylanicola* and were able to ferment D-xylose. Further, Morais *et al*. (2013b) reported the extraordinary biotechnological potential of these strains due to their ability to produce xylanase and ferment D-xylose. The screening and isolation of xylanase-producing strains were based on the formation of a clear halo around colonies on xylan agar medium. Some other species such as *Lindnera. fabianii* and *Wickerhamomyces. pijperi* have been reported by Morais *et al*. (2013b) to produce xylanase when cultivated on a xylan-yeast extract medium.

1.5.2 Microbial sources of xylosidase

Only a few studies have focused on microbial β-xylosidases. Rohman *et al*. (2019), classified β-xylosidase into families of 3, 39, 43, 52 and 54 glycosyl hydrolases based on their amino acid sequence similarities. Fungal xylanases only belong to 3, 43 and 54 glycosyl hydrolases. Xylosidases from filamentous fungi have been studied but very few have been purified and characterized (Yan *et al*. 2008). Fungal xylosidases are an interesting source because they secrete enzymes freely inside the media (Knob, Terrasan and Carmona (2010). Fungal xylosidases have elevated activity levels and specificity, therefore enabling them to have various industrial applications in the processing of agro-industrial residues into fuels and chemicals.

1.5.2.1 Production of fungal xylosidase

Many research papers have focused on newly isolated fungal β-xylosidases. Filamentous fungi are generally preferred as they are more effective producers of xylanolytic enzymes (Paul *et al*., 2020). Fungal xylosidases are recovered from the production medium or by lysis of mycelium as it becomes associated during early phases of growth (Knob, Terrasan and Carmona 2010) whereas other fungal xylosidases remain to interact with the cell (Katapodis *et al*. 2006). β-xylosidases from filamentous fungi belong to three GH families namely; 3, 43 and 54 (Knob, Terrasan and Carmona 2010). The majority of fungal β-xylosidases are members of the glycoside hydrolase (GH) 3 family (Wang and Arioka, 2021), while presumptive β-xylosidases like *Penicillium herquei* and *A. oryzaeare* are grouped under GH43 (Machida *et al*. 2005; van den Brink and de Vries 2011). Presently most β-xylosidases are produced from fungal (*Aspergillus niger*, *Trichoderma reesei*) and bacterial (*Bacillus sp*.) sources. Interestingly, Jordan and Wagschal (2010) and Kanna *et al*. (2011) reported *Acremonium cellulolyticus* as a primary producer of cellulase which secretes a lower β-xylosidase yield than the previously reported fungal xylosidases. Patel, Divecha and Shah (2018) isolated *Aspergillus niger* ADH-11 for β-xylosidase and reported increased production of 2.85-fold after optimization using response surface methodology. The crude extract had several other xylanolytic and cellulolytic enzymes making the microorganism advantageous for both xylanase and cellulose degradation. This allows minimal use of commercial enzymes for saccharification of pretreated SCB (Patel, Divecha and Shah 2018).

1.5.2.2 Production of bacterial xylosidases

There are few reports on β-xylosidase production by a bacterial strain. Most bacterial β-xylosidases are intracellular (Kim and Yoon 2010). (Bosetto *et al*. 2016) isolated GH43 β-xylosidases from *B. subtilis subsp.subtilis str.168, B. pumilus, Alkaliphilus metalliredigens* and *Lactobacillus brevis* ATCC367, which are of major industrial significance. Silva *et al*. (2020) reported a 62% increase in activity of xylosidase (CcXynB2) from recombinant *Caulobacter crescentus*.

1.5.2.3 Production of yeast xylosidases

Many yeast species are capable of producing β-xylosidases (Paul *et al*., 2020). Romero, Mateo and Maicas (2012) isolated, purified and characterized a pH, temperature and ethanol tolerant β-xylosidase from *Pichia membranifaciensiso*. López, Mateo and Maicas (2015) identified

Hanseniaspora vineae, *Pichia membranifaciens*, *H. uvarum* and *Wickerhamomyces anomalus* as xylosidase producers and used them to treat wine. *Hanseniaspora vineae* and *Wickerhamomyces anomalus* contributed higher 2-phenyl ethanol in wines than others. It would be beneficial to obtain a cost-effective xylosidase from yeast (Romero, Mateo and Maicas 2012).

1.6 Purification and characterization of xylanolytic enzymes

Xylanases are purified using classical biochemical techniques which include ammonium sulphate precipitation, ion exchange (Teng *et al*., 2021), and gel-filtration chromatographic steps (Bouhlel *et al*., 2021). Purification techniques allow the characterization of proteins possible for easy industrial application. Generally, a high state of purity is not necessary for applications in food processing, detergents and paper and pulp industries but may be essential to eliminate contaminating enzymes based on application requirements (Price and Stevens 1999). Shah and Madamwar (2005) successfully produced xylanase from newly isolated *Aspergillus foetidus* MTCC 4898 and partially purified the enzyme. The authors obtained a yield of 84.7% from 40–70% ammonium sulphate fraction with a purification fold of 4.98. Xylanase from *Streptomyces rameus* L2001 appeared to be monomeric with an estimated molecular weight of 21.1 kDa based on SDS-PAGE analysis. The enzyme was purified 13.3-fold by 40 – 60% ammonium precipitation followed by DEAE-52 and CM Sepharose fast flow ion exchange chromatography (Li *et al*. 2010). The molecular weight for xylanase generally ranges around 20 kDa. The low molecular weight of enzymes offers easy access to the lignocellulosic network for efficient degradation of hemicelluloses (Kocabaş, Güder and Özben 2015).

Classical purification of β-xylosidases involves the same steps as described for β-xylanases. Extracellular β-xylosidases are much cheaper and easy to purify than intracellular xylosidases as they require costly and time-consuming cell-lysis and extraction from biomass (Ja'afar and Shitu, 2022). β-xylosidase from *Themoanerobacterium saccharolyticum* JW/SW-YS485 showed a molecular weight of 78 kDa on SDS PAGE. The enzyme was purified by gel-filtration on Superose 6 (10/30) column and DEAE-Sephacel ion-exchange chromatography (Shao *et al*. 2011). Intracellular β-xylosidase from *B. thermantarcticus* isolated from soil by (Lama *et al*. 2004) was purified 160-fold by gel filtration chromatography using Sephacryl S-200 (2.5×110 cm) column, ion-exchange chromatography and hydrophobic interaction chromatography (HIC). SDS and

native PAGE and gel filtration on Sephacryl S-200 column (2.5×49 cm) was used to report a molecular weight of 150 kDa and pi of 4.2. Terrasan, Guisan and Carmona (2016) isolated a fungal xylosidase from *Penicillium janczewskii,* and purified the protein with 55% ammonium sulphate, dialysis, and cation exchange chromatography using CM Sephadex C-50 column (Sigma Aldrich, 1.4×17.0 cm). The molecular mass of 110 kDa was estimated by SDS-PAGE and gel filtration. Mhetras, Liddell and Gokhale (2016) purified xylosidase to homogeneity as a glycoprotein with 23% glycosylation and obtained 8.3-fold from *Pseudozyma hubeiensis* NCIM 3574 (PhXyI). The purification steps in this investigation included ammonium sulphate precipitation, QAE-Sephadex A50 ion-exchange chromatography and Sephacryl-200 column chromatography with a yield of 53.12%. The purified enzyme exhibited a prominent band of 110 kDa on SDS-PAGE.

1.7 Nanoparticles (NPs) as promising support matrices

Nanomaterials have become a leading edge of the rapidly developing field of nanotechnology due to their unique size-dependent properties which make them superior and indispensable in many areas of human activity (Murray, Kagan and Bawendi 2000). They range from 1-100 nm depending on the type and chemical composition of the nanomaterial. However, in most applications, particles perform best when they are in the range of 10-20 nm (Lu, Salabas and Schüth 2007). Nanoparticles have been studied for over a decade and have now entered a commercial exploration phase (Kah *et al.*, 2021).

The physical and chemical characteristics of nanomaterials are influenced by size-related properties such as shape and inter-particle distance to the core, charge, dielectric properties of the conjugated system, refractive index, polarizability, dielectric medium surrounding particles (solvent) and the composition of moieties (Doria *et al*. 2012). Nanomaterials are not only attractive in medical fields but are also routinely used for many biotechnological applications with enzyme immobilization processes being the most appealing. Nanoparticles support ideal characteristics such as a larger specific surface area for attachment of enzymes leading to higher enzyme loading per unit mass of particles (Jia, Zhu and Wang 2003), mass transfer resistance and effective enzyme loading.

Enzymes are highly specialised protein catalysts that are commonly used in biofunctionalization due to their great potential in biotechnology and biomedicine because of their convenience in

handling ease of separation from the reaction mixture and reuse (Tilahun Bekele *et al*., 2021). Immobilization in nanoparticles often reduces diffusion limitations and/or enhances the catalytic activity of the enzymes (Conde *et al*. 2014). Moreover, enzymes immobilized on nanoparticles showed broader working pH and temperature range and higher thermal stability than native enzymes (Kaur *et al*. 2021). When comparing conventional immobilization methods, nanoparticle-immobilization offers advantages such as easy production of nano-enzyme with high solid content without using surfactants and toxic reagents, a homogeneous and well-defined core-shell of nanoparticles with a thick enzyme shell and convenient tailoring of particle size within utility limits. Due to the growing interest in cascade enzymatic reactions and in vitro synthetic biology, nanoparticles might be able to co-immobilize multiple enzymes (Ansari and Husain 2012).

Several materials such as chitosan, gold, metals, and diamonds have been used at nano-size for immobilization processes (Cipolatti *et al*. 2014). Immobilization of protein is effective to solve difficulties with poor enzyme stability and difficult recovery of free enzymes. Moreover, it is crucial to select a proper protein immobilization basis, designed to leads to increased rigidity of the heterogeneous adsorbed materials in the biological sphere ranging from antibodies to biocatalysts. Subunit dissociation is reduced and reuse of enzyme is entertained thus, the immobilization of enzymes and proteins results in improved stability, simple separation from the reaction mixture, possible modulation of the catalytic properties, prevention of microbial growth, and in certain cases, results in higher activity or selectivity (Polizzi *et al*. 2007). Metal nanoparticles are receiving great research attention (Tilahun Bekele *et al*., 2021). The physical and chemical properties of NPs are directly related to their chemical compositions, sizes, and surface structural characteristics (Mirkin *et al*. 1996). Fe_3O_4 nanoparticles have been intensively employed because of their unique magnetic performance, improved stability, and reusability. These nanoparticles can be easily isolated from the reaction medium using an external magnetic field (Peng, Liang and Qiu 2011). But the superparamagnetic behaviour implies that its magnetization may disappear once the external magnetic field is removed (Wu *et al*. 2007).

Immobilization of enzymes has inherent problems with recovery during centrifugation or filtration processes, which can easily be overcome using magnetic nanoparticles and recovery by magnets that can be reused in the next cycle (Ren *et al*., 2021). NPs are potential support matrices for enzymes, nucleic acids, peptides and antibodies (Liao and Chen 2001). Additionally, immobilized

enzymes are much cleaner and easier for enzymatic transformations. The use of carrier substrates increases the ability and stability of enzymes (Singh and Ahmed 2012) due to the specific interaction between them and the immobilized enzyme. Mostly enzyme activity decreases on immobilization due to mass transfer limitations. Singh and Ahmed (2012) immobilized amylase by adsorption on carboxymethyl cellulose-silver nanoparticle (AgNp)-silica hybrid and optimized the hydrolysis of soluble starch in comparison to a free enzyme. The physical and chemical properties of NPs are directly related to their chemical composition, size and surface structural characteristics (Mirkin *et al*. 1996).

1.7.1 Magnetic nanoparticles (MNPs) as promising enzyme carriers

Magnetic nanoparticles (Fe_3O_4) are widely used nanomaterials due to their excellent structural, chemical and thermal and storage stability, and reusability (Ashkan *et al*., 2021). Enzymes immobilized on MNPs are active under a wide range of pH and temperature and display more enhanced stability than free enzymes. During the past few years, various approaches for the functionalization of MNPs have been suggested to improve the immobilization efficiency and characteristics of enzymes (Bilal *et al*., 2018). Chitosan is a polymer of great interest due to its biocompatibility, biodegradability and the presence of polycationic reactive groups, and therefore it is suitable for coating of MNPs. Chitosan-coated magnetic nanoparticles have been produced by physically adsorbing chitosan onto oleic acid-coated nanoparticles, resulting in spherical shaped CCMNPs with a diameter of 15 nm (Kim *et al*. 2005), and their application in the removal of metals has been reported by Yuwei *et al*. (2011). They are generally inert, but with an intravenous injection, their surface can be adsorbed by plasma proteins or opsonisation as the first step in their clearance by the reticuloendothelial system (Berry and Curtis 2003). Their low toxicity was reported by Dyal *et al*. (2003) with improved lipase enzyme activity, loading and stability after immobilization.

There are few reports on the preparation, characterization and adsorption properties of chitosan-MNPs composite. Two methods are widely used for the preparation of these nanoparticles, and this study uses the one step *in situ* co-precipitation method (Feng *et al*., 2022). Recently, the use of highly structured physical and biosynthetic activities of microbial cells has emerged as a novel approach for the synthesis of metal nanoparticles. The interaction between microorganisms and

metals has been widely studied. Microorganisms' ability to extract accumulated metals is already being utilized in biotechnological processes such as bioleaching and bioremediation. The ability of CCMNPs to chelate metal ions is attributed to the presence of amine and hydroxyl groups in the chitosan chain.

MNPs can also be used for enzyme immobilization other than biomedical applications which are achieved by physical absorption, covalent bonding and bioconjugation. Coupling nanoparticles with reagents like glutaraldehyde,1-ethyl-3-(3-dimethylaminopropyl) carbodiimide hydrochloride (EDC) (Sui *et al*. 2012) and sodium tripolyphosphate (TPP) are better suited to achieve appreciable immobilization stability by covalent bonding.

Huang *et al*. (2010) covalently bound glucose oxidase to Fe_3O_4/silicon dioxide nanoparticles using glutaraldehyde and showed an activity of immobilized glucose oxidase of 4570 U/g at pH 7 at 50 °C. The immobilized glucose oxidase retained 80% activity after 6 h at 45 °C while free enzymes could only retain 20% activity under similar conditions. Immobilized glucose oxidase retained 60% of its initial activity after six repeated cycles, and retained 75% of its activity when stored for a month at 4 °C compared to 62% of free cells (Xu *et al*. 2014). The role of surface modification of nanoparticles was also demonstrated by Esmaili *et al*. (2021) when they modified MNPs 3-Aminopropyltriethoxysilane (APTES) and trichlorotriazine (TCT).

There are several applications of MNPs conjugated with enzymes, for instance, MNPs produced by biopolymer immobilization are useful in the food industry as food processing units (Gharibzahedi and Jafari, 2017). Their renewable biocatalyst characteristic allows them to be implemented for greener generation of biofuels (Ansari and Husain 2012) by co-immobilizing xylanolytic enzymes on nanoparticles including MNPs. Another greener potential of NP conjugation is the cost-effective production of cellulosic ethanol by saccharification of cellulose when cellulase was immobilized on silica NPs followed by yeast fermentation (Maier-Hauff *et al*. 2011). MNPs possess many advantages for immobilization of enzymes and their repeated use remarkably

decreases the production costs (Khoshnevisan *et al*. 2011). However, immobilizing lactase to deplete lactose in milk for lactose intolerant individuals was costly (Talbert and Goddard 2013). MNPs conjugation to enzymes does not have strict requirements for colloidal stability of enzymes

like MNPs for drug delivery. It is important to preserve enzymatic activity on MNPs. MNPs are also applied in biosensing and proteomics. For example, Pečová *et al*. (2013) reported trypsin conjugated MNPs as a promising platform for proteomic analysis, the combination decreased autolysis of the enzyme and increased re-usability (Hola *et al*. 2015). Bhattacharya and Pletschke (2014) studied characteristics of *Bacillus gelatin* ABBP-1 immobilized on magnetic nanoparticles and exhibited higher specific activity. He further suggested that immobilization might have a protective effect on a protein structure which has also led to optimization of its catalytic efficiency.

1.7.2 Advantages and disadvantages of NPs

Despite several advantages of NPs as stated previously in section 1.6, there are certain limitations as well. For instance, their small size and large surface area can lead to particle-particle aggregation and may result in limited loading of functional components. In fact, only NPs with the appropriate size and surface chemistry are not immediately recognized by the immune system and show increased circulation times (Shvedova, Kagan and Fadeel 2010). Nevertheless, their unique and broad-based optical properties, their ease of synthesis and facile surface chemistry and, most importantly, their appropriate size scale can overcome these drawbacks and have been generating much eagerness in clinical diagnostics and therapy (Sperling and Parak 2010).

Magnetic nanoparticles can also be used to carry drugs, they are concentrated in cancer tissue using external magnetic field used (Hosseini, Seyedsadjadi and Farhadyar 2014). The synergistic interaction of immobilization techniques with special features on nanomaterials has led to unpredictable successes (Lee *et al*. 2010).

1.7.3 Recent applications of nanoparticles for bioethanol production

Bioenergy from lignocellulosic biomass has drawn attention lately because of its advantageous low carbon dioxide emissions over the complete fuel cycle and its raw materials for production are not food sources (Reshmy *et al*., 2022). This occurs as an indirect CO_2 emission from biofuels when the logging residues are emitted into the atmosphere simultaneously through combustion instead ofbeing released incrementally as a result of decomposition at the harvest sites (Repo *et.al*, 2011). Recently, Mariño *et al*. (2021) worked on the hydrolysis of cellulose isolated from orange bagasse using immobilized commercial cellulases onto amino-functionalized magnetic

beads. In addition, Dey *et al*. (2021) outlined that nanotechnology can refine lignocellulosic biomass (LCB) into a high-performance fuel source. Furthermore, NPs can reduce toxicity and the costs involved in conventional methods can be reduced when applied to LCB. The use of enzymes in NPs promotes the green hydrolysis of LCB. Furthermore; Sánchez-Ramírez *et a*l. (2017) utilized chitosan cellulase immobilized coated magnetic nanoparticles on the hydrolysis of agave fibre. An increase of 1.60-fold in bioethanol production was obtained from pre-treatment and fermentation of potato peels when Sanusi *et al*. (2021) employed nickel oxide (NiO) NPs immobilized with amylase and amyloglucosidase

Besides using enzymes Kim *et al*. (2014) and Kim and Lee (2016) enhanced bioethanol production from syngas by *Clostridium ljungdahlii* using silica and magnetic nanoparticles respectively being the best at enhancers of gas-liquid mass transfer during fermentation. After intense reading and to my knowledge, the is no single report on xylanolytic bound chitosan-coated magnetic nanoparticles in an attempt for bioethanol production/enhancement from plant biomass. Only recently there have been reports on biomass degradation from cellulase immobilized magnetic nanoparticles. This can be evidenced by a study by Ozyilmaz *et al*. (2021) and lastly, Shalini *et al*. (2021a) who hydrolyzed cellulose from *Allamanda schottii L* by cellulase bound MNPs using *S. cerevisiae*. These findings and studies are conclusive that immobilization of enzymes on NPs improves enzymatic activity and thus increased bioethanol production Ozyilmaz *et al*. (2021) while Kaur *et al*. (2021), Taggar and Kalia (2021) and Shalini *et al*. (2021a) demonstrated that cellulose derived from Allamanda schottii L can be hydrolyzed by cellulase bound MNPs using *S. cerevisiae*.

1.8 Purpose of the study

South Africa produces a significant amount of lignocellulosic biomass annually. The Province of KwaZulu-Natal is especially known for its high production of sugarcane bagasse as waste. Bioethanol production using sugarcane waste has emerged as a renewable, environmentally friendly, and sustainable alternative to non-renewable fossil fuels. The purpose of this study is to investigate the efficacy of a xylanolytic biodegradable nanoparticle co-immobilized enzyme system for enhanced saccharification and bioethanol production. An attempt was also made to assess the production of xylitol. *T. lanuginosus,* which produces high titres of xylanase and acts as a source of the xylosidase gene, was selected for this study. This study focuses on using sugarcane

waste to produce bioethanol and xylitol using a consorted biotechnological-nanotechnological approach. Despite the huge need for bioethanol worldwide, the supply is limited mostly due to poor saccharification of C5 sugars and low yield. The xylanolytic system of *T. lanuginosus* SSBP and its applications has been extensively studied by Singh et al. 2003 from our research group, however studies presenting utilization of pentose sugar is still new. The present investigation attempts to address this supply gap using an environmental-friendly approach which will be instrumental for the sustainable development of South Africa.

Objectives

1. To produce and purify xylanase from *T. lanuginosus* and recombinant β-xylosidase from *P. pastoris* harbouring the *Tlxyn1* gene from *T. lanuginosus*

2. To synthesize chitosan-coated magnetic nanoparticles (CCMNPs) and produce xylan from sugarcane bagasse

3. To co-immobilize xylanolytic enzymes on CCMNPs and study enzymatic saccharification under batch, repeated batch, and fed-batch modes

4. To produce bioethanol and xylitol using a saccharified product

CHAPTER 2: PRODUCTION AND PURIFICATION OF XYLANASE AND RECOMBINANT β-XYLOSIDASE FROM *T. LANUGINOSUS* SSBP

2.1 INTRODUCTION

The global industrial enzyme market is expected to grow from $5.6 billion in 2019 to $7.0 billion in 2023 (https://www.newschannelnebraska.com/news). Despite the global industrial decline in demand due to the current COVID-19 pandemic, the need for carbohydrases is expected to reach USD 5.4 billion by 2027 (https://www.marketresearchfuture.com/reports/carbohydrase-market-5338). Therefore, the production of enzymes in appropriate quantities is the first and most critical step for its application in different bioprocesses. Laboratory production of enzymes often involves studies in shake flasks and laboratory bioreactors. While shake flask studies are routinely used for the initial optimization of enzyme production, bioreactors are preferred for optimum production under controlled temperature, pH, aeration and agitation (Selden and Fuller 2018). Submerged fermentation (SmF) is often preferred over solid-state fermentation (SSF) as medium components are homogeneously dissolved in an aqueous medium for maximum utilization by microorganisms. Most fermenter designs used in laboratory SSF processes are shake flasks or, Erlenmeyer bioreactors.

The degradation of xylan requires a range of xylanolytic enzymes including xylanase and β-xylosidase. The use of filamentous fungi as microbial sources of xylanolytic enzymes has been well-studied (Kumar, Dangi and Shukla 2018). There is a growing interest in xylanases for lignocellulosic hydrolysis (Sutay Kocabaş, Güder and Özben (2015), biofuel production (Basit, Jiang and Rahim 2020) and bioconversion of xylan to value-added products such as xylitol (Zhang et al. 2019) and xylooligosaccharides (Arumugam *et al*. 2018). Cekmecelioglu and Demirci (2020) optimized xylanase from *Trichoderma reesei* on shake flasks and laboratory bioreactor. A total activity of 18.7 IU/mL from a benchtop scale bioreactor was obtained which confirmed that of shake flasks 18.5 IU/mL. Ghoshal, Banerjee and Shivhare (2014) performed experiments to optimize xylanase production from shake flasks to stirred tank laboratory bioreactor. The xylanase was from *Penicillium citrinum,* the production increased by 2.5 times when compared to shake flasks after 96 h. In contrast, Khanahmadi *et al*. (2018) observed reduced time by 24 h on a tray

bioreactor compared to the corresponding batch on shake flasks. The maximum xylanase activity was 1491 U/g and 1157 U/g respectively on the bioreactor and shake flasks.

Similarly, β-D-xylosidases are widely used as one of the xylanolytic enzymes in a diverse range of applications, such as food, fuel, and the pharmaceutical industries. This has resulted in an increase in studies for bioprospection of thermostable and xylose-tolerant β-D-xylosidases (Li *et al*. 2018). β-xylosidases are crucial because they are able to hydrolyze more glycosidic bonds than any other xylanolytic enzyme (Jin *et al*. 2020). There are several reports on microbial production of β-xylosidases with desirable characteristics required for applications. However, the production levels of xylosidases in wild strains are generally low. Therefore, recombinant strains are preferred over wild strains for the production of xylosidases (Mustafa *et al*. 2016).

Bacterial hosts are known to produce misfolded inclusion bodies. Additionally, the instability of plasmids after a few generations is a major concern. Recombinant yeast strains are preferred over bacterial hosts due to appropriate folding and easy methods of cultivation. There are only a few xylosidases reported from filamentous fungi.

Abdeshahian, Samat and Wan Yusoff (2010) cultivated *Aspergillus niger* FTCC 5003 from palm kernel cake for three independent variables on RSM on an aerated packed-bed bioreactor; the activity was 6.13 Units/g after 7 days of incubation. In search for an enzyme to be used as feedstock for bioethanol production, Prasoulas *et al*. (2020) produced xylosidase from a fungus *Fusarium oxysporum* F3 under solid-state cultivation using different agro-industrial residues. A maximum of 0.052 U/g xylosidases was observed on shake flasks. The β-xylosidase from *Aspergillus* sp. BCC125 expressed in *P. pastoris* resulted in a very high yield (Wongwisansri *et al*. 2013). Wild strains of *A. terricola, A. ochraceus* are also known for the production of β-xylosidase (Michelin *et al*. 2012).

Enzyme purification is mandatory for the removal of unwanted proteins and contaminants prior to the characterization of the desired protein. The concentration of proteins using ammonium sulphate and/or acetone is one of the most important steps during the initial steps of enzyme purification. Purification steps may vary from a simple one-step process to multiple steps. Generally, more than one purification step is required to achieve a high level of enzyme purity. The classical chromatographic method of enzyme purification is based on differences in specific properties of

proteins such as charge (ion-exchange), size (gel-filtration), hydrophobicity (hydrophobic interaction and reverse-phase) and biorecognition (affinity chromatography). Therefore, the selection of the appropriate purification strategy is crucial to attain maximum yield with the highest catalytic activity and maximum possible purity of the target enzyme. The homogeneity of purified proteins after every step is most routinely visualized on SDS-PAGE gels. The purification process is directed towards achieving a distinct single prominent band corresponding to the protein of interest (Berg, Tymoczko and Stryer 2012).

Mostly, standard column chromatographic techniques involving ion-exchange and gel-filtration steps are required for the purification of microbial xylanases (Singh, Singh and Verma 2017). However, some reports also indicate the use of hydrophobic interaction chromatography (Becker *et al*. 2020). Frequently used fungal xylanases from *Thermomyces.* sp. and *Trichoderma* sp., have been successfully purified to electrophoretic homogeneity (Harris and Ramalingam 2010). Xylosidase from *Aspergillus oryzae* (Matsuzawa, Kameyama and Yaoi 2020) and *Rhizophlyctis rosea* (Huang*et al*. 2019) expressed in *P. pastoris* has been reported.

Enzyme production in the bioreactor has ability to reduce costs associated with the entire process. This chapter focuses on the production and purification of two xylanolytic enzymes, xylanase and xylosidase. These integrated enzymes play a significant role in the biorefinery. Xylanase (TlxylA) was produced by a wild fungus strain *T. lanuginosus* SSBP on course corn-cob media, and xylosidase (Tlxyn1) was produced from a recombinant strain of *P. pastoris* G115. All enzyme productions were explored through submerged fermentation of the previously optimized medium.

2.2 MATERIALS AND METHODS

2.2.1 Growth of microorganisms and enzyme production

2.2.1.1 Production of xylanase from T. lanuginosus SSBP

T. lanuginosus SSBP was grown on PDA plates for 7 days, followed by inoculation of 9 mm (3×) mycelial growth in 100 mL statistically optimized medium as described previously (Singh, Pillay and Prior 2000). The medium was composed of 30 g/L corn cobs, 5 g/L KH_2PO_4 and 15 g/L yeast extract at pH 6 (Lin *et al*. 1999). Cultivation was carried out in 250 mL flasks at 50 °C for 7 days at 180 rpm. A cell-free culture supernatant was obtained by centrifugation at 3 500 × g for 20

minutes at 4 °C and used as crude enzyme extract. TlxylA activity was measured by determining the amount of reducing sugars released at 50 °C using 1% birchwood xylan in 50 mM citrate buffer at pH 5 (Kambourova *et al*. 2007) as the substrate, as described by Miller *et al*. (1960). The substrate was pre-heated at 50 °C for 5 min then incubated with appropriately diluted enzyme solution for 5 min and 0.9 mL DNS reagent was added, reaction was stopped by boiling the reaction mixture for 5 min. Finally, it was cooled to room temperature, thereafter the absorbance was read at 540 nm. The substrate and enzyme blanks were subtracted from the value of the analysed sample (Breuil and Saddler 1985). One unit of xylanase activity was defined as the releaseof one nmol of product per second by hydrolyzing xylan substrate, per min at 50 °C.

2.2.1.2 Production of β-xylosidase from recombinant P. pastoris GS115

Host *P. pastoris* GS115 harbouring the β-xylosidase gene from *T. lanuginosus* SSBP was expressed in 100 µg/mL zeocin (Sigma-Aldrich) supplemented yeast extract, peptone, dextrose (YPD) medium containing 10 g/L yeast extract, 20 g/L peptone, 20 g/L glucose and 20 g/L solidifying agar (Gramany *et al*. 2016). A loopful of *P. pastoris* was inoculated in 50 mL YPD broth medium on arotary shaker at 200 rpm at 30 °C. An overnight culture was then inoculated into the fermentationbroth of 50 mL and incubated for 5 days at 200 rpm at 30 °C. Produced Tlxyn1 was harvested bycentrifugation and stored at 4 °C. One unit of β-D-xylosidase was defined as the amount of enzymerequired to release 1 µM of p-nitrophenol per minute under optimal conditions.

2.2.2 Purification of xylanase and xylosidase

TlxylA from *T. lanuginosus* SSBP was produced in a 5 L laboratory fermenter and the crude extract was concentrated by 25 – 50% ammonium sulphate precipitation. The precipitate obtained after overnight incubation at 4 °C was resuspended in 50 mM citrate buffer pH 5.0. This was followed by desalting through Hi-Prep^{TM} 26/10 column (GE Healthcare, Sweden) against 20 mM citrate buffer (pH 5.5) using AKTA purifier system (GE Healthcare, Sweden). DEAE column and Resource Q anion-exchange columns were tested for their efficacy in purifying the proteins using ÄKTA purifier. To study the binding of target proteins, both columns were operated using 20 mM Tris – HCl pH 8.0- and 50 mM Na-citrate pH 5.3 as separate running buffers. To elute the proteins, 0 – 1 M sodium chloride was used at a flow rate of 1 mL/min. Active fractions from the eluted peaks were pooled and applied on a Superdex^{TM} 200 increase 10/300 column (GE Healthcare, Sweden) to elute with 50 mM sodium acetate buffer (pH 5.5) at 0.75 mL/min. Eluted fractions

were collected and concentrated with Biomax (MW. cut-off 10 000 Da) ultrafiltration membrane (Millipore, USA). The concentration for total proteins was estimated using the Bradford method with bovine serum albumin (BSA) as the standard. Tlxyn1 from *P. patoris.* G115 was produced and purified in a similar manner as that of TlxylA, except that the crude extract was concentrated by 75-90% ammonium sulphate precipitation.

Purified proteins were visualized on SDS-PAGE as described by Laemmli (1970) using a Mini PROTEAN gel electrophoresis unit (BioRad) to run a 12% separating gel of pH 8.80 containing 10% SDS.

2.3 RESULTS

2.3.1 Production of enzymes

2.3.1.1 Comparative xylanase production in shake flask and a 5 L laboratory bioreactor

TlxylA production by *T. lanugenosus* SSBP was observed over a period of 7 days by determining xylanase activity every 24 h in a statistically optimized medium as shown in Figure 2.1. The highest production of 3450 U/mL was observed on the sixth day. Thereafter, the production remained almost constant. For large-scale production of TlxylA, a 5 L laboratory bioreactor was used. Similarly, to shake flasks, TlxylA production by *T. lanugenosus* SSBP was observed over a period of 7 days by determining xylanase activity every 24 h; with the highest production of 3735 U/mL was observed on day 6. During the first 48 h of fermentation, the enzyme units were almost the same on the shake flasks and the laboratory bioreactor.

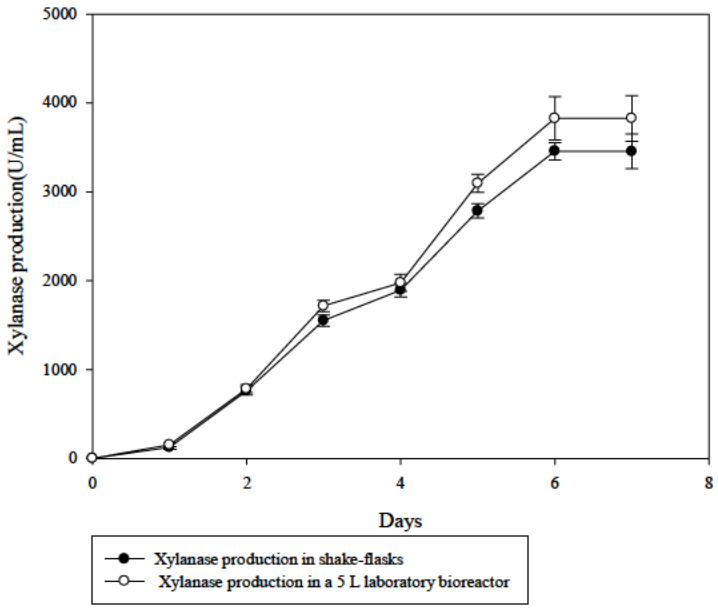

Figure 2. 1: Comparative TlxylA production profile in 250 mL shake flask and in a 5 L laboratory bioreactor at 50 °C for 7 days

2.3.1.2 Comparative xylosidase production in a shake flask and in a 5 L laboratory bioreactor

A time course (Fig.2.2) Tlxyn1 production by *P. pastoris* was carried out over 4 days of fermentation on a YPD fermentation medium supplemented with zeocin. There was an almost constant increase in the production in the shake flasks. A steep gradual production was observed. The highest production of 59.45 U/mL was on day 4 of fermentation. Production declined slightly on the fifth day. Tlxyn1 was upscaled on a 5 L laboratory bioreactor and the production was monitored every 24 h for a period of 5 days. The production pattern was like that of the shake flasks. There was a difference of 23.92% – 39.01% from flasks to the bioreactor. A maximum of 82.84 U/mL was observed on the 4th day of fermentation. There was no significant increase in production after day 4.

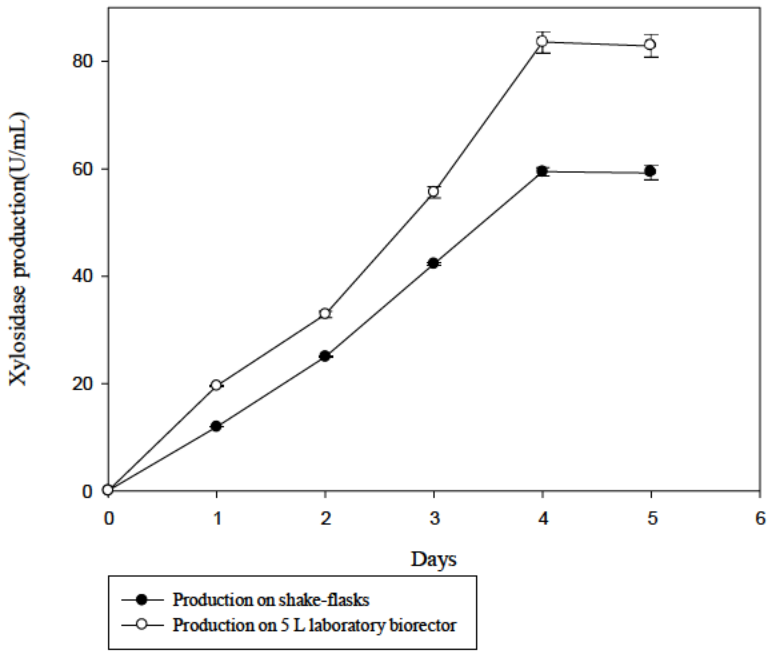

Figure 2. 2: Comparative Tlxyn1 production profile in a 250 mL shake flask and in a 5 L laboratory bioreactor at 30 °C for 5 days

2.3.2 Purification of xylanase and xylosidase on the ÄKTA purifier

TlxylA and Tlxyn1 were concentrated using ammonium sulphate precipitation and purified by classical chromatography using ion-exchange and size-exclusion chromatographic steps. Concentrated enzyme solutions were desalted with Hi-PrepTM 26/10 column (GE Healthcare) and then passed through HiTrap DEAE (GE Healthcare) and Resource Q (GE Healthcare) columns on the ÄKTA purifier 100 (GE Healthcare).

The purification chromatogram for Tlxyn1 on the ÄKTA purifier is shown on the chromatogram (Fig.2.3 (A)). Two peaks were observed namely peak 1 (P1) and peak 2 (P2). P1 consists of fractions from A4 to B15 which have failed to bind at the matrix, as a result they passed as flow through. After elution with a linear gradient of 0 – 1 M NaCl in 50 mM Tris-HCl buffer (pH 8.0), a second peak (P2) was observed and eluted at a concentration of approximately 70% NaCl. P2 showed a visible separation of fractions E4 and E7. After performing the standard xylosidase assay, the most active fractions were found to be those of D3, E1 and E4. Therefore, these active fractions were pooled and concentrated using 10 000 kDa cut-off membrane and used for gel filtration

chromatography on a Superdex G-75 column. The concentrated fraction appeared as a single band SDS-PAGE after silver staining (Fig 2.4). A complete summary of the chromatographic details including purification fold, yield, activity, and the recovery rate is presented in Table 2.1.

The purification profile for TlXYnA on the ÄKTA purifier is shown on the chromatogram (Fig.2.3(b). Two peaks were observed namely peak 3 (P3) and peak 4 (P4). The third (P3) consists of fractions from A5 to A15 which shows the adsorption of the sample and washof unbound proteins. These unbound proteins are referred to as waste, they are eluted before the gradient begins. Peak 4 was observed from D6 to F13 after elution with a linear gradient of 0–1 MNaCl in 50 mM Tris-HCl buffer (pH 8.0), at a concentration of approximately 70% NaCl. The second peak showed a slight separation of fractions D3 and D4. After performing the standard xylanase assay, the most active fractions were found to be those from D6 to E3, E1. Thereafter, these active fractions were pooled and concentrated using 10 000 kDa cut-off membrane and usedfor gel filtration chromatography on a Superdex G-75 column. The concentrated fraction appearedas a single band SDS-PAGE after silver staining (Fig 2.5). A complete summary of chromatographic details including purification fold, yield, activity, and the recovery rate ispresented in Table 2.2. During optimization, TIxynA and Tlxyn1 purification using 50 Mm sodiumcitrate buffer, pH 5.30 and DEAE column and vice versa on ÄKTA did not produce desirable results (data not shown). Fractions with the highest activity on TIxynA and Tlxyn1 appeared witha single band on the SDS-PAGE (Fig 2.4 and 2.5). A complete summary of TIxynA purification containing purification folds, yield, activity, and recovery is presented in Table 2.2 and Table 2.2.

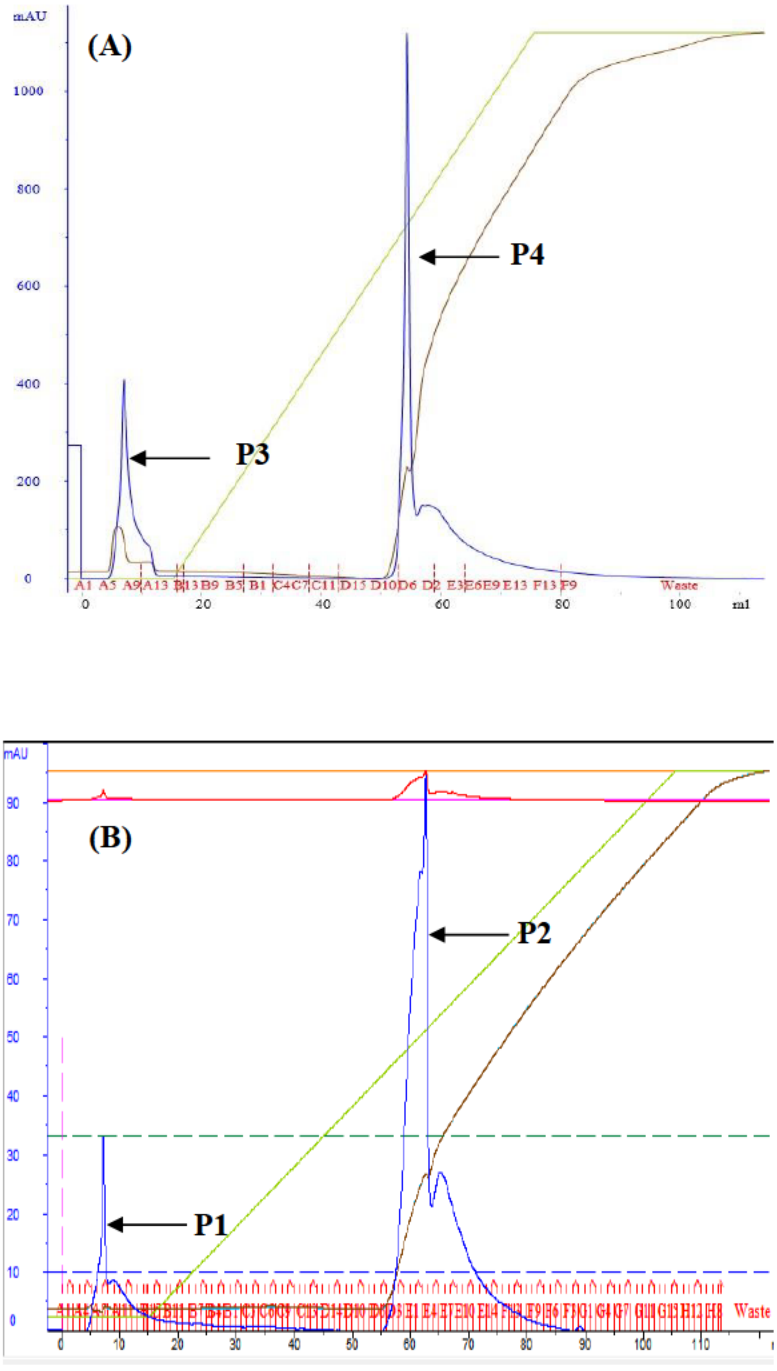

Figure 2. 3: Elution profiles of TlxylA (A) and recombinant Tlxyn1 (B) after anion exchange chromatography using Resource Q column. The columns were eluted with 50 mM Tris-HCl buffer (pH 8.0) at a flow rate of 1.0 mL/min.

Table 2. 1 Summary of purification steps for xylanase from T. lanuginosus SSBP

Purification Steps	Total activity (U)	Total protein (mg)	Specific activity (U/mg)	Yield (%)	Fold purification
Crude filtrate	19179	134.3	144.97	100	1
$(NH_4)_2SO_4$ precipitation	16891	98.54	171.41	88.07	1.18
Anion exchange (DEAE FF)	11252	21.30	528.26	58.67	3.64
Gel filtration (Superdex™)	9137	13.97	654.04	47.64	4.51

TlxynA from *T. lanuginosus* SSBP was successfully purified with an overall 4.51 purification fold and 47.64% yield with a specific activity of 654.04 U/mg (Table 2.1). The purified enzyme had an apparent molecular mass of 23 kDa on SDS-PAGE gel (Fig.2.5).

Table 2. 2: Summary of purification steps for recombinant xylosidase

Purification steps	Total activity (U)	Total protein (mg)	Specific activity (U/mg)	Yield (%)	Fold purification
Crude filtrate	16716	111.75	149.58	100	1
$NH_4)_2SO_4$ precipitation	12517	78.42	159.62	74.88	1.07
Anion exchange (Resource Q)	5779	10.23	564.71	34.57	3.78
Gel filtration (SuperdexTM)	2453.88	2.08	1179.75	14.67	7.89

Recombinant Tlyyn1 was purified to homogeneity with an overall purification fold of 7.89-fold and a yield of 14.67% with a specific activity of 1179.75 U/mg (Table 2.2). The purified enzyme had an apparent molecular mass of 55 kDa on SDS-PAGE gel (Fig.2.4).

2.3.3 Molecular mass determination of enzymes

Homogeneity of the purified proteins was confirmed on SDS-PAGE. The SDS-PAGE revealed multiple bands on lanes 2 and 3. A single band in each sample after the purification steps on lane 5 was observed. The molecular masses estimated by this method were 50 kDa for Tlxyn1 (Fig.2.4)

and 23 kDa for TlxynA (Fig.2.5). The effectiveness of the purification can be evident from the band for the protein of interest becomes more prominent relative to other bands.

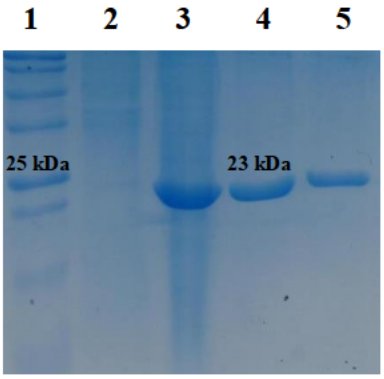

Figure 2. 4: SDS-PAGE analysis of purified xylanase from T. lanuginosus SSBP. Lane 1: Native protein molecular weight marker (Sigma-Aldrich), lane 2: Crude filtrates, lane 3: Ammonium sulphate precipitated enzymes (crude extract), lane 4: Ion exchange chromatography (Anion exchange-DEAE FF), lane 5: Gel filtration (Superdex^{TM})

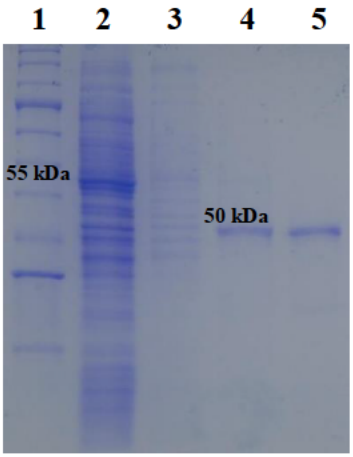

Figure 2. 5: SDS-PAGE analysis of purified recombinant xylosidase produced in P, pastoris as host. Lane 1: Native protein molecular weight marker (Sigma-Aldrich), lane 2: Crude filtrates, lane 3: Ammonium sulphate precipitated enzymes (crude extract), lane 4: Ion exchange chromatography (Anion exchange-DEAE FF), lane 5: Gel filtration (Superdex^{TM})

2.4 DISCUSSION

Laboratory production of industrial enzymes is important to further scale up to a pilot-scale level. For characterization and immobilization of enzymes, all non-desirable proteins must be removed. The discovery of novel enzymes is often followed by purification, characterization, and optimization to suit industrial use and multifarious applications. Catalysts for the synthesis of amide bonds are highly desired based on an environmental perspective (Huisman and Collier 2013).TlxynA (Fig 2.1) and Tlxyn1 (Fig 2.2) were produced in a 5 L bioreactor.

Complete hydrolysis of xylan requires the synergistic action of various enzymes, known as a xylanolytic system. Endo-β-1,4-xylanase (E.C.3.2.1.8) and β-D-xylosidase (E.C.3.2.1.37) are the most important, well studied xylanolytic enzymes responsible for the degradation of the polymer main chain (Terrasan, Guisan and Carmona 2016). The present investigation focused on the production and purification of β-TlxynA and β- Tlxyn1 enzymes. Thermophilic filamentous fungus *T. lanuginosus SSBP* super producer was used to produce xylanase in a laboratory reactor. Xylanase from *T. lanuginosus* was previously reported by Kumar *et al*. (2009) where *T. lanuginosus* MC 134 mutant was used to obtain high levels of extracellular xylanase (346 ± 10 U/mL) observed on the fifth day of fermentation. The production was further enhanced to 3299 ± 95 U/mL using corn cobs under optimized growth conditions. During the present study, a total of 3454 U/mL and 3735 U/mL were obtained on day six from shake flasks and a laboratory bioreactor, respectively. *Aspergillus fumigatus* JCM 10253 was shown as a potential producer of extracellular xylanase (EI 1.18) with 2.6 IU/mL activity over 6 days of incubation at 50 ℃ (Saroj, Manasa and Narasimhulu 2018).

On shake flasks production of Tlxyn1, a maximum of 59.45 U/mL and 82.84 U/mL was observed in shake-flasks and laboratory reactor respectively after 96 h of incubation. After 96 h of incubation, there was no significant production. These enzymes generally operate at slightly acidic pH, mesophilic temperatures. Kim*et al*. (2017) reported a novel intracellular glycoside hydrolase family 43 β-xylosidase gene (xyl43) from *Penicillium oxalicum* 114-2 that was successfully overexpressed in *P. pastoris* to produce high levels of xylosidase. After incubation of 4 days, the Xyl43 protein concentration in the culture supernatant reached approximately 92.8 mg/L. An enhanced production of β- Xylosidase was also achieved from *K marxianus* M125 mutant up to 1.5 to 2-fold more than that of wild strain (Mustafa *et al*. 2016. *P. pastoris* GS115 was shown to be a good gene host. This is

evident in a study by Wang *et al*. (2014) who transformed pGAPHα-*MAP*30 gene into *Pichia pastoris* GS115 by electroporation successfully. The second part of this chapter focuses on enzyme purification. This involved precipitation by ammonium sulphate followed by concentration using ultrafiltration (Millipore 5 L benchtop ultrafiltration unit, 10 kDa and 50 kDa cassettes). Further, binding conditions of TIxynA and xylosidase on different anionic and cationic chromatographic columns (GE Healthcare) were optimized. This included optimization of flow rate (0.5 mL/min to 1.5 mL/min), buffer strength (10 mM– 80 mM) and pH (4 – 10) on the ÄKTA purifier. TIxynA andTlxyn1 were purified using ion-exchange and size-exclusion chromatographic steps on the ÄKTApurifier.

Most of the protein remained unbound and detected in the flow-through fractions when using DEAE, indicating that DEAE was not the appropriate matrix for binding of β-TlxynA and β-Tlxyn1. Therefore, purification steps were attempted on another matrix Resource Q (50 mM Tris-HCl buffer (pH 8.0). As expected, both enzymes were successfully attached to the changed column and buffer, which was further eluted in fractions as peaks 1,2,3,4. Non-attachment of proteins to matrices is common during protein purification and has been previously reported during the development of protein purification methods on the BioRad NGC and GE ÄKTA by Winters *et al*. (2020) and during the purification of protease as reported by Matkawala *et al*. (2019). A Resource Q column was used for the successful purification of human epidermal growth factor receptors (EGFR) (Seetaha, Ratanabanyong and Choowongkomon 2019) and serine proteinase (Azzolini *et al*. 2003).

DEAE is an excellent and preferred matrix, which has been used for the purification of a large number of proteins with recent reports by Vidya *et al*. (2020) on β-galactosidases from a fungus *Aspergillus terreus* (KUBCF130), purification of thaumatin-like protein-1 (Ma *et al*. 2020) and Urokinase Enzyme from serum blood of patients with pneumonia (Mohammed and Shaker 2020).

β-TlxynA and β- Tlxyn1 were successfully homogenously purified with an overall purification of 4.51-fold, 47.64% yield (Table. 2.1) and 7.89%, yield of 14.69% (Table. 2.2) respectively after gel filtration although the purification fold of xylanase is lower than those reported from other fungal strains. Purification using Sephacryl S-200 resulted in 7.43-fold (Heinen *et al*. 2018), 7.06-fold (Teixeira *et al*. 2010), 6.0 (Li *et al*. 2005a) and 7.7-fold from the Sephadex G-100 column

(Khucharoenphaisan, Tokuyama and Kitpreechavanich 2010) which are still within the same range as obtained.

The purity of proteins was evidenced by size-exclusion chromatography in the SDS-PAGE analysis on a 12% gel. Purified, TlxynA and Tlxyn1 were found to be homogeneous and detected as a single protein band on SDS-PAGE (Fig 2.4, Fig.2.5). The molecular weight of purified TlxynA was estimated to be 23 kDa and Tlxyn1 was estimated to be 55 kDa (Fig.2.4) using SDS-PAGE, suggesting that purified enzymes might be a monomer. To our advantage, xylanases with low molecular weight are preferable in the pre-treatment of lignocellulosic biomass. This is evidenced by Subramaniyan (2012) during his pre-treatment of Kraft cooked pulp. This is because they can easily generate pores allowing penetration into pre-treated xylan for effective xylan hydrolysis. The size of recombinant Tlxyn1 is not in agreement with the previous reports as per (Li *et al*. 2005a) and (Dehnavi *et al*. 2016). The size of TlxynA agrees with the previous reports as per Khucharoenphaisan *et al*. (2010) with an intense protein band of 24.9 kDa. The molecular masses (23 kDa) of the enzymes are similar to the values of 24 kDa by Bokhari, Latif and Rajoka (2009) and (Prajapati *et al*. 2020) with a molecular weight of 22.5 kDa from *Aspergillus tubingensis*. The size of molecular weight from different species can diverge greatly for homologous enzymes as their common gene ancestor has not evolved the same way in these microorganisms. On the opposite side, same/similar enzyme activity can be obtained from two different proteins (i.e., not originating from the same gene ancestor) which have evolved in a convergent way to catalyse the same reaction but with different architectures/strategies. Secretorypathways are highly complex systems requiring many assisting proteins for maturation, folding and secretion (Celińska and Nicaud 2019). Genetic background also affects molecular weight during gene expression within the same expression cassette and same locus (Swietalski *et al*. 2020).Extensive glycosylation increases molecular weight, it is critical for a wide range of biological processes, including cell attachment to the extracellular matrix and protein-ligand interactions in the cell (Bonzom *et al*. 2019).

2.5 Conclusions

Extracellular β-xylanase was purified from the culture of *T. lanuginosus* SSBP and xylosidase from *P. pastoris* G115 grown on zeocin supplemented YPD medium. The molecular masses and

purity of these enzymes were evidenced by the presence of a single band on the SDS-PAGE. The results put the enzymes at a suitable stage for their application in biomass degradation.

CHAPTER 3: SYNTHESIS OF CHITOSAN-COATED MAGNETIC NANOPARTICLES (CCMNP) AND PRODUCTION OF XYLAN FROM SUGARCANE BAGASSE

3.1 INTRODUCTION

There have been numerous reports on applications of biomass-degrading enzymes in industrial processes during the past few decades (Kumar et al. 2008; Solomon et al. 2016; Bilal et al. 2017; Sharma et al. 2019). Despite extensive industrial applications of enzymes, their use is presently limited by several factors such as high costs (Ávila *et al*. 2020), loss of stability on prolonged use, availability in small amounts, susceptibility to proteases and presence of inhibitors (Husain and Jan 2000). Asgher *et al*. (2014) and Cao *et al*. (2021) suggest immobilizing enzymes with an insoluble matrix to increase their effectiveness as industrial biocatalysts. Immobilization of enzymes on support matrices, such as nanoparticles, may offer possible solutions to these limitations as it improves the stability of enzymes, which in turn, enhances their reusability. Moreover, enzyme-bound nanoparticles allow Brownian movement when dispersed in an aqueous solution, which may improve the activities of immobilized enzymes more than free enzymes (Gupta *et al*. 2011). Therefore, immobilized enzyme systems are preferred over free enzymes, especially for repeated cycles of continuous bioreactor operations (Fernández-Fernández, Sanromán and Moldes 2013). A wide range of nanoparticles has been synthesized and investigated for their suitability as support matrices for the immobilization of enzymes. Nanoparticles are preferred over other available immobilizing matrices as they offer a large surface area for immobilizing and stabilizing enzymes.

Magnetic nanoparticles offer unique characteristics such as superparamagnetism, high coercivity, low Curie temperature and high magnetic susceptibility, which has attracted considerable scientific interest (Tai *et al*. 2011). Uncoated metallic nanoparticles have a large surface area-to-volume ratio and can be easily oxidized in air, thereby losing magnetic properties and dispersibility. Coating of the magnetic nanoparticles is required for the addition of functional groups for specific applications (Alzaidi, Alzahrani and El-Mouhty 2016). Mohammadi *et al*. (2019)produced gold-coated MNPs for immobilization of inulinase. Similarly, attempts have been madeto coat MNPs with polyaniline (Tahmasebi *et al*. 2012), silica (Du *et al*. 2012), dextran (Mou *et al*. 2015) and many other polymers. Functionalization of MNPs has grabbed considerable interest

as it introduces important functional groups for effective immobilization of industrially important enzymes (Bilal *et al*. 2018a; Bilal et al. 2018b). It also allows easy detection of functional groups that can be identified using FTIR (Zhou *et al*. 2009). Gou *et al*. (2020) reported a novel magnetic nanocarrier for immobilization of laccase to digest corn stover for improvement of bioethanol production.

This chapter starts with the synthesis of chitosan-coated magnetic nanoparticles (CCMNPs) for co-immobilization of xylanolytic hemicellulases from *T. lanuginosus* SSBP. Co-immobilization of xylanolytic β-xylanase and β-xylosidase on CCMNP can overcome some of the mentioned limitations by improving certain enzyme characteristics. Major immobilization advantages include an increase in thermostability and its resistance to extreme conditions (Georgieva *et al*. 2008; Arıca, Altıntas and Bayramoğlu 2009).

The remaining part of this chapter is focused on producing xylan as a substrate, from sugarcane bagasse. Globally, lignocellulosic biomass is abundant and underutilised. It is considered one of the cheapest substrates to produce value-added compounds. Annually, 1.3 billion tons of lignocellulosic waste is produced from food and food-processing industries (Ravindran and Jaiswal 2016). A wide range of value-added products can be obtained by using sugarcane by-products such as bagasse, sugarcane tops, molasses, and vinasse. This study employs the use of sugarcane bagasse as the preferred lignocellulosic biomass to produce xylan. The produced xylanase was used as a substrate for bioethanol production.

For extraction of xylan from SCB or any other biomass, pre-treatment is required for the removal of lignin and the disintegration of the structure to enhance enzymatic hydrolysis of xylan (Reddy and Krishnan 2016). Alkali pre-treatment using sodium hydroxide or potassium hydroxide is an effective method for the recovery of xylan (Jayapal *et al*. 2013).

3.2 MATERIALS AND METHODS

3.2.1 Production of nanoparticles

3.2.1.2 Synthesis of Chitosan–coated magnetic (Iron oxide) nanoparticles

The nanoparticles were prepared using the method described by Chen *et al*. (2011). This involved using a ratio of 2:1 $FeCl_3$. $6H_2O$ and $FeCl_2.4H_2O$ at 60 – 80 °C under an inert nitrogen atmosphere and stirring at 400 rpm for 15 min. This was followed by the addition of 8 M NaOH to the solution until pH 9.5 was attained, as indicated by a change in colour from orange to yellow to black. The solution was then stirred for 30 min at 400 rpm and washed 5 times with ethanol and 3 times with double deionised water (DDIW) by magnetic decantation. Chitosan solution was prepared by dissolving 0.125 g of chitosan in 100 mL of 2% acetic acid. Ten millilitres (50 mg/mL) of prepared magnetic nanoparticles were added to 40 mL of chitosan with vigorous mixing. Thereafter, the resulting solution was sonicated for 40 min (Sonics, USA). This was followed by washing with 250 mL of 50 mM citrate buffer (pH 5.3) and dispersing the resulting solution by ultra-sonication for 30 s to reach a concentration of 10 mg/mL for storage at 4 °C.

3.2.2 Activation, functionalization, and modification of NPs

3.2.2.1 Oleic acid (OA)

Oleic acid (5.3 mL) was added dropwise to 150 mL NP solution during synthesis to cover their surface and stirred for an hour. Resulting NPs were washed 5 times with ddH_2O and ethanol to remove unwanted material then oven-dried overnight (Xiao *et al*. 2016).

3.2.2.2 APTES

An amount of 0.5 g dried OA-coated NPs obtained above were dissolved in 10 mL ethanol and sonicated for 10 minutes. This was followed by the addition of 0.2 mL APTES (99%), stirred for 24 h at room temperature and NPs were then washed with ddH_2O.

3.2.2.3 Glutaraldehyde (GA)

Glutaraldehyde was used as a cross-linking coupling agent, where 0.5 g of OA+APTES coated NPs were dispersed in 10 mL 10% GA in citrate buffer (50 mM pH 5.3). The solution was stirred for 2 h, washed and dried (Shaw *et al*. 2006).

3.2.3. Characterization of produced nanoparticles

Produced nanoparticles were microscopically characterized using SEM, and TEM. The temperature profile was studied using differential scanning calorimetry (DSC) and Thermogravimetric analysis (TGA), while Zeta potential was used for the estimation of the surface charge.

3.2.3.1 SEM

Synthesized nanoparticles with and without enzymes were diluted and a drop was dispersed onto carbon tape and dried under a standard table lamp with a 60W incandescent light bulb, placed about 5 – 10 cm above the sample. The fixed sample was loaded on Field Emission Gun Scanning Electron Microscope (FEG-SEM) in the Microscopy and Microanalysis Unit, University of KwaZulu-Natal (UKZN) for imaging.

3.2.3.2 HRTEM

Similarly, to SEM, the analysis was done by diluting nanoparticles with and without enzymes, dispersed dropwise onto carbon paper and dried under a lamp. The samples were then placed onto the Joel 2100 Electron Microscope in the Microscopy Unit at the University of KwaZulu-Natal for size imaging.

3.2.3.3 FTIR

Discs containing nanoparticles with and without enzymes were prepared with 150 mg of KBr blended with 1.5 mg of sample (NPs, NPs with enzymes). This was then ground with a mortar and pestle to obtain a homogeneous powder. After the prepared mixture had been loaded onto the die, a plunger was used to evenly distributed it by rotating the die. The pellet was then dropped and pressed down lightly with the plunger and the sample was exposed to a vacuum pump (2 mm Hg) for 5 minutes. The die was removed from press by tweezer and the disc obtained was transferred to holder of Varian 800 FTIR for analysis over a full range of available wavenumber.

3.2.4 TGA and DSC analysis

Thermogravimetric and differential scanning calorimetric analysis was performed on a DSC-TGA (TA instruments) facility equipped with a computerized thermal data analyser in the department of mechanical engineering at the Durban University of Technology. Thermogravimetric and calorimetric properties were studied by heating 4 mg of samples at a rate of 10 °C per min from 25 °C – 600 °C and the difference in mass and heat flow was observed.

3.2.5 Zeta potential measurements

Zeta potential measurements were performed using Litesizer500 (Anton Paar). An analysis was performed using omega cuvettes. Cuvettes were thoroughly cleaned with distilled water prior to each measurement. The instrument pre-equilibrates itself with an aliquot of the sample before acquiring data.

3.2.6 Pre-treatment of lignocellulosic waste by alkaline for the liberation of xylan

Sugarcane bagasse from Durban in Southern Africa was used as raw material. The solid biomass at a loading of 100 g milled sugarcane bagasse (particle size, 0.45 – 0.9 mm) was treated with 6% NaOH at a ratio of 1:10 for 4 h. The slurry was pH adjusted to 6.50 using 6 M HCl and filtered through Whatman no. 1 paper to separate residues from the filtrate. The residue was washed several times until neutral pH was achieved. The filtrate was air-oven dried at 45 °C until the volume was reduced to one-third of the initial volume. Thereafter, three times the volume of ethanol was added to concentrate the filtrate as precipitated hemicellulose. The precipitate was decanted and dried at 65 °C for eight hours (Brienzo, Carvalho and Milagres 2010).

3.3 RESULTS

3.3.1 Production of magnetic nanoparticles

The magnetic nanoparticles (MNPs) were successfully produced as seen in Fig.3 (A), using the method described by Zhang *et al*. (2011b). The magnetic property of the produced nanoparticles was confirmed by placing an external magnet Fig.3 (B). CCMNPs can be observed in Fig 3.3(C).

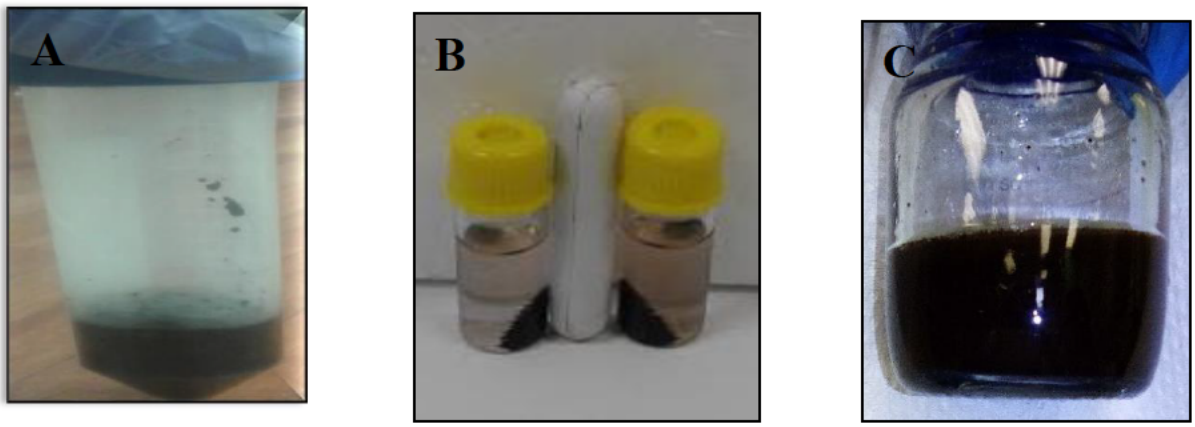

***Figure 3. 1**: Magnetic nanoparticles prepared by coprecipitation of $FeCl_3.6H_2O$ and $FeCl_2.4H_2O$ under inert nitrogen atmosphere (A). Separation of MNP from solution by external magnet (B). Magnetic nanoparticles coated with chitosan for protection against oxygen (C)*

3.3.2 Characterization of CCMNP

The above-produced nanomaterials were characterised using a variety of techniques such as scanning electron microscopy (SEM), HRTEM, FTIR, TGA and DSC to study and confirm their physical and chemical characteristics.

3.3.2.1 SEM

From Fig.3.2 (A) the clumping of MNPs can be clearly seen, resulting in an unclear/undefinedshape. However, Fig 3.2(B) shows distinctive spherical morphology.

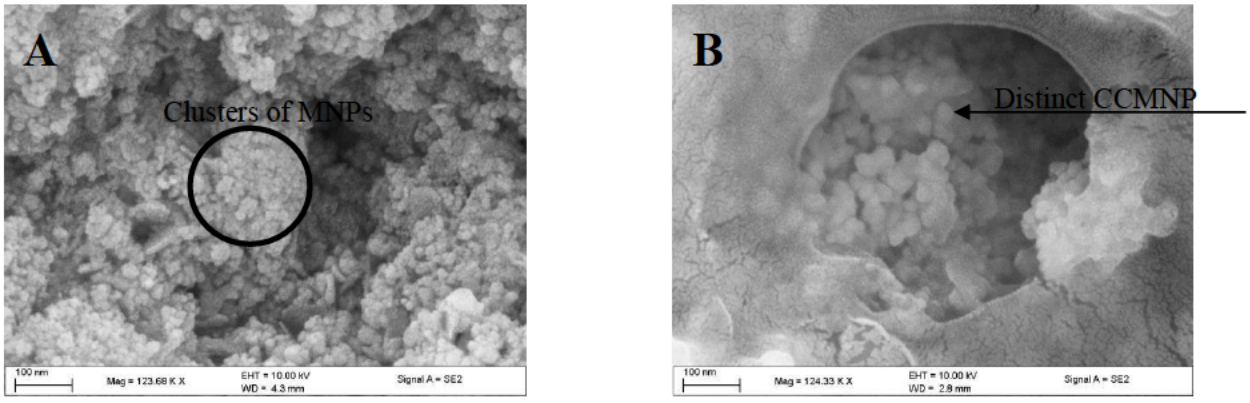

Figure 3. 2: SEM images showing clumping of naked MNPs (A) and distinct spheric MNPs obtained after coating with chitosan (B)

3.3.2.2 HRTEM

A high-resolution transmission electron microscope revealed the morphology of produced MNPs and CCMNPs. Figure 3.3(A) and (B) also show the agglomeration of nanoparticles. The average size range was 1.738 nm to 3.07 nm with semi-spherical and spherical shapes on synthesized CCMNPs. Micrographs in Fig.3.3 (A) and (B) shows naked CCMNPs and CCMNP without the use of APTES.

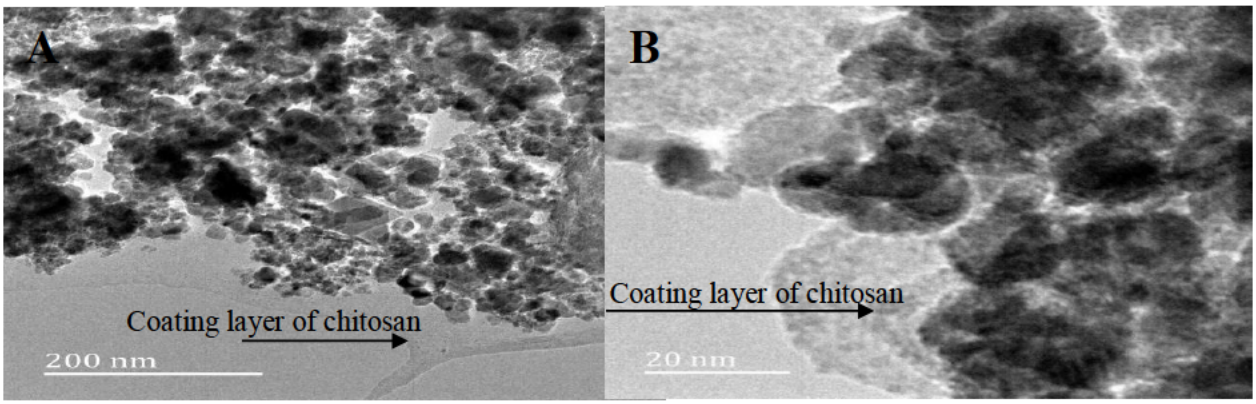

Figure 3. 3: Agglomeration of CCMNPs in the absence of APTES showing clear appearance of chitosan

The HR-TEM images in Fig.3.4. (A) and (B) shows almost a uniform size with spherical morphology. Most particles are sized ranging from 4.65 – 17 nm using image J. Improved dispersion was also observed on CCMNPs.

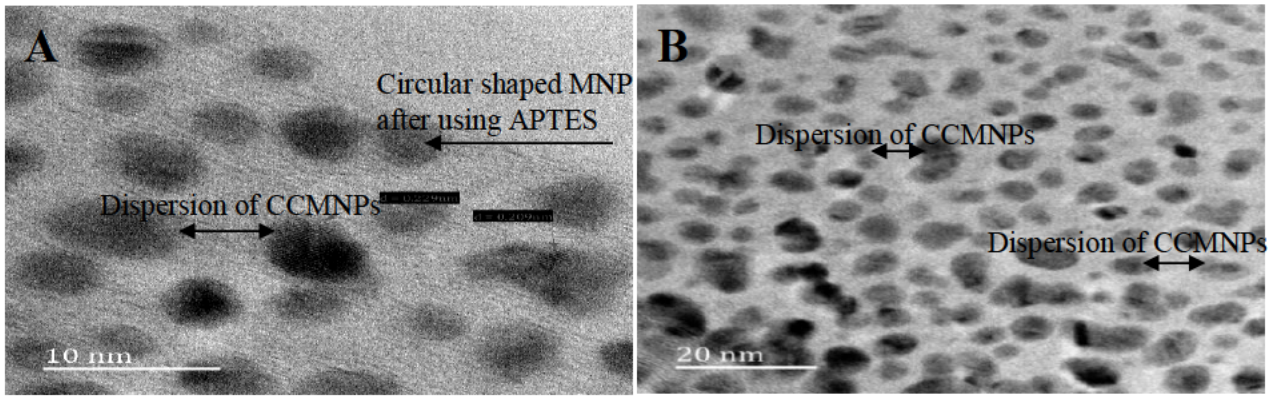

Figure 3. 4: Evenly dispersed CCMNPs after using APTES showing circular shape

3.3.2.3 FTIR analysis

Figure 3.5 depicts the FTIR spectra for MNPs. A stretching vibration of the Fe – O bond was observed at an absorption peak of about 563 cm^{-1} (Guo *et al*. 2021). An amine group at about 1637 cm^{-1} is observed, the resulting amine bond is due to the interaction between the aldehyde(-CHO) group and the amino(-NH_2) group. Another report by Sukprasert *et al*. (2021) indicated glutaraldehyde cross-linkage in the vicinity of 1653 cm^{-1}. The peak at approximately 1386 cm^{-1} is assigned as C–H bending vibration of CH_2 in aliphatic compounds.

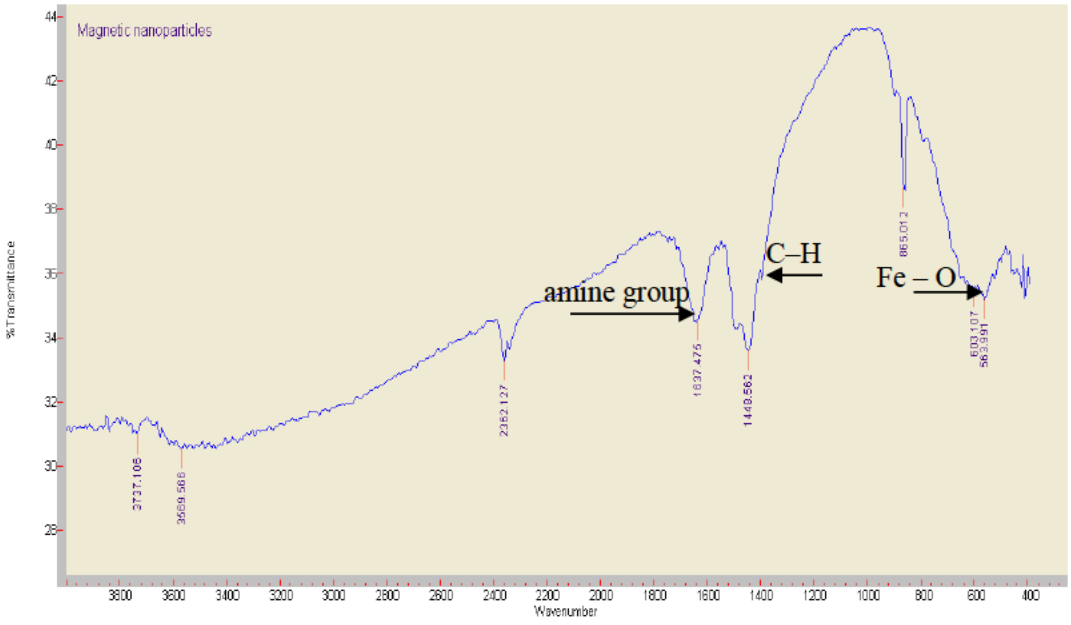

Figure 3. 5: FTIR spectra of synthesized naked MNPs showing major functional groups

The FTIR spectra of chitosan-coated magnetic nanoparticles before and after immobilisation with enzymes are shown in Figure 3.6. A strong peak stretching at 1653 cm^{-1} in both free and co-immobilized CCMNPs corresponds with -NH_2 group bend scissoring. A peak observed at around 1547 cm^{-1} on the CCMNPs without enzymes is assigned to an amide II band with C–N stretching and N–H bend (Sukprasert *et al*. 2021). There was a formation of Schiff's base at 1423 cm^{-1} (Nordin *et al*. 2021).

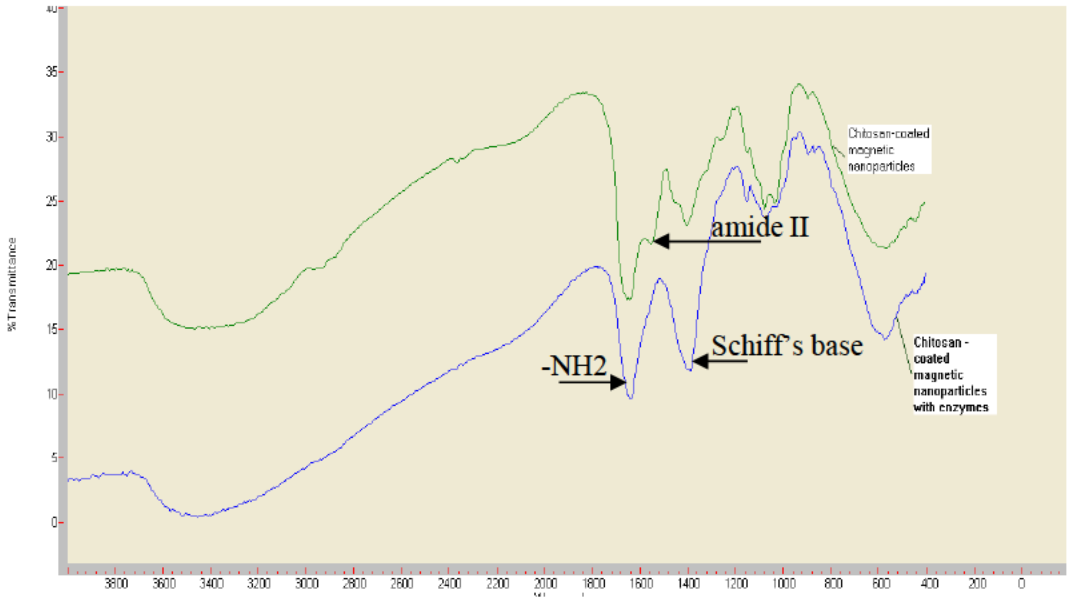

Figure 3. 6: FTIR spectra of CCMNPs and co-immobilized CCMNPs with xylanase and xylosidase confirming co-immobilization

3.3.2.4 TGA/DSC

The TGA-DSC of bare MNPs (Fig.3.7A) shows about an 8% decrease in weight at 70 °C. A further decrease of 5% after 8% at a temperature of 75 – 150 °C was observed. The MNPs remained stable from 150 – 600 °C as evidenced by a stationary line. The MNPs retained about 87% of their weight at 600 °C. A melting peak/point was noted at about 70 °C in both Fig.3.9A and Fig.3.7. A second melting peak was observed at about 175 °C of MNPs while an exothermic peak was observed at 125 °C. At 75 °C CCMNPs retained about 50% of their weight. Crosslinking was observed after 100 °C of CCMNPs. The CCMNPs retained about 25% of their weight at 600 °C.

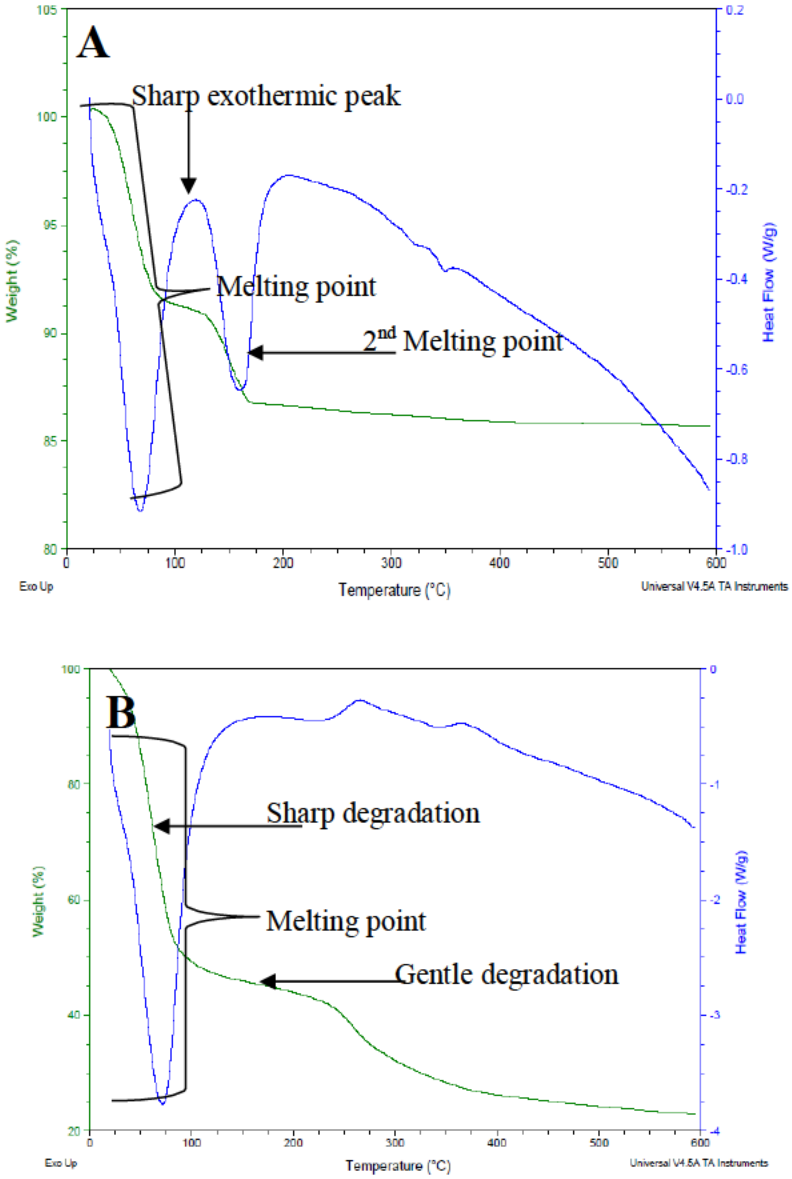

Figure 3. 7: TGA and DSC profile of MNPs and CCMNPs obtained at a heating rate of 10 °C min^{-1}. Uncoated MNPs (A), CCMNPs (B). Where green line represents TGA profile, and blue line represents DSC profile.

3.3.2.4 Surface electric charge and size determined by zeta potential

According to Table 3.1, MNPs has an average zeta potential of 30.58 mV. The charge units decreased by over 50% when the MNPs were coated with chitosan. This trend is also observed on the pH.

Table 3. 1: Zeta potential and size of produced MNPs and CCMNPs (without enzymes) with respective to pH

Nanoparticle	Zeta potential (mV)	Size (nm)	pH
MNP	30.36	1.738	5.65
	30.81	3.07	5.65
CCMNP	14.49	17	2.85
	14.36		2.84

3.3.3 Extraction of xylan from sugarcane bagasse

Powder form of xylan was obtained after pre-treated sugarcane bagasse (Fig.3.8A). Produced dried xylan was dissolved in a citrate buffer (Fig.3.8B) to be used on following experiments.

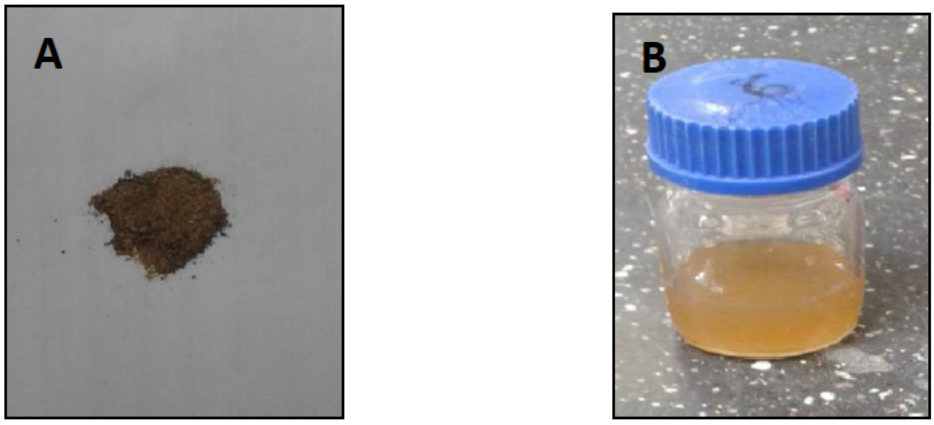

Figure 3.8: Dried precipitate of extracted xylan powder from pre-treated sugarcane bagasse (A), extracted xylan (1%) dissolved in a Na-citrate buffer (B)

3.3.4 FTIR of xylan from sugarcane bagasse

An evident band at 1040 cm^{-1} was observed in Fig.9, the peak attributed to C–O, C–C, stretching and the glycosidic bond as C–O–C (Srinivasan *et al*. 2021). Arabinosyl side chains are observed at around 1161 cm^{-1} and 992 cm^{-1} (Liu *et al*. 2021a). The prominent asymmetric and symmetric vibration mode at 1559 cm^{-1} and 1415 cm^{-1} of the carboxyl group, confirm glucuronic acid component while the peak at 1642 cm^{-1} exhibited water absorption (Sharma *et al*. 2020). A broad

band at 3440 cm^{-1} signify the presence of the hydroxyl group. Peaks displayed at 2800 cm^{-1}, 600 cm^{-1} and 1800 cm^{-1} are distinctive for xylan (Hema *et al*. 2021).

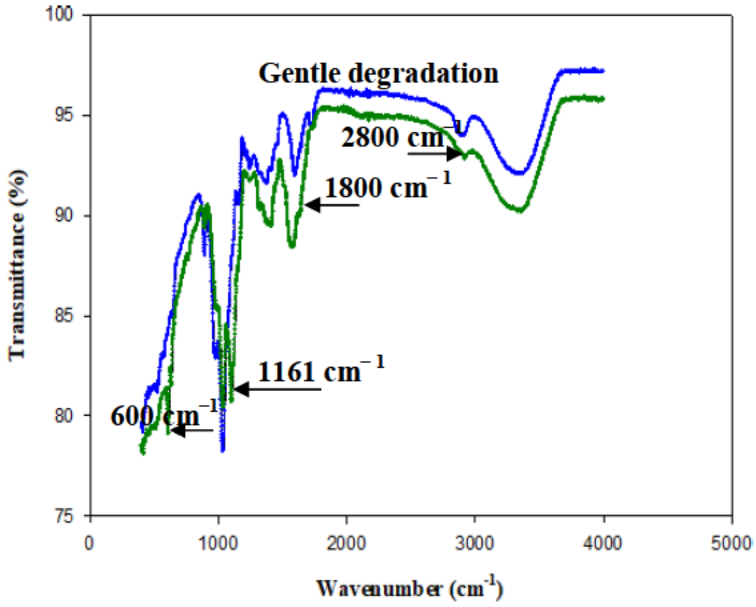

Figure 3. 9: FTIR spectra showing extracted xylan (green) against commercial xylan (blue)

3.4 DISCUSSION

The stability of industrial enzymes under harsh conditions is often the most important factor for the cost-effective application of immobilized enzyme systems (Asgher *et al*. 2014). Many nanomaterials have been used for immobilization in order to enhance enzyme stability and activity (Tian *et al*. 2016). Bare magnetic nanoparticles and CCMNPs were successfully synthesised. Synthesised NPs were able to be separated from a solution with an external magnet. Coating of MNPs with chitosan protected them from oxidation.

Agglomeration was observed in Fig.3.2 because the MNPs were freely exposed to the environment without protection coating and APTES, resulting in oxidation to MNPs. A high-resolution transmission electron microscope agrees with the results obtained from SEM shown in Fig.3.3. Nanoparticles without chitosan and APTES agglomerated. Bare nanoparticles revealed a high

degree of agglomeration due to dipole-dipole interaction. Employing chitosan and APTES on the nanoparticles resulted in less agglomeration with a distinctive spherical shape. The polydispersity of the overall NPs was spherical, whereas Alzaidi, Alzahrani and El-Mouhty (2016) obtained nearly cubic MNPs. The possible reason may be the use of chitosan in the present study while glycine was used as a coating agent by Alzaidi, Alzahrani and El-Mouhty (2016).

Typical HRTEM micrographs for CCMNPs are shown in Fig.3.4 (A) and Fig.3.4(B). It was observed that the nanoparticles showed a lower degree of agglomeration after coating with chitosan and the use of APTES. This can be attributed to the presence of a non-magnetic chitosan layer on the magnetic nanoparticle surface. Treatment of small clusters of CCMNPs with APTES resulted in obtaining evenly dispersed nanoparticles with less or no agglomeration, as observed on the HRTEM. Jadhav *et al*. (2013) previously indicated the relationship between the extent of dipolar coupling and the distance between particles. Although the coated nanoparticles were distinct, they generated small clusters, mainly because of the magnetic nature of the particles. Both NPs were spherical which agrees with the observations from reported SEM micrographs in the present study. Using image J, the diameter of NPs was estimated to range from 1.738 nm to 3.07 nm of MNP. On encapsulation with chitosan, the size of particles increased to 17 nm, indicating successful encapsulation of particles by chitosan. After surface modification by chitosan and APTES, particles maintained their original spherical shape without any deformation and aggregation.

The FTIR spectra of MNPs presented in Fig.3.5 shows a stretching vibration of the Fe – O bond at about 563 cm^{-1}, the bond is located at the tetrahedral site of the inverse spinel structure of the oxide (Vadivel *et al*. 2015). The stretching vibration peak was exhibited at about 563 cm^{-1} (Guo *et al.* 2021). The glutaraldehyde linkage can be used as quality control for the immobilization of antibodies on the produced magnetic nanoparticles. An amine(C=N) bond at about 1653 cm^{-1} was due to the interaction occurring between an aldehyde (-CHO) group of glutaraldehyde and an amino ($-NH_2$) group on the surface of MNPs (Sukprasert *et al.* 2021).

Analysis of FTIR was mandatory following the coating of MNPs with chitosan and co-immobilized with TlxylA and Tlxyn1 onto the surface of Fe_3O_4 MNPs (Fig 3.6). The peak at 1386 cm^{-1} can be attributed to the CH bend vibration of CH_2 in aliphatic compounds (Sukprasert *et al.*

2021). Results confirmed successful surface modification with GA on MNPs. A sharp and broad peak at 3440 cm^{-1} regions in all samples corresponds with the OH bond stretching (Boddu *et al*. 2008; Ghosh *et al*. 2011; Yan *et al*. 2017). The peak at 1637.47 cm^{-1} assigns to the -NH_2. Thedips at 1386.577 cm^{-1} correspond with C–H bending (Shete *et al*. 2014a), and the dips at 1180 cm^{-1} relate to the C-O stretching vibration of the primarily alcoholic group (Hong, Chang and Rhee 2010; Dhoble *et al*. 2011). The C-O-C stretching vibration is visible at 1076 cm^{-1} which is consistent with a previous report by Gao *et al*. (2008). The strong absorption band at 570.07 cm^{-1}corresponds with the Fe-O that validates the presents of Fe_3O_4 core (Li *et al*. 2005; Ma *et al*. 2007;Shete *et al*. 2014b; Chaichi and Ehsani 2016). These results indicate that Fe_3O_4 MNPs were successfully coated with chitosan without a phase change. Evidence of strong stretching of the NH_2 peak at 1637 cm^{-1} was observed. The peak slightly shifted from 1637.47 cm^{-1} to 1653 cm^{-1} after coating and enzyme co-immobilization. A similar characteristic was observed by Sukprasert*et al*. (2021). The GA enzymes assisted as an antigen-binding site of the enzymes. The strong peakat 1653 cm^{-1} serves as the absorption spectrum of proteins. This is also characteristic of the absorption spectrum of protein, thus confirming the tethering of the enzymes. Co-immobilized enzymes remained active after attachment to the CCMNPs.

Thermal properties of nanoparticles were investigated by simultaneous TGA-DSC curves of the MNPs with a heating rate of 10 °C/min are depicted in Fig.3.7A, MNP, Fig 3.7A CCMNPs. The loss of weight from the MNP and CCMNP was due to the loss of residual water in the sample (Hojnik Podrepšek, Knez and Leitgeb 2013). The two endothermic peaks were observed from the corresponding DSC thermogram at around 70 °C and 175 °C from the MNPs. The endothermic peaks indicated that both free and hydrogen-bound water MNPs were dehydrated (Bui *et al*. 2021). A similar trend of endothermic peaks at 70 °C was also demonstrated from CCMNPs. The exothermic peak on MNPs was caused by the crystallization process (Yang *et al*. 2021). The weight loss on TGA curves is attributed to the cross-linking agent (GA) present on the NPs. Degradation results from combustion of the organic layer present (Arévalo-Cid *et al*. 2021). The TGA curve of CCMNPs shows that there was a sharp degradation of about 50% at 75 °C. The sharp decrease in weight loss from CCMNPs was mainly because chitosan is susceptible to high temperatures (Dongre 2019). This was due to the free H_2O molecule in the sample that was adsorbed on the surface of the NPs being lost (Han *et al*. 2018) but this does not affect our study

because only 50 °C will be used later in the study. Degradation further occurred from 75 °C to 230 °C, thereafter the remaining weight remained constant. CCMNPs retained about 25% of their weight at 600 °C which is very less compared to that of MNPs. The biopolymer chitosan decomposes at about 200 °C (Arévalo-Cid *et al*. 2021) which explains further weight loss from 230 °C to 600 °C.

Surprisingly, though the CCMNPs had retained very little of their weight, there were very tiny exothermic peaks at 275 °C and 350 °C, implying that they were still stable. These results are in accordance with those of Hojnik Podrepšek, Knez and Leitgeb (2013) where one exothermic peak was obtained at around 300 °C. The crosslinking peak observed at the CCMNPs was clearly visible due to the presence of GA and chitosan sharing a common functional group.

The zeta potential of functionalized MNPs and CCMNPs was measured and is shown in Table 3.1. The duplicate zeta potential of uncoated MNPs is 30.36 mV, 30.81 mV and 14.49 mV, 14.35 mV of CCMNPs. Stable dispersion is formed at zeta potential above 30 mV. With these clear indications, it was noticed that the zeta potential of coated and uncoated MNPs decreased from 30.36 mV, 30.81 mV to 14.49 mV, 14.35 mV. Functionalized nanoparticles showed inherent hydrophobicity due to the indole side chain, thus the change in zeta potential with a decrease in pH. At pH less than 7.3 the surface charge of NPs is positive and at pH value above 7.3, the charged surface of NPs is negative (Li *et al*. 2021). These physicochemicals enable enzyme attachment to the NPs. Similar observations were also reported by (Lee, Chen and Lee 2021). Functionalization with APTES shifts the negative surface of MNP to a positive surface. Adding more APTES on MNPs introduces a positive charge (Zhang *et al*. 2015). However, increasing APTES concentration causes zeta potential to be less prominent suggesting saturation of particles surface with the NH_3^+ groups. This makes it possible to control the magnetic properties of super magnetic hybrid particles (Digigow *et al*. 2014).

Numerous methods are used for the pretreatment of sugarcane bagasse such as using acids, alkali, surfactant-assisted ultrasound, surfactant-assisted acid pretreatment, and sequential pretreatment. After sequential pretreatment of lignocellulosic, produced dry xylan (Fig.3.8a) was dissolved in a 50 mm citrate buffer (Fig.3.8b). Among the used methods, Sindhu *et al*. (2016) reported the highest

reducing sugar of 0.796 g/g with sequential pretreatment and 0.775 g/g by alkali pretreatment. In the present study, SCB was pretreated with alkali and 69% of xylan was recovered, which is 19% higher than previously reported by Doner and Hicks (1997). Moreover, the yield varies greatly depending on the type of wood, presence of lignin, hydrogen bonds, hemicellulose content and the nature and concentration of alkali used for pretreatment (Bian *et al*. 2010).

It was mandatory to substantiate successful extraction of xylan from SCB by confirmation of functional groups (Fig.3.9). The band appearing at 1040 cm^{-1} corresponds with the C–O, C–C or C–O–H bending present in the hemicellulose structure (Kačuráková *et* al. 1994; Srinivasan *et al*. 2021). This is an affirmation of xylan obtained from SCB (Liu *et al*. 2021a). The absorbance at around 900 cm^{-1} represents a dominant β-glycosidic bond (Bian *et al*. 2010; Gullón *et al*. 2011b) holding xylose sugar units in hemicellulose. The peak at 2800 cm^{-1} assured the purity of xylan after alkali pre-treatment while 600 cm^{-1} corresponds with the C=O stretching vibration of the ester group in xylan (Kumari and Das 2015). The overall region of 1200 – 900 cm^{-1} is typical of arabinoxylan type oligomers and polymers with a low degree of the branched backbone which is indicated by the signal at around 992 cm^{-1} (Robert *et al*. 2005). The asymmetric C–O stretching vibration at 1500 cm^{-1} confirms the presence of uronic acid residues in ionized form (Gullón *et al*. 2011a) as xylans have linear β-(1→4)-d-xylopyranan backbone consisting of various substitutes including uronic acid derivatives, arabinofuranosyl and glucopyranosyl (Singh, Banerjee and Arora 2015). The band appearing at 1642 cm^{-1} was due to the bending mode of water which is identical to FTIR spectra of SCB xylan obtained after precipitation with different levels of ethanol (Kačuráková *et al*. 1998; Samanta *et al*. 2012). The additional vibration at 2990 cm^{-1} corresponds with C–H stretching (Bian *et al*. 2010; Maziero *et al*. 2012). The broad peaks centred at around 3440 cm^{-1} can be attributed to the stretching vibration of hydroxyl group, which is widely distributed over the monosaccharide rings, hydroxymethyl, uronic acid and absorbed water (Wang *et al*. 2015). The bending deformation at 570 cm^{-1} is the linkage for hemicellulose (Kumari and Das 2015). Additionally, the absorbance band at 3440 cm^{-1}, around 1400 – 1500 cm^{-1},1040 cm^{-1},900 cm^{-1}, 1020 cm^{-1} were typical of xylan structure (Jayapal *et al*. 2013).

3.5 Conclusions

Co-precipitation of iron in an inert atmosphere successfully generated MNPs. Produced MNPs were functionalized and activated using APTES, GA, and OA. The use of pure magnetic

nanoparticles may not be very useful since they are more likely to aggregate, undergo quick degradation and altered magnetic properties. Therefore, coating of MNPs with chitosan provided improvement and stability. This greatly provides new opportunities for the development of environmentally friendly nanoparticles as support matrices for enzymes. Sugarcane bagasse remains the top agro-industrial residue in several countries. The use of sugarcane bagasse for energy generation is of immense benefit and a possible solution to the stockpiled sugarcane waste in sugar mills. Production of ethanol from SCB required hydrolysis of xylan by synthesized nanoparticles co-immobilized by xylanolytic enzymes in this study.

CHAPTER 4: CO-IMMOBILIZATION AND CHARACTERIZATION OF XYLANOLYTIC ENZYMES ON CCMNP FOR ENHANCED SACCHARIFICATION

4.1 INTRODUCTION

There have been several attempts to immobilise enzymes on a range of nanoparticles for different industrial applications (Darwesh *et al*. 2020). Self-assembled enzymes on nanoparticles are promising and have shown great improvement in different biotechnology industries. Different enzymes have been immobilized successfully on a variety of nanoparticles. Properties of enzymes usually change when using nanobiotechnology systems (An *et al*. 2020). Enzyme stabilities are more remarkable than enzyme activities. Mohapatra (2021) immobilized β-mannase on chitosan nanoparticles while Alam *et al*. (2021) reported immobilization of L-asparaginase as a food enzyme on magnetic nanoparticles to reduce acrylamide formation in fried and baked products. However, there are few reports on the immobilization of more than one enzyme on a single nanomaterial.

Cascade reactions catalysed by more than one enzyme have been widely used in industries due to their advantages over the use of single-enzyme systems (Liao *et al*. 2020). Co-immobilization of enzymes in a single matrix can save more lag-time during the fermentation process than independently immobilized in different particles in cascade reactions (Arana-Peña *et al*. 2020). The immobilized enzyme systems display exceptional thermal stability, and reusability compared to free forms (Yao *et al*. 2020a). Recently, Qiu *et al*. (2021 co-immobilized laccase and 2,2-binamine-di-3-ethylbenzothiazolin-6-6 sulfonic acid (ABTS) on chitosan-coated magnetic nanoparticles to enhance the removal of 2,4-dichlorophenol pollutant in water at 25 ℃ with a removal efficiency of 100%. However, coating of magnetic nanoparticles with an active biodegradable, biocompatible and bioactive polysaccharide like chitosan is required to provide protection against oxidation of MNPs and provides amino functional groups for attachments of foreign antibodies (Naskar, Sharma and Kuotsu 2019). The biocompatible polymer, chitosan was previously used as a coating agent of MNPs by physical absorption by Xu *et al*. (2014). During the study by Hojnik Podrepšek, Knez and Leitgeb (2013), chitosan has shown to improve the activity of immobilized cholesterol oxidase by 74.5% on chitosan-coated magnetic nanoparticles. Additionally, immobilization on MNPs can reduce protein unfolding in addition to the stability

and performance of enzymes (Mattos and Ringe 2001) and is effective for the refolding of proteins (Ghaeidamini *et al*. 2018).

The present chapter focuses on the co-immobilization of TlxylA and Tlxyn1 on synthesized CCMNPs for saccharification of extracted xylan to yield fermentable xylose. The chemical and physical characteristics of co-immobilized enzymes were studied. The size, structure and magnetic properties of the resultant NPs were characterized by SEM, HRTEM, and Zeta potential. The binding of co-immobilized enzymes to NPs was confirmed by FTIR spectroscopy. In addition, binding efficiency, thermal properties, pH stability and shelf life of co-immobilized enzymes were also examined. Finally, response surface methodology (RSM) was used to optimize temperature, enzyme dose, and pH as the most significant factors affecting the hydrolysis of xylan. To the best of our knowledge, this is the first study involving the co–immobilization of xylanase andxylosidase on either MNPs or CCMNPs.

4.2 MATERIALS AND METHODS

4.2.1 Confirmation of co-immobilized enzyme CCMNPs activity

Xylan (1 mg/mL) was added to a freshly prepared co-immobilized enzyme CCMNPs with a preliminary 2:1 xylanase to xylosidase ratio and incubated at 50 °C, 150 rpm for 12 h. Control reactions contained substrate and CCMNPs without enzymes. Thin-layer chromatography (TLC) was used for the development and observation of produced xylose due to co-immobilized enzyme CCMNP action. TLC was developed on pre-coated silica gel plates (Merck) by using ethyl acetate/acetic acid/2-propanol/formic acid/ water (25:10:5:1:15 by volume) as eluent. Two microlitres xylose standard, test and control samples were loaded on the TLC, dried, and carefully placed on the eluent for an hour. The product was detected by spraying the plate with 1% orcinol dissolved in 10% sulfuric acid into ethanol. The plate was then dried and heated at 100 °C for 10 minutes for the detection of xylose. The method helped to detect the produced xylose (Jayapal *et al*. 2013).

4.2.2 Enzyme activity and protein binding efficiency of co-immobilized CCMNPs

4.2.2.1 Activity of co-immobilized CCMNPs and comparative xylose yield

CCMNP-xylanase activity and CCMNP-xylosidase activity were assayed according to the method as described in sections 2.2.1.1 (xylanase assay) and 2.2.1.2 (xylosidase assay). Activity recovery of enzymes was determined by calculating the ratio of total bound protein as per respective enzyme activity:

$$Activity\ recovery\ \ (\%) = \frac{a_i}{a_f} \times 100$$

Where,

a_i = activity of immobilized enzyme

a_f= activity of free enzyme added to immobilization system

Xylose yield (%) was calculated according to the following formula:

$$Xylose\ yield\ (\%) = \frac{xylose\ released\ (g)\ due\ to\ enzymatic\ hydrolysis \times 0.88}{Amount(g)\ of\ xylan\ in\ substrate} \times 100$$

4.2.2.2 Protein binding efficiency

The total amount of protein in the form of enzymes co-immobilized on CCMNPs was estimated using Bio-Rad Protein Assay Dye Reagent, which is based on the Bradford assay (Bradford 1976). However, not all the protein was bound to the CCMNPs. Therefore, loosely bound proteins were removed by deionized water and buffer (Abraham *et al*. 2014). The unbound protein in the wash solution was also estimated using the Bradford assay. The binding efficiency of the enzyme was determined by calculating the ratio of total protein bound to the total amount of protein initially used for co-immobilization:

Binding efficiency (%) = Total amount of bound protein ÷Total amount of protein added ×100

4.2.3 Characterization of co-immobilized TlxylA and Tlxyn1 on CCMNPs

4.2.3.1 Morphology, size, and charge of co-immobilized enzyme CCMNPs

Co-immobilized enzyme CCMNPs were characterized using SEM, HRTEM, FTIR and zeta potentials as described in section 3.3 of this study.

4.2.3.2 Effect of pH on the activity of free and immobilized xylanolytic enzymes

The optimum of free and immobilized xylanolytic enzymes was studied based on substrate hydrolyzed over a pH range of 4.0 – 8.0. The optimums of free and immobilized enzymes were determined by carrying out enzyme assays at these pH values. The reaction mixtures were incubated at 50 ℃ for the enzyme assay and the optimal activities for immobilized and free enzymes were taken as 100%. The pH stability of free enzyme, solely immobilized enzyme and co-immobilized CCMNPs was investigated by measuring the relative activity of enzymes after incubating in different pH values (pH 4 – 7) for 4 h for each enzyme. The pH stability was determined at 4 ℃ in all the above-mentioned buffers by incubating and calculating the residual activities after taking samples every hour. Enzyme activities were determined by the DNS method as described in sections 2.2.1.1 and 2.2.1.2 previously. Experiments were performed in triplicate and average values were reported.

4.2.3.3 Effect of temperature on the activity of free and immobilized xylanolytic enzymes

The temperature stability of free enzyme, solely immobilized enzyme and co-immobilized CCMNPs was investigated for each enzyme. Using the standard procedure, the temperature stability of xylan was studied over a temperature range of 40 – 90 °C. The temperature stability for Tlxyn1 was studied over a temperature range of 30 – 80 °C. The residual activity was measured at 50 ℃ in a 50 mm citrate buffer. Xylan without enzyme addition was assigned a relative activity of 100% for xylanase and uninoculated p-nitrophenol was assigned a relative activity of 100% for xylosidase. Experiments were done in triplicate and average values were reported. The initial activity was regarded as 100% and residual activities with respect to initial activity were measured at an interval of every 1 h for 4 h using standard xylanase and xylosidase assay. Each point represents the mean ± SD of triplicate experiments

4.2.3.4 Storage stability

To investigate the shelf-life of free and immobilized enzymes, the enzyme activities were monitored every week for 10 weeks at 4 ℃.

4.2.4 Statistical optimization for enhanced saccharification

The extracted SCB xylan was used as substrate [1% (w/v); Jayapal *et al*. (2013)] and hydrolyzed using co-immobilized CCMNP. The enzyme doses, pH and temperature were statistically optimized using the response surface methodology (RSM) to improve the enzymatic production of xylose. The design consisted of 30 experiments (Table 4.1) to be performed in triplicate. For this study, different buffers were prepared, where 30 mg/mL of CCMNPs were used to immobilize different doses of enzymes according to the RSM design and as per the immobilization method explained previously (3.2.1.2). The enzyme-bound NPs were recovered after 12 h and 48 h of saccharification using a strong magnet. Aliquots of the resulting supernatant were used for enzyme and protein assays (Jordan *et al*., 2011). Samples were quantified for xylose using Shimadzu HPLC (LCMS-2020).

4.2.5 Xylose quantification on HPLC

HPLC analysis was performed on HPLC Shimadzu with an Aminex column. All samples were filtered through a 0.22 µm syringe filter. 5 Mm H_2SO_4 was used as a mobile phase with a flow rate of 0.5 mL/min and an oven temperature maintained at 50°C. The ELSD drift tube was at 635 °C at a carrier gas pressure of 300 kPa. The concentration of xylose was determined by ELSD, and the total run time was 15 min for each sample. Xylose standard was prepared together with the samples and used to plot a standard curve to be used for xylose calculations from the samples.

4.3 RESULTS

4.3.1. Qualitative and quantitative confirmation of co-immobilized enzymes

Extracted xylan (1%) from sugarcane bagasse (refer to chapter 3) was hydrolyzed with co-immobilized CCMNPs. The hydrolysis resulted in xylose due to the combined action of immobilized β-xylanase and β-xylosidase as confirmed by a thin layer chromatography (Fig.4.1). A spot corresponding to a xylose standard in lane 1 was observed, confirming the activity of co-

immobilized enzymes. The control reaction without immobilized enzymes on CCMNPs did not show any hydrolysis spot in lane 2.

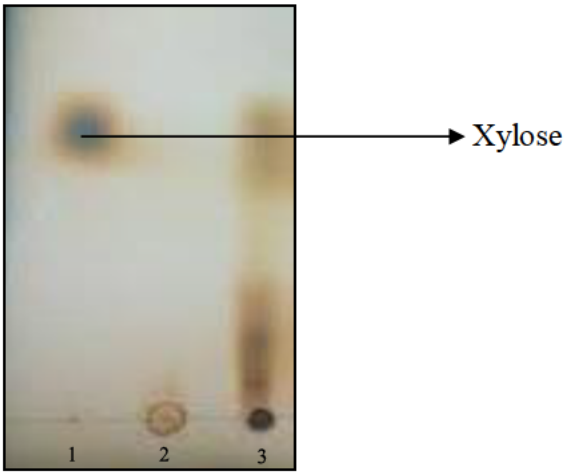

Figure 4. 1: Thin layer chromatography (TLC) of xylan hydrolyzed by co-immobilized CCMNPs with β-xylanase and β-xylosidase. Lane 1: Xylose standard (Sigma Aldrich) lane 2: Control (CCMNPs without enzymes), lane 3: Test

Three different enzyme systems were used to produce xylose from 1% of the synthesized xylan from the previous chapter. As shown in Fig.4.2, xylose yield for the co-immobilized enzyme was slightly lower than the free enzyme but greater than the yield of the solely immobilized enzyme mixture. A maximum of 28.62% xylose yield was achieved using free enzyme systems; a co-immobilized system and the mixture of solely immobilized system showed a yield of 25.91% and 18.34%, respectively, after 36 h.

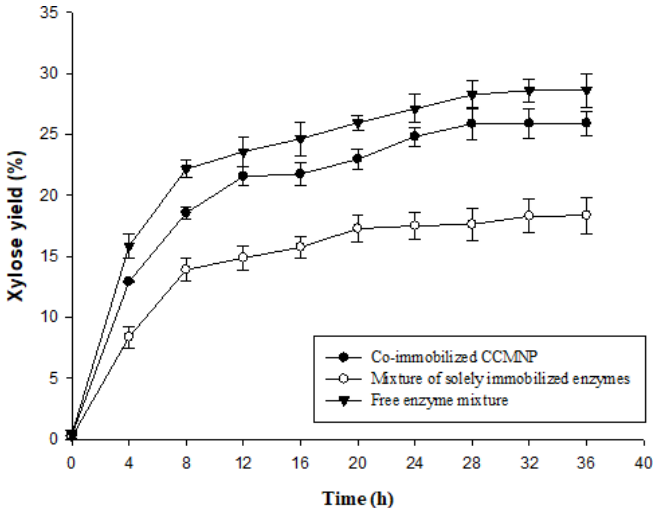

Figure 4. 2: Quantitative confirmation of enzyme activity on co-immobilized CCMNP (—●—) and comparative xylose yield using a mixture of solely immobilized enzymes (—○—) and free enzymes (—▼—)

4.3.2 Binding efficiency

Immobilized xylanase lost 18% activity while xylosidases remained more active showing 92% activity after co-immobilization. These results are in accordance with 75 – 90% protein binding efficiency determining the amount of unbound protein in the unreacted fraction considering the contribution of both purified proteins.

4.3.2 Characterization of physical co-immobilized CCMNP

4.3.2.1 SEM

Figure 4.3 shows uncoated co-immobilized MNPs (A) and co-immobilized CCMNPs (B). The illustrations below show an average of 17 nm size and morphology of crystalline phase and semi-homogenous samples. Similar observations were also reported by Mohammadi and Shaterian (2019).

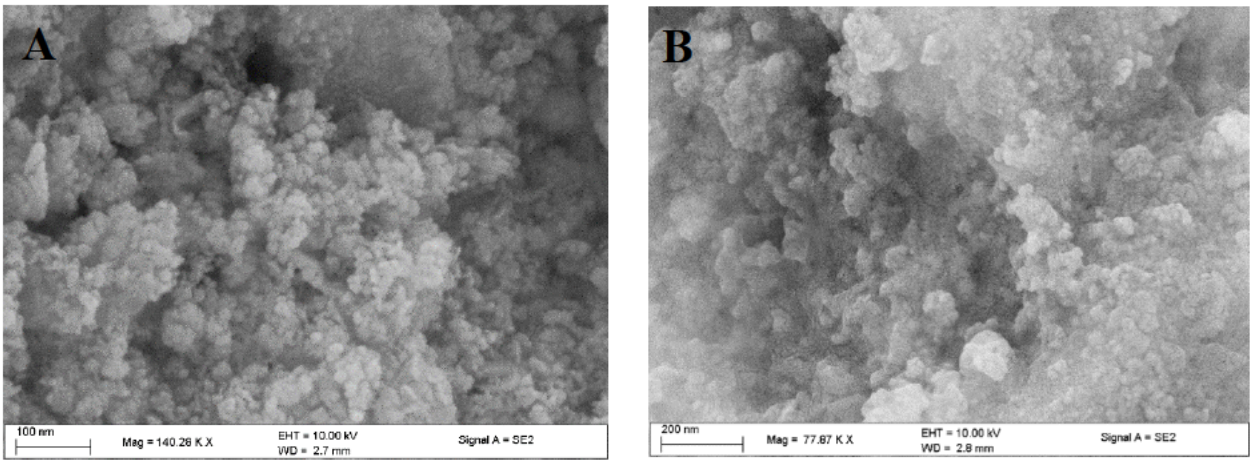

Figure 4. 3: SEM images of uncoated co-immobilized MNPs (A) and enzyme co-immobilized CCMNPs (B)

4.3.2.2 HRTEM

The diameter of co-immobilized CCMNPs ranged from 18.24 nm to 24.43 nm. These results are within the minimum range of particle size that was reported by (Hojnik Podrepšek, Knez and Leitgeb 2013). An increase in size due to chitosan-coating was noted in a study by Zhu *et al*. (2010) where the uncoated NPs ranged from 2–10 nm while coating increased the size to 20 – 30 nm.

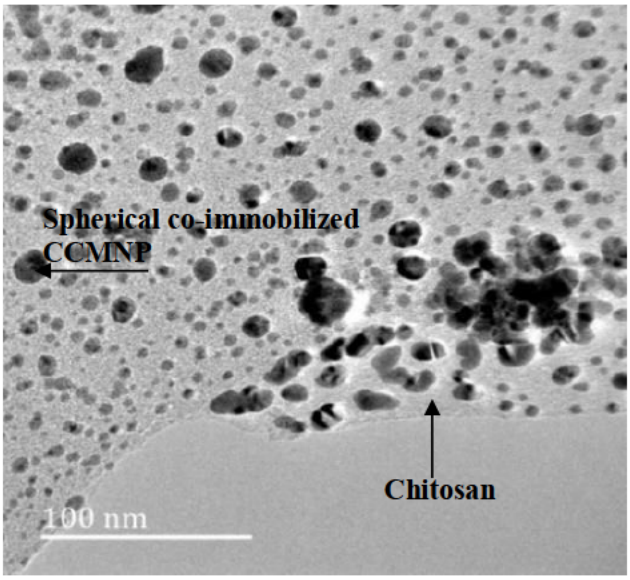

Figure 4. 4: HR-TEM image of co-immobilized CCMNPs with a slight increase in size from MNPs without enzymes

4.3.2.3 Surface electric charge and size determined by zeta potential

Table 4.1 shows duplicate values of the charge for co-immobilized CCMNPs. Produced co-immobilized CCMNPs show an average zeta potential of 28.96 mV while the pH remained constant.

Table 4. 1: Summary of produced co-immobilized CCMNPs nanoparticles with respective to their zeta potential, size and pH

Nanoparticle	**Zeta potential (mV)**	**Size (nm)**	**pH**
Co-immobilized CCMNP	29.057	24.43	5.85
	28.87	18.24	5.85

4.3.2.4 FTIR analysis of co-immobilized CCMNPs

After enzyme immobilization onto a surface cross-linked by GA (refer to Fig.3.5), a strong peak at about 1637.47cm^{-1} was observed. This confirms the successful co-immobilization of the enzymes on NPs. A peak against 1423 cm^{-1} was also observed, which indicates the formation of Schiff's base due to a reaction between the aldehyde and amine groups (Dhiraj *et al*. 2020). Schiff's base structure is a form of a bridge between reactive sites on NPs allowing them to adsorb proteins.

4.3.2.5 TGA/DSC

Initially, the TGA thermogram of CCMNPs (Fig.4.5A) indicated 85% weight retention at 70 °C which reduced to 36% at 600 °C. After co-immobilization, the stability of CCMNPs was improved as shown on the DSC-TGA thermogram Fig.4.5B. This is evidenced by over 90% weight recovery at 70 °C, retaining almost 60% weight at 600 °C. A tiny endothermic peak for CCNMPs was observed at 25 °C and similar tiny exothermic peaks were also observed at 175 °C and 300 °C, respectively. The endothermic was more intense and sharper with co-immobilized CCMNPs at 52 °C without any notable exothermic peaks.

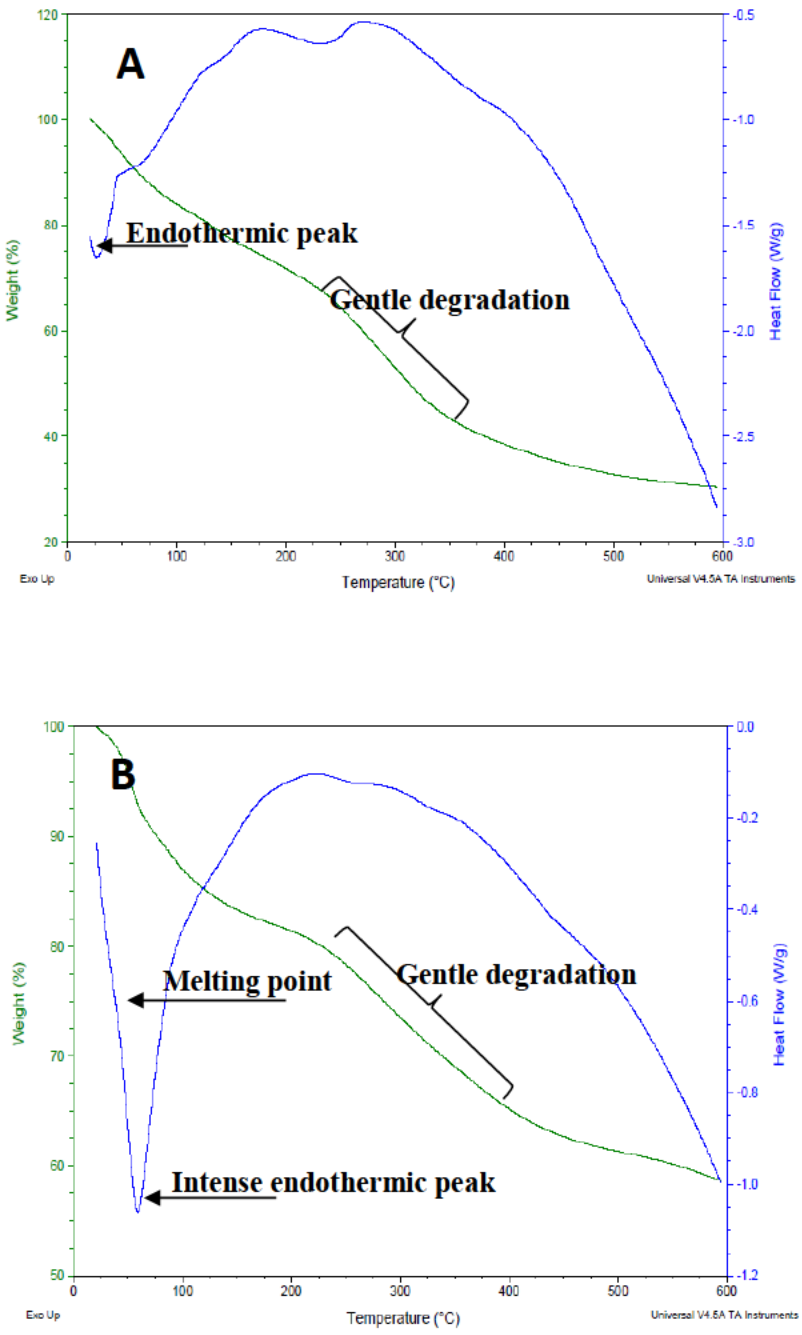

Figure 4. 5: TGA and DSC profile of CCMNPs obtained at a heating rate of 10 °C min-1 (A) and co-immobilized CCMNPs (B). Where green line represents TGA profile, and blue line represents DSC profile

4.4.3 Chemical characterisation of free, solely immobilized, and co-immobilized enzymes

After the production, purification and co-immobilization of enzymes, characterization is critical for confirming its suitability before application/s. Characterization involves the determination of different chemical and physical attributes of the co-immobilized enzyme system. It is required to ensure purity, identity, structural and conformational integrity, and enzyme activities.

4.4.3.1 pH optimum for free, solely immobilized, and co-immobilized of TlxylA and Tlxyn1

The free and co-immobilized xylanase exhibited maximum activity at pH 6.0 while solely immobilized TlxylA exhibited the highest activity at pH 5.50 (Fig.4.6). A steep increase in the relative activity of xylosidase is noted in Fig.4.7 from pH 5.5 to 6.0. All enzyme systems for Tlxyn1 retained higher than 80% activity in the steep slope. Solely immobilized Tlxyn1 and co-immobilized enzyme showed maximum activity at pH 6.00 and the and free enzyme exhibited the highest activity at pH 5.50. Both TlxylA and Tlxyn1 activities started to drop after pH 6.0. The shift in optimal activity may be due to the chosen immobilization method, support matrix or change of enzyme confirmation after binding with the support matrix.

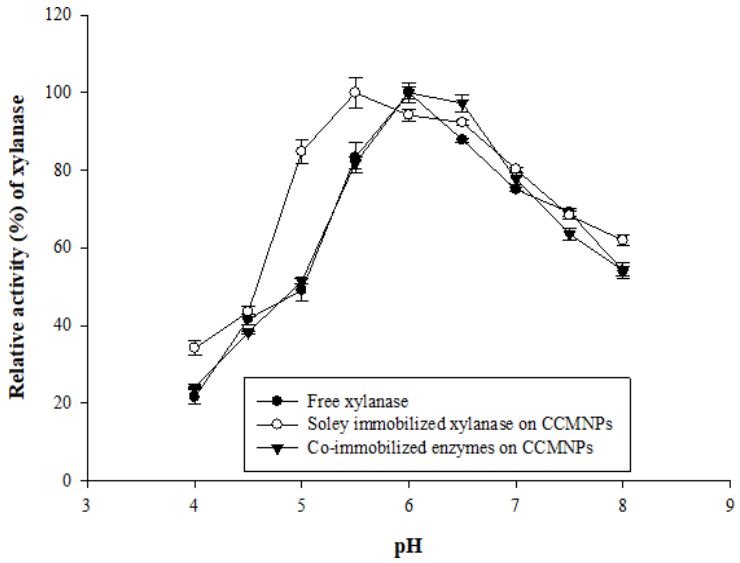

Figure 4. 6: pH optimum of TlxylA on 1% substrate hydrolyzed at 50 °C over a pH range of 4.0 – 8.0

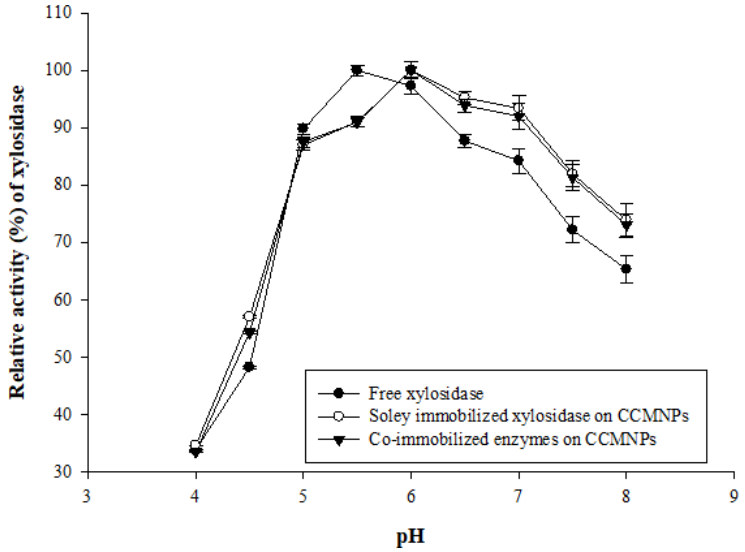

Figure 4. 7 pH optimum of Tlxyn1 on 1% substrate hydrolyzed at 50 °C over a pH range of 4.0 – 8.0

4.4.3.2 pH stability of free, solely immobilized, and co-immobilized TlxylA on CCMNPs

Free TlxylA showed the highest stability at pH 6.50 while it was least stable at pH 4.0 as evidenced by the retention of 56.21% and 23.19% activity, respectively, after 4 h incubation (Fig.4.8). Immobilization of the sole TlxylA improved the pH stability. Solely immobilized TlxylA was comparatively more stable retaining 66.28% of activity at pH 6.0 (Fig.4.9). The enzyme lost 33.1 % activity at pH 6.0 over 4 h, while a loss of 41.73% and 39.49% was observed at pH 5.0 and 5.5, respectively, over 4 h. Furthermore, the pH stability of co-immobilized TlxylA on CCMNPs was also studied (Fig.4.10). There was an even greater improvement in pH stability compared to that of free or solely immobilized enzymes. The co-immobilized TlxylA lost 47.9%, 46.66% and 39.67% of activity after 4 h at pH 4.5, 5.0 and 6.50, respectively. After 2 h, there was 72, 74.48 and 85.28% of retained activity at pH 4.50, 5.0 and 6.50, respectively. It was noted that all enzyme systems for TlxylA were less stable at lower pH. There was a slight shift in maximum pH stability from pH 6.5 to pH 6.0, when the free TlxylA was immobilized, either solely or with xylosidases.

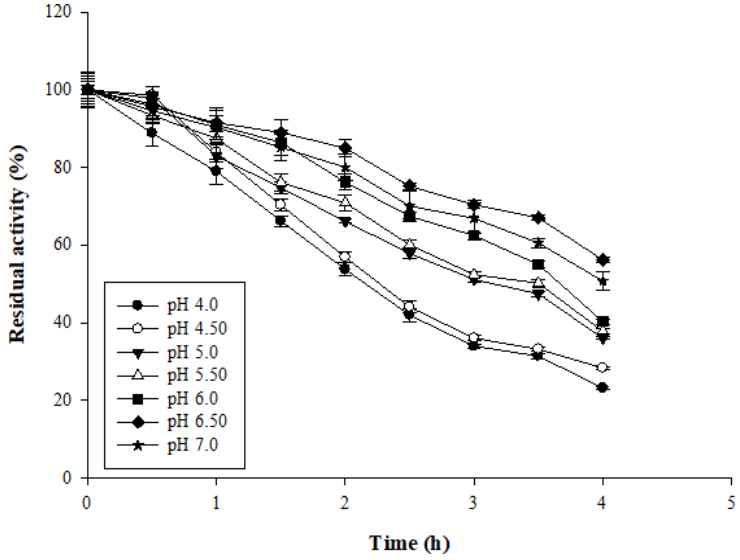

Figure 4. 8: Effect of pH on free TlxylA after incubating in different pH values (4 – 7) for 4 h

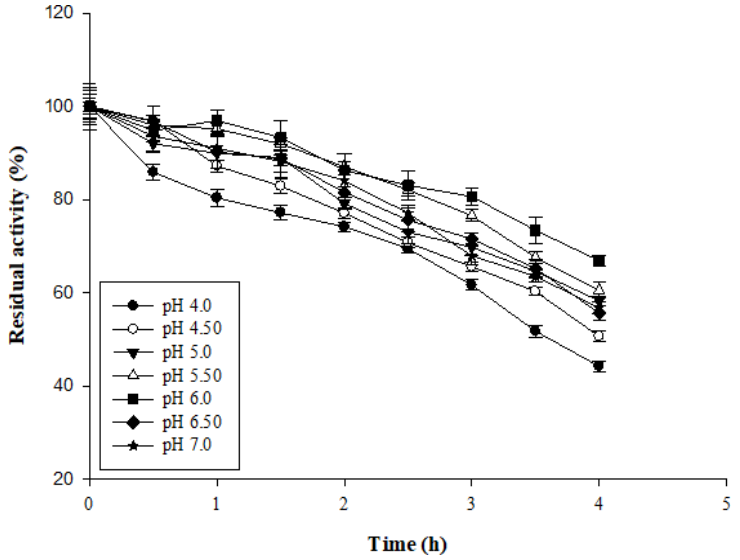

Figure 4. 9: Effect of pH on solely immobilized TlxylA after incubating in different pH values (4 – 7) for 4 h

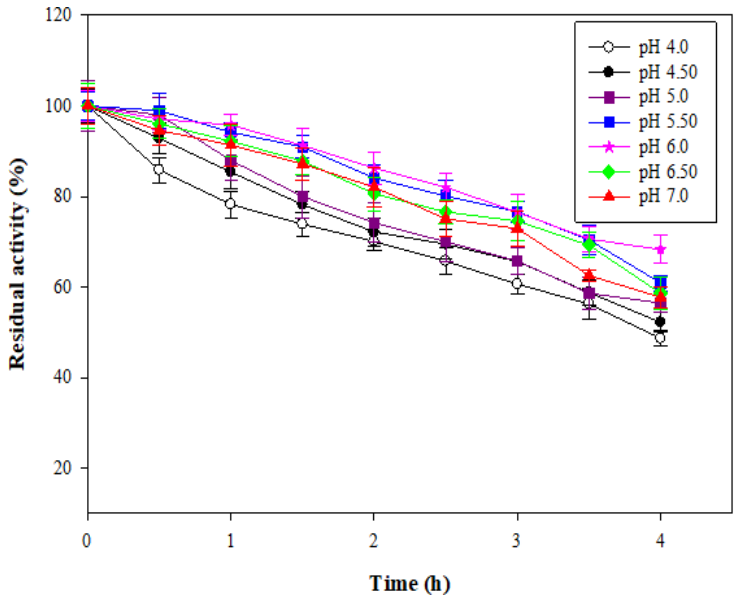

Figure 4. 10: Effect of pH on co-immobilized TlxylA on CCMNPs after incubating in different pH values (4 – 8) for 4 h

4.4.3.3 pH stability for free, solely immobilized, and co-immobilized Tlxyn1 on CCMNPs

A sharp loss of free Tlxyn1 activity was observed at pH 4.0 within the first hour of incubation retaining almost negligible activity after 4 h (Fig.4.11). The enzyme at pH 4.50 was more stable than pH 5.0 for the first 1 h. After 1 h, the activity at pH 4.50 started to decrease more than the activity at pH 5.0. Free Tlxyn1 showed maximum stability at pH 5.50 retaining 36.39% activity, while it retained 28.75% of activity at pH 6.0. There was no significant difference in free enzyme stability between pH 6.50 and pH 7.0 after 4 h. A similar trend of improved pH stability as section 4.4.3.1. was also observed with solely immobilized Tlxyn1 (Fig.4.12). Solely immobilized Tlxyn1 was fairly stable from pH 5.0 – 6.50. The solely immobilized Tlxyn1 was most stable at pH 6.0, with a loss of only 10.88% activity over 4 h while it showed the least stability at pH 4.0 with a loss of 52.81% activity. The co-immobilized Tlxyn1 retained 69.42%, 75.04% and 73.71% activity when the enzyme was incubated for 4 h at pH 5.50, 6.50 and 7.0, respectively. After 2 h, there was 84.75%, 88.12%, 88.53% activity was retained at pH 5.50, 6.50 and 7.0, respectively. Co-immobilized Tlxyn1 was most stable at pH 6.0, retaining 76.85% activity after 4 h (Fig.4.13).

Although the residual activity of co-immobilized Tlxyn1 shows similar stability patterns as the solely immobilized enzyme, a difference was noticed with respect to the rate of declining enzyme activity in the range of pH 6 – 7.0. The highest loss in activity was noted at pH 4.0 and pH 4.50 on all enzyme combination systems used in this study. Free Tlxyn1 was most stable at pH 5.50 while both solely immobilized and co-immobilized CCMNPs showed maximum stability at a slightly higher pH 6.0 for Tlxyn1.

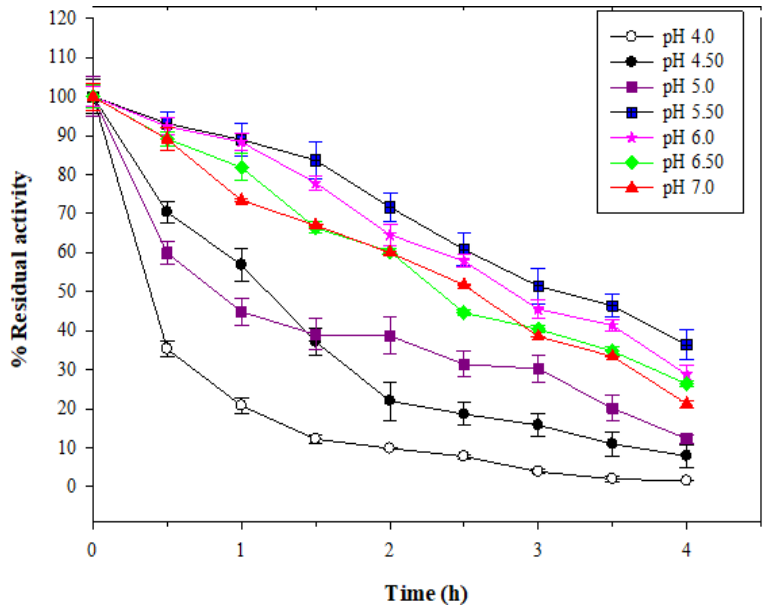

Figure 4. 11: Effect of pH on free Tlxyn1 after incubating at different pH (4 – 7) for 4 h

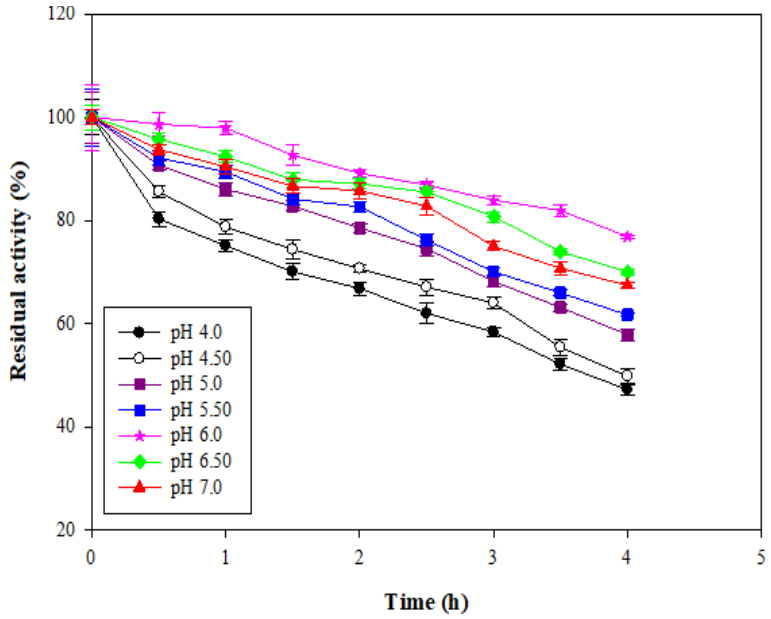

Figure 4. 12: Effect of pH on solely immobilized Tlxyn1 after incubating at different pH values (4 – 7) for 4 h

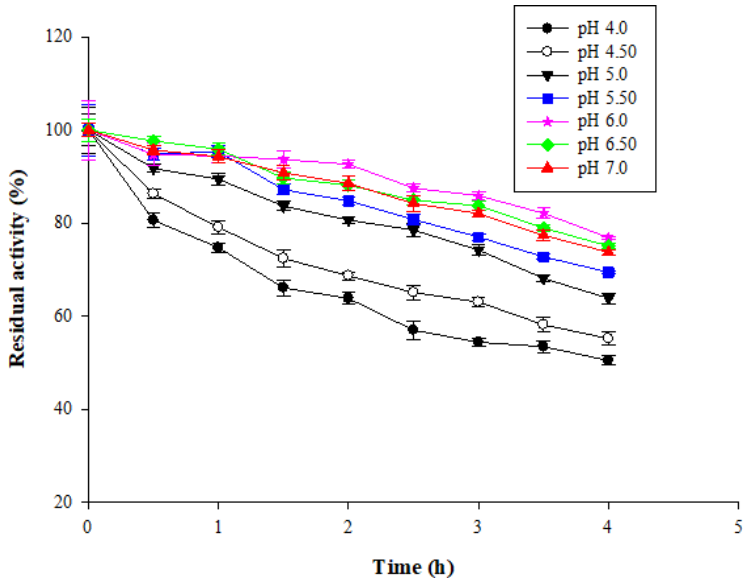

Figure 4. 13: Effect of pH on co-immobilized CCMNPs on Tlxyn1 after incubating at different pH (4 – 7) for 4 h

4.4.3.4 Temperature stability for free, solely immobilized, and co-immobilized TlxylA on CCMNPs

Xylanase from *T. lanuginosus* SSBP was stable in the temperature range of 40 – 90 °C for free, solely immobilized, and co-immobilized TlxylA on CCMNPs. The free enzyme was fairly stable between 60 and 70 °C for 4 h (Fig 4.14). The enzyme also showed appreciable stability at 50 °C retaining 67.67% activity after 4 h. However, free enzyme stability decreased when the temperature was further reduced below 50 °C. Similarly, the solely immobilized xylanase was fairly stable between 50 and 70 °C for 4 h (Fig 4.15). Solely immobilized enzymes retained 80.56%, 100% and 98.87% TlxylA activity during the first 2 h of incubation at 50 °C, 60 °C and 70 °C, respectively. Further increments to 80 °C and 90 °C resulted in 50.53% and 46.68% retention of activity, respectively after 4 h. Temperature stability profiles of co-immobilized TlxylA showed improved thermostability compared to that of free and solely immobilized enzymes. The enzyme was fairly stable in all combinations at 60 and 70 °C. The enzyme was more stable between 80 °C and 90 °C than at 40 °C. This implies the thermostable nature of the enzyme.

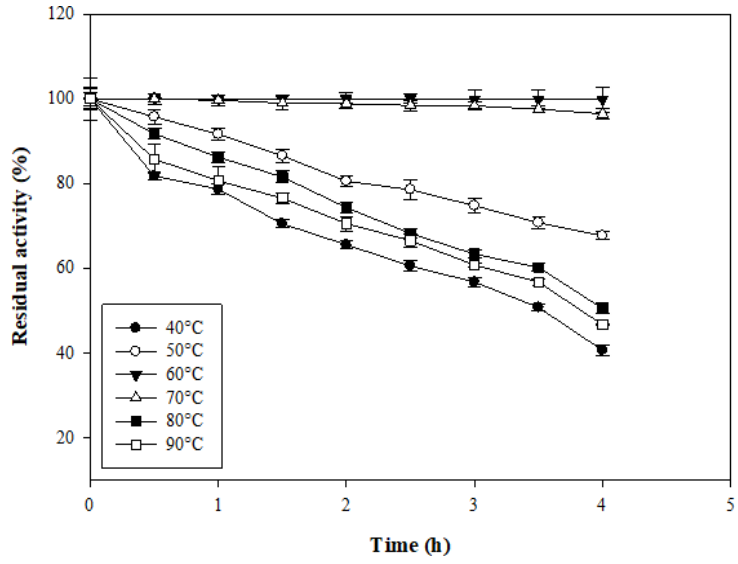

Figure 4. 14: Effect of temperature on free TlxylA after incubating in different temperature range of 40 – 90 °C for 4 h

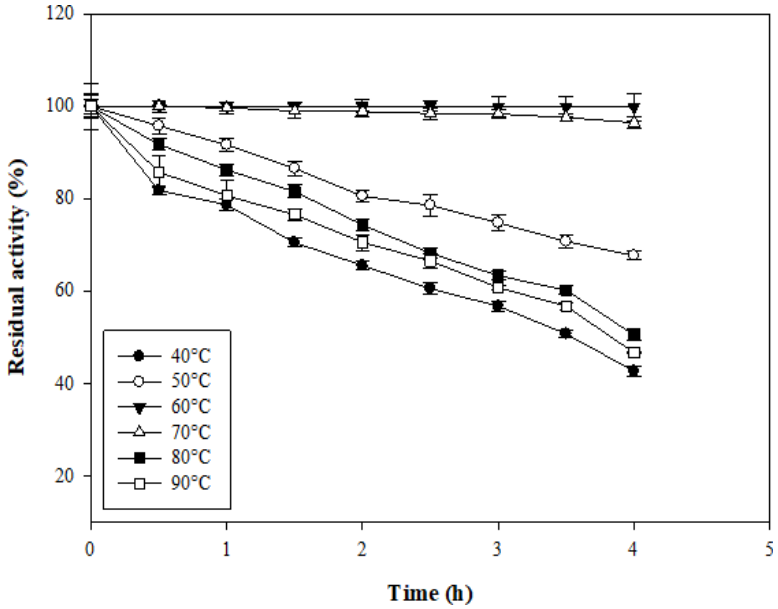

Figure 4. 15: Effect of temperature of solely immobilized TlxylA on CCMNPs after incubating at 40 – 90 °C for 4 h

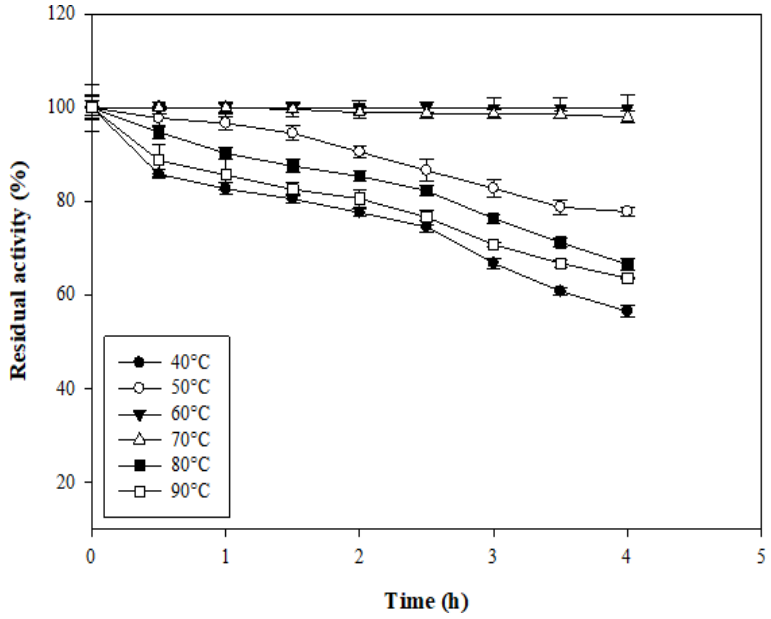

Figure 4. 16: Effect of temperature on co-immobilized TlxylA on CCMNPs after incubating at 40 – 90 °C for 4 h

4.4.3.5 Temperature stability for free, solely immobilized, and co-immobilized Tlxyn1 on CCMNPs

The stability of xylosidase as a free and immobilized enzyme was studied in the range of 30 – 80 °C. Free Tlxyn1 was fairly stable between 30 and 40 °C for 4 h (Fig 4.17). The enzyme only lost 29.47% activity at 30 °C after 4 h incubation. A gradual loss of activity was observed at 50 °C retaining 24.77% after 4 h. When the temperature was further raised from 60 – 80 °C, more than 80% of its activity was lost within 1 h. Only 11.5%, 10.45% and 6.65% activity remained at 60 °C, 70 °C and 80 °C, respectively. The activity was completely lost at 80 °C after 1 h incubation. As shown in Fig.4.18, the temperature stability for solely immobilized Tlxyn1 on CCMNPs was slightly improved. The solely immobilized Tlxyn1 was also active between 60 – 80 °C for 4 h. It was most stable at 30 °C, retaining 74.5% activity followed by retention of 66.77% activity after 4 h at 40 °C. The least stability was observed at 80 °C when only 19.76% of activity was retained. This is over 30% improvement from the free Tlxyn1 enzyme. The temperature stability profile for co-immobilized Tlxyn1 on CCMNPs (Fig.4.19) matches that of solely immobilized enzymes on CCMNPs. The enzyme was fairly stable at 30 °C and 40 °C retaining 69.51 and 60.26% residual activity, respectively, after 4 h. The enzyme stability of co-immobilized Tlxyn1 on CCMNPs was slightly lower than solely immobilized enzyme but with improved enzyme stability. From all the enzyme combination systems used in this study for Tlxyn1, it appears that the enzyme prefers lower temperatures; however, the stability was improved after immobilization.

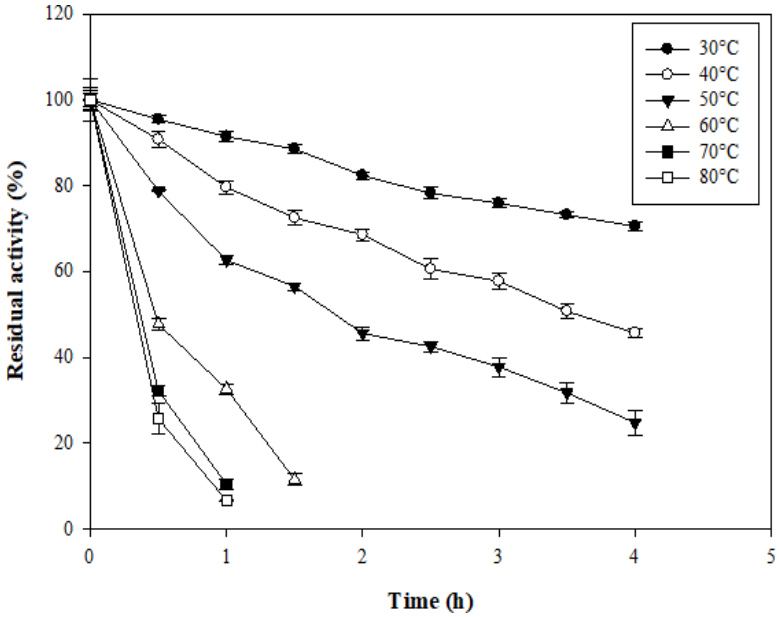

Figure 4. 17: Effect of temperature on free Tlxyn1 after incubating at 30 – 80 °C for 1 (70 and 80 °C),1.5 (60 °C), and 4 h (30 – 50 °C)

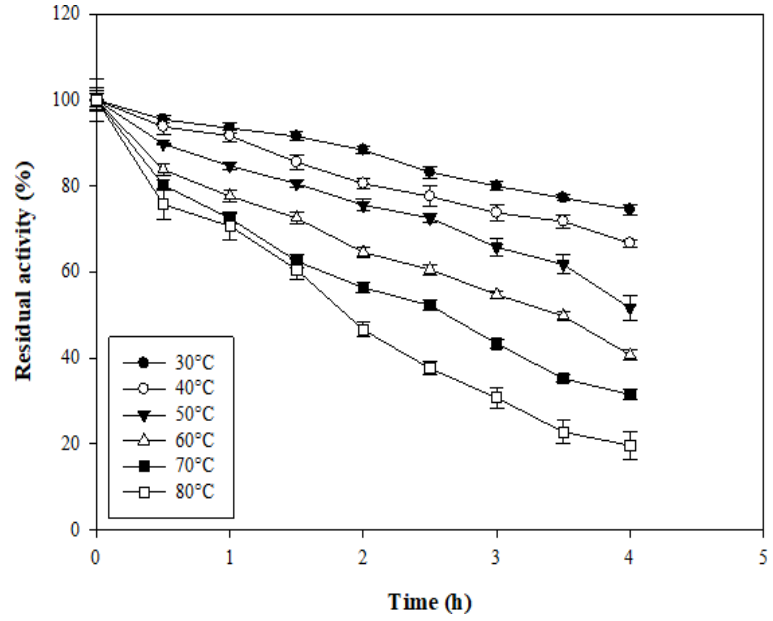

Figure 4. 18: Effect of temperature on solely immobilized Tlxyn1 on CCMNPs after incubating at 30 – 80 °C for 4 h

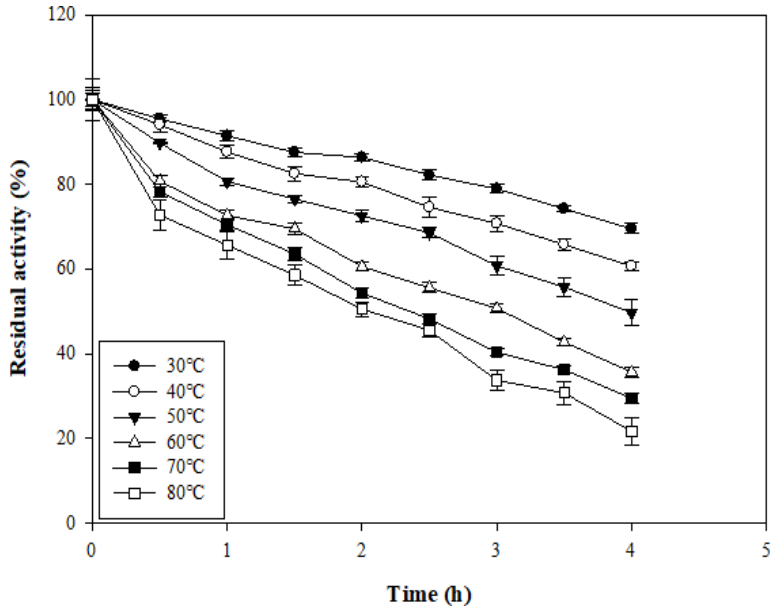

Figure 4. 19: Effect of temperature on co-immobilized Tlxyn1 on CCMNPs after incubating at 30 – 80 °C for 4 h

4.4.4 Shelf life of enzymes at 4 °C

The study included free enzymes, solely immobilized enzymes, a mixture of solely immobilized enzymes and co-immobilized enzymes on CCMNPs. Results showed that enzyme immobilization enhanced the enzymes' storage stability (Fig 4.20 and Fig 4 .21). Storage stability for TlxylA was greater than Tlxyn1 on all combinations. Solely immobilized enzymes and co-immobilized enzymes showed better stability for both enzymes studied. A maximum of 61.89% and 58.89% activity was retained for solely immobilized and co-immobilized enzymes on CCMNPs for TlxylA, respectively, after 10 weeks. Residual activity of 90.67%, 95.36%, 87.67%, and 93.36% was observed after 2 weeks on the free enzyme, solely immobilized, mixed solely enzymes and co-immobilized enzymes on CCMNPs, respectively. A maximum of 56.72 % and 51.87% activity was retained for solely immobilized and co-immobilized enzymes on CCMNPs, respectively, after 10 weeks at 4 °C. Residual activity of 82.67%, 90.67%, 82.36% and 86.41% was obtained after 2 weeks on free enzyme, solely immobilized, mixed of solely enzymes and co-immobilized enzymes on CCMNPs of Tlxyn1 respectively. Immobilization protects enzymes from deactivation and enhanced enzymes stability.

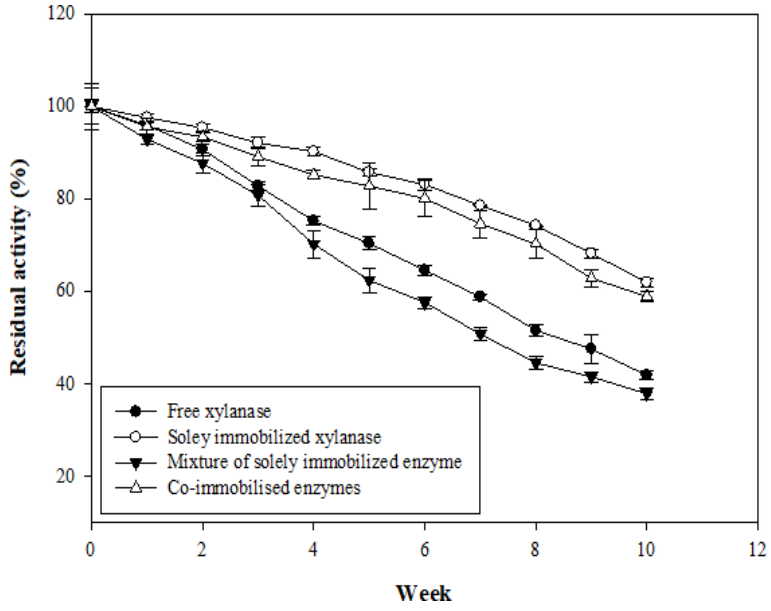

Figure 4. 20: Storage stability of TlxylA at 4 ºC for 10 weeks. Samples were taken and assayed every week at 50 ºC

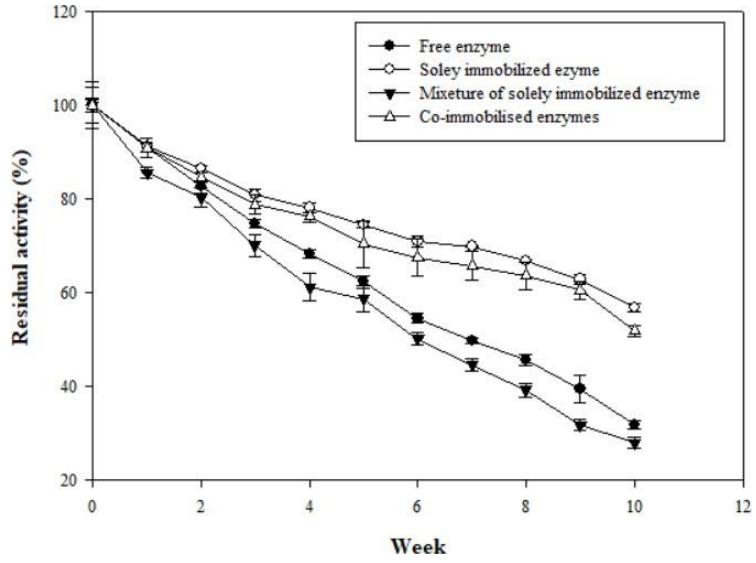

Figure 4. 21: Storage stability of Tlxyn1 at 4 ºC for 10 weeks. Samples were taken and assayed every week at 50 ºC

4.4.5 Statistical optimization for enhanced saccharification of xylan using RSM

RSM using CCD was used to optimize xylanase, xylosidase, pH and temperature variables that can influence the production of xylose. Selected variables were studied for their optimum levels and to study their interactions for improved xylose production. Table 4.2a shows the experimental range of independent variables at five different levels. Responses of experiments are shown as xylose production in Table 4.2b. The highest xylose production of 7.51 ± 0.38 g/L was observed near the centre of the model while run 23 resulted in the lowest production of 2.34 xylose. The results of the experiments were further analysed by standard ANOVA (section 4.2c). The following second-order polynomial equation was obtained that explains xylose production as a function of the four variables:

Xylose production (g/l) = 5.63+0.24A+0.31B+0.32C+0.28+D-0.63A_2-0.72B_2-0.13C_2-0.88D_2-0.36AB+0.15AC+0.48AD+0.038BC+0.17BD+0.035CD

Table 4. 2 Experimental range (a) and design (b) for optimization of xylose production by CCMNPs co-immobilized with xylanase and xylose on 1% xylan response surface methodology

(a) Experimental range and level of independent variables

Variables	**Symbol**	**Range and level**				
		-α	**-1**	**0**	**+1**	**+α**
Xylanase (U/mL)	x_1	20.00	40.00	60.00	80.00	100.00
Xylosidase (U/mL)	x_2	10.00	20.00	30.00	40.00	50.00
pH	x_3	4.00	4.75	5.50	6.25	7.00
Temperature (°C)	x_4	40.00	45.00	50.00	55.00	60.00

(b) Experimental design for R studies

Run no.	Values of variables				Xylose production (g/L)	
	x_1	x_2	x_3	x_4	after 12 h	after 48 h
1	40.00	20.00	4.75	45.00	2.45 ± 0.20	3.13 ± 0.19
2	80.00	20.00	4.75	45.00	2.53 ± 0.13	3.21 ± 0.17
3	40.00	40.00	4.75	45.00	3.43 ± 0.98	3.7 ± 0.83
4	80.00	40.00	4.75	45.00	2.02 ± 0.79	3.22 ± 0.76
5	40.00	20.00	6.25	45.00	2.45 ± 0.44	3.15 ± 0.53
6	80.00	20.00	6.25	45.00	3.01± 0.11	4.47 ± 0.19
7	40.00	40.00	6.25	45.00	3.00 ± 0.14	4.34 ± 0.20
8	80.00	40.00	6.25	45.00	2.74 ± 0.18	4.82 ± 0.18
9	40.00	20.00	4.75	55.00	2.13 ± 0.15	4.78 ± 0.21
10	80.00	20.00	4.75	55.00	4.12 ±0.19	4.66 ± 0.21
11	40.00	40.00	4.75	55.00	3.56 ± 0.19	4.8 ± 0.25
12	80.00	40.00	4.75	55.00	4.05 ± 0.22	4.32 ± 0.23
13	40.00	20.00	6.25	55.00	1.96 ± 0.08	4.34 ± 0.17
14	80.00	20.00	6.25	55.00	4.78 ± 0.17	5.7 ± 0.27
15	40.00	40.00	6.25	55.00	3.97 ± 0.15	5.45 ± 0.25
16	80.00	40.00	6.25	55.00	4.90 ± 0.21	6.12 ± 0.30
17	20.00	30.00	5.50	50.00	2.97 ± 0.16	3.89 ± 0.13
18	100.00	30.00	5.50	50.00	3.52 ± 0.10	4.23 ± 0.16
19	60.00	10.00	5.50	50.00	2.02 ± 0.05	3.34 ± 0.10
20	60.00	50.00	5.50	50.00	3.71 ± 0.13	4.05 ± 0.19
21	60.00	30.00	4.00	50.00	4.02 ± 0.18	4.88 ± 0.20
22	60.00	30.00	7.00	50.00	6.42 ± 0.23	6.9 ± 0.25
23	60.00	30.00	5.50	40.00	2.43 ± 0.16	2.34 ± 0.11
24	60.00	30.00	5.50	60.00	2.06 ± 0.15	3.89 ± 0.14
25	60.00	30.00	5.50	50.00	5.87 ± 0.26	7.62 ± 0.33

26	60.00	30.00	5.50	50.00	5.42 ± 0.30	7.41 ± 0.30
27	60.00	30.00	5.50	50.00	5.75 ± 0.27	7.5 ± 0.28
28	60.00	30.00	5.50	50.00	5.55 ± 0.23	7.62 ± 0.32
29	60.00	30.00	5.50	45.00	5.60 ± 0.19	7.41 ± 0.27
30	60.00	30.00	5.50	45.00	5.48 ± 0.24	7.5 ± 0.26

* x_1–-xylanase (U/mL), x_2–xylosidase (U/mL), x_3–pH, x_4–Temperature(°C)

(c) ANOVA values for xylose production

R-Squared	:	0.9897
Adj R-Squared	:	0.9800
Pred R-Squared	:	0.9430
Adeq Precision	:	33.596

4.4.6 Optimization of xylose production on RSM

Figures 4.2 (A) and (B) show the interaction of two variables while keeping the remaining variable fixed. Figure 4.2 (A) and (B) represent three-dimensional response surface curves for xylose production. Figure 4.2a shows an increase in xylose production with an increase in β-xylanase and β-xylosidase concentration up to 66.33 U/mL and 33.07 U/mL, respectively. Any further increase in these variables did not have a significant increase in xylose production. Furthermore, an increase in temperature to 52.31 °C and a pH of 6.18 had a favourable impact on xylose production (Fig.4.2B). Therefore, the statistically optimized parameters of 66.33 U/mL xylanase, 33.07 U/mL xylosidase, pH 6.18 and a temperature of 52.31 °C were selected for further validation experiments.

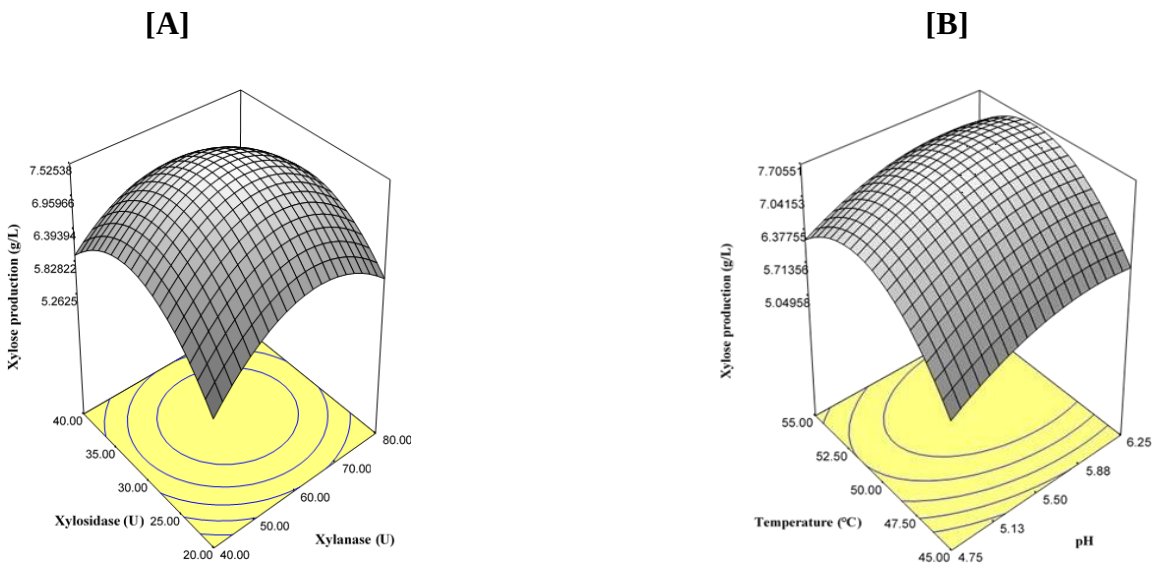

Figure 4. 22: Response surface curves to study the interaction of xylosidases and xylanase (A) and pH and temperature (B) on xylose production using 1% xylan

4.4. DISCUSSION

Successful co-immobilization of the two enzymes was confirmed qualitatively and quantitatively. The hydrolysis of xylan to xylose was confirmed as a dark spot corresponding to standard xylose (Sigma) on a developed TLC plate (Fig 4.1). There are several reports on the hydrolysis of xylan using xylanases and xylosidases (Okamoto *et al.* 2021). Liu *et al*. (2019) reported a TLC of xylose from the hydrolysis of beech wood xylan due to xylanase and xylosidase action. The qualitative and quantitative confirmation of enzyme activities of co-immobilized CCMNPs formed the basis of further optimization using a central composite design. The intermediate xylose yield of the co-immobilized system may be explained based on slightly higher activities of free enzymes.

The protein corona around nanoparticles obstructs the binding of competing proteins to the CCMNPs. Therefore, it was mandatory to estimate the protein binding efficiency. In the present study, xylanase and xylosidase from *T. lanoginosus* SSBP were immobilized on CCMNPs using a GA cross-linker. Solely immobilized enzymes had a protein binding efficiency of 82 – 90% while the co-immobilized system showed 75 – 80%. Reduced binding efficiency on the co-immobilized system was presumably due to a hindrance caused by the accommodation of two

enzymes on the same binding site on CCMNPs. Recently, Salem *et al*. (2021) showed 92% of amylase and 87% of xylanase immobilized on biomimetic MNPs. Another recent report on the use of MNPs for cellulase immobilization reported a binding efficiency of 65.55% (Kaur *et al*. (2021b).

Comparative morphological study of the uncoated and immobilized MNPs is required to observe changes before and after immobilization (Mohammadi and Shaterian 2019). Therefore, the morphology of uncoated co-immobilized MNPs and co-immobilized CCMNPs was studied using SEM micrographs (Fig.4.3). Based on HRTEM results in Fig.4.4, it was determined that immobilization did not significantly change the size of the nanoparticles after enzyme co-immobilization, indicating that agglomeration and particle compaction did not occur, primarily due to the use of APTES. Previously, Jadhav and Bongiovanni (2012) noted a very small change in particle size in the absence of APTES that was associated with agglomeration and energy associated with the high surface area to volume ratio of the nano-size particles. HRTEM confirmed the spherical shape of co-immobilized CCMNPs with an average size of 21.34 nm. The thin film layer surrounding MNP in this study indicated successful coating of the CCMNP with chitosan.

The co-immobilized CCMNPs showed an average zeta potential of 28.96 mV, which was almost doubled that of CCMNPs without enzymes (Table 3.1). This infers that enzyme immobilization resulted in increased zeta potential (Fig.4.4). Recently, Ahmadi *et al*. (2021) reported -35mV MNPs zeta potential. The structure and functional groups of CCMNPs and co-immobilized CCMNPs were further characterized by FTIR (Fig.4.5). The displayed typical peaks of amide I at 1637 cm^{-1} and amide II at 1653 cm^{-1} confirm the presence of enzymes. Thermal degradation of CCMNPs and co-immobilized CCMNPs with xylanolytic enzymes was shown in Fig.4.6A and 4.6B. TGA-DSC showed thermostable CCMNPs and co-immobilized CCMNPs. Tiny exothermic peaks obtained from CCMNPs without enzymes were eliminated on co-immobilized CCMNPs, which may be attributed the absence of crystallization (Neamţu *et al*. 2011). The intense endothermic peak from the co-immobilized CCMNPs at around 52 °C resulted from the elimination of water. The weight loss of CCMNPs and co-immobilized CCMNPs between 50 °C and 200 °C was the result of evaporation of water and unreacted APTES groups (Todan *et al*. 2013). At a range from 200 – 600 °C, CCMNPs and co-immobilized CCMNPs retained about 36%

and 60% weight, respectively, at 600 °C. Improved stability was observed on co-immobilized CCMNPs (Fig.4.5a). However, our results contradict those reported by Long *et al*. (2020) where β-fructofuranosidase and glucose oxidase were co-immobilized by sol-gel encapsulation, showing significant weight loss on TGA-DSC. After 200 °C, TlxylA and Tlxyn1 started to decompose. Characterization using SEM, TEM, FTIR, Zeta potential and DSC-TGA studies confirmed successful immobilization of TlxylA and Tlxyn1 on CCMNPs.

pH plays an important role in reaction and biological systems as it can affect enzyme stability and consequently its activity (Emamdadi, Gholizadeh and Housaindokht 2021). The optimum pH of free, solely immobilized, and co-immobilized TlxylA were 6.0, 5.50 and 6.0 respectively (Fig.4.6). Maximum activity occurred at a pH of 5.50 (Fig.4.7) indicating an increase in the net charge of the co-immobilized enzymes, which is favour of the study because the co-immobilized system of these enzymes will be used in the next chapter for saccharification. The shift of pH on other enzyme systems seems to be related to the changes in microenvironments and steric hindrance around the enzymes. A shift in optimum activity was also seen in a study by Al-Najada *et al*. (2019).

Stability of pH reflected conformation stability of enzymes under varying pH media. Improved enzyme stability was obtained from co-immobilized CCMNPs with TlxylA. Co-immobilized enzymes maintained higher residual activity due to the covalent bond between TlxylA and CCMNPs. The covalent bond may be attributed to a more stable molecular structure. Both free and immobilized xylosidase exhibited their highest elevated activities at pH 6.50. There was no significant difference in the activity of free Tlxyn1 between pH 6.50 and pH 7.0. Similarly, for Tlxyn1, solely immobilized Tlxyn1 (Fig.4.12) showed improved pH stability in comparison to free Tlxyn1. The pH stability was significantly improved when Tlxyn1 was co-immobilized on CCMNPs with. Co-immobilized Tlxyn1 was more stable at pH 6.0, retaining 76.85% of activity after 4 h. Both enzymes were most stable at pH 6.0 for solely immobilized, and co-immobilized Tlxyn1 on CCMNPs. The pH stability of xylosidase shifted from 5.5 on free xylosidase to pH 6.0 on co-immobilized xylosidase. Basaran and Ozcan (2008) reported xylosidase pH stability at range 4.8 – 5.0 from mutant *P.stipitis*. The enhanced optimum and stability towards alkaline pH might be due to the multipoint covalent achieved by immobilization and been reported as one of the most

promising possibilities in improving enzyme stability. Multipoint covalent attachment configured the xylanolytic enzymes and fixed them on the surface of the carriers so the tolerability of enzyme to pH variance in the surroundings increased (Souza *et al*. 2016). Another possibility of enhanced stability is that the covalent interaction between particles and enzymes increased the rigidity of the enzymes also inhibiting external distortion and non-specific aggregation of the enzymes, therefore allowing them for better resilience to a pH change (Sun *et al*. 2017). All patterns of xylosidase pH stability were similar but co-immobilized xylosidase showed higher activities.

Enzymes are generally susceptible to heat, therefore enhanced thermal stability is one of the required properties of enzymes for industrial applications. Enhanced thermal stability of co-immobilized TlxylA may be described on the basis of covalent cross-links between amino-functionalized MNPs, the enzyme molecules were enclosed or entrapped on the CCMNPs, which could contribute to increased rigidity of enzyme molecules, protecting them from conformational changes at high temperatures (Poorakbar *et al*. 2018).

On the other hand, free xylosidase (Fig.4.17) lost almost all its activity at 50 °C retaining only 24.77% of its activity after 4 h incubation at 50 °C. Tlxyn1 was most stable at its optimum temperature retaining 70.53% at 30 °C. This resistance at elevated thermal conditions may be due to the success of the covalently bonded systems, which played the role of inhibiting the conformational denaturation of the enzymes at higher temperatures, thus making it more heat-resistant (Sun *et al*. 2017. Jain *et al*. (2015), performed thermal stability of amylase ranging from 25 – 75 °C and the maximum activity was obtained at 35 °C for immobilized amylase and 25 °C for free amylase. There was also a noticeable rapid decrease of free enzymes at higher temperatures, the immobilized amylase retained about 70% of its activity after 1 h incubation at 65 °C. Between the range of 60 – 80 °C, free Tlxyn1 was observed to be more susceptible to heat. Therefore, immobilizing Tlxyn1 has remarkably improved thermostability at 60 °C, 70 °C and 80 °C, because almost all activity was lost within 1 h. Furthermore, covalent bonds between CCMNPs and Tlxyn1 reduce thermal vibrations and enzyme mobility while preventing aggregation and enzyme unfolding (Gashtasbi *et al*. 2014). The study indicated that the lifetime of enzymes increased drastically, resulting in CCMNP-enzyme conjugate that is more stable, efficient, and economical. From the results, it has been predicted that CCMNPs provided a shield to the enzymes

preventing them from getting oxidized. McGrath (1977) indicated that enzyme stability increases in the presence of its substrate. Much attention was also paid to the stability of stored TlxylA and Tlxyn1.

The preservation of the enzyme activity and promoting synergistic activity by co-immobilization of multiple enzymes on nanoparticles have become routine practices in bio-nanotechnology (Liang *et al*. 2016). Long-term storage stability and NP reusability are the most significant characteristics in determining an enzyme's industrial application. Solely immobilized enzymes on CCMNPs showed the best enzyme stability followed by co-immobilized enzyme system with a difference of less than 10%. Even though solely immobilized enzymes showed better storage stability, the present study focused more on the co-immobilized enzyme system. Co-immobilized enzyme system retained 93.36% and 86.41% of TlxylA and Tlxyn1, respectively, after 14 days. A similar study was performed by Liang *et al*. (2016), where co-immobilized enzymes on metal coordinated hydrogel nanofibers retained 70% activity after 15 days of storage at 4 °C while free enzymes nearly lost all of their activity. Ranjbakhsh *et al*. (2012) immobilized lipase alone on the matrix and retained an average of 64% of its activity after 21 days whereas free lipase only retained 47% of activity.

It was important to monitor and optimize the amount of TlxylA and Tlxyn1 to immobilize maximum xylose liberation from 1% produced xylan. Xylose maximal liberation greatly depends on the hemicellulose oligomer that is present in the biological liquid and the choice of enzymes with their loading concentration and also with substrate composition (Qing, Yang and Wyman 2010). Chapla, Pandit and Shah (2012), pointed out that substrate concentration plays a huge role during enzymatic hydrolysis. During their study, he found that increasing the concentration from 1 to 3% did not have a significant increase in the production of end-products. While on the other hand decreasing the substrate from 1– 0.1% drastically reduced the production.

The optimum conditions for xylose production predicted by RSM were validated by carrying out experiments in triplicates. At optimized conditions, the maximum cumulative xylose production was 7.51 g/L using HPLC for quantification. This can be seen on the correlation chart in Fig.4.22 that predicted cumulative xylose. Thakur *et al*. (2021b) reported a xylan to xylose of 69.6%

conversion using HPLC. When referring to the statistical quality (R^2=0.9897), it was predicted that the results are in good agreement with the experimental data. While Liu *et al*. (2021) obtained an R^2 value of 0.9737 from wheat straw using maleic acid as a catalyst between experimental data and RSM for xylose optimization. The results of the validation model showed great agreement with experimental parameters, as they show close parameters to that of RSM. The validation model revealed 66.33 U xylanase, 33.07 U xylosidase, a temperature of 52.3 °C and a pH of 6.18 These results provide optimization parameters to successfully achieve enhanced levels of xylose using xylan extracted from sugarcane bagasse for this study. Improved production of xylose has a direct effect on bioethanol and xylitol production as discussed in the next chapter.

4.5 Conclusions

Biological catalysts are now key players in various industrial processes and are increasingly replacing conventional chemical methods. This study has the potential to minimize the costs involved in the commercialization of enzymes and their processes. In this study, the technique for co-immobilizing xylanase and xylosidase on chitosan-coated magnetic nanoparticles was demonstrated and confirmed by HRTEM and FTIR. The co-immobilized enzyme system was effective in enhancing the pH, temperature, and long-term storage stability of xylanolytic enzymes. These results indicate that the synthesized CCMNPs have the potential to be excellent support matrices for enzymes. This study described the co-immobilization of xylanase and xylosidase enzymes on CCMNPs for saccharification of xylan. Immobilized enzymes can be separated with great ease from the reaction medium allowing reusability on a fresh medium. Additionally, conditions for maximum xylose production were optimized by RSM. Conclusively, produced CCMNPs are potentially useful for multiple industrial applications.

CHAPTER 5: BATCH, FED-BATCH AND REPEATED BATCH PRODUCTION OF XYLOSE FOR BIOETHANOL PRODUCTION USING CCMNP CO-IMMOBILIZED ENZYME SYSTEM

5.1 INTRODUCTION

There are different processes for the industrial production of commercially important secondary metabolites. Different approaches for saccharification of lignocellulosic biomass using immobilized enzyme systems have been reported (Sharma and Aggarwal 2020). Broadly, these approaches can be categorized into batch, repeated-batch, and fed-batch processes. Enhanced saccharification of xylan-containing C5 sugars is critical for improvement in bioethanol production (Saleem *et al*. 2021). While batch production is routinely used for several studies, the process becomes limited due to an insufficient amount of substrate and/or other limiting factors. Batch productions have a low risk of contamination, are easy to operate but have low productivity due to the presence of inhibitors resulting from substrate and products (Rawoof *et al*. 2021).

Repeated batch strategy involves inoculation with free or immobilized enzymes into a batch of fresh medium (Lapeña *et al*. 2020). Immobilized enzymes are separated from the fermentation medium at regular time (batch) intervals and a new medium is added for further substrate utilization/conversion to products. Repeated batch fermentations allow the reusability of immobilized enzymes on matrices for multiple cycles. Fed-batch fermentation involves a time-dependent addition of a substrate to the fermentation medium throughout the cultivation process to improve production (Abdel-Rahman, Tashiro and Sonomoto (2011). This also minimizes the production of inhibitors (Ramírez *et al*. 2021). Changes in feed composition and feed rate are the most significant factors contributing to increased yields of the products. Sharma, Bhardwaj and Pathak (2021 reported a more than two-fold increase in production by adopting fed-batch production as compared to batch production using the same medium. Using this methodology, xylose can be produced by gradually feeding xylan into the laboratory bioreactor to favour and increase xylose production.

The present study used *Scheffersomyces stipitis* for fermentation. Engineered xylose-fermenting yeasts are mostly preferred to produce second-generation ethanol from lignocellulosic material. *S. stipitis* can ferment xylose and have been extensively exploited for bioethanol production using a medium containing fermentable sugars in shake flasks or laboratory bioreactors (Germec *et al*. 2020). This xylose-fermenting yeast promise industrial-scale production of ethanol with a high yield (35 – 44%) due to its thick cell wall and resistance to contamination from bacteria and viruses (Kurian *et al*. 2010). Bioethanol is primarily produced by biological saccharification and fermentation of biomass to yield monosaccharides (Kootstra *et al*. 2009) such as xylose, which is then fermented to ethanol using yeast. Immobilization of enzymes for bioethanol production can eliminate most industrial problems associated with cost. Co-immobilization on a single matrix has a huge economic impact as it can reduce enzyme and matrix costs during fermentation.

This chapter focuses on comparing industrially important approaches for xylose production by co-immobilized CCMNPs using batch, repeated-batch, and fed-batch processes from 1% of xylan under conditions statistically optimized by RSM. This study aimed to ferment the resulting xylose from xylan by 1% *S.stipitis* for bioethanol production. Variables such as feeding time, pH, agitation, substrate concentration and aeration were carefully monitored during ethanol production in a laboratory bioreactor. This is the first report on biomass hydrolysis from co-immobilized TlxylA and Tlxyn1 on CCMNPs for bioethanol production.

5.2 MATERIALS AND METHODS

5.2.1 Validation of the experimental model

Predicted statistical parameters were validated for xylose production in 250, 500, 1000 and 2000 mL shake flasks and in a 5 L laboratory bioreactor (Minifors, Infors HT, Switzerland). The pH of the medium was adjusted to 6.20 before autoclaving and the fermenter was operated at 52.3 °C, 150 - 200 rpm and 1 vvm of aeration rate. Samples were collected as per experimental design intervals, and harvested samples were used for xylose analysis. All experiments were conducted in triplicate.

5.2.2 Batch production of xylose in a 5 L laboratory bioreactor

Xylose was produced using co-immobilized CCMNPs with statistically optimized units of TlxylA and Tlxyn1. Batch production was conducted in 500 mL shake flasks containing 100 mL of 1% xylan. Batch fermentation was performed at 52.3 °C and 200 rpm for 48 h. Samples were withdrawn (2 mL) every 12 h and the batch was terminated after 48 h. All experiments were performed in triplicate and the data was represented as the average of the triplicate values.

5.2.3 Preliminary optimization for fed-batch fermentation

5.2.3.1 Selection of time of feed

Fermentation was conducted in 500 mL shake flasks containing 100 mL of 10 g/L initial xylan for 72 h. Different fed-batch points in the exponential phase (12, 24, 36, 48 and 60 h) were fed with 2.5 mL of xylan (4 g/L) and were evaluated in separate experiments to find the best time of feed. Samples were withdrawn every 6 h, and harvested samples were used for xylose analysis.

5.2.3.2 Selection of xylan concentration

To select the appropriate concentration of xylan to be fed into the bioreactor, a range of concentrations (2, 4, 6, 8, 10, 15 g/L) was investigated. These concentrations were fed in separate experiments in the production medium after 36 h xylose production profile was studied. All other variables were kept constant.

5.2.4 Fed-batch and repeated batch production of xylose

5.2.4.1 Fed-batch production of xylose

Fed-batch cultivations were performed in a 5 L laboratory bioreactor (Minifors, Infors HT, Switzerland) containing 2700 mL of statistically optimized medium to which was added a 1% (v/v) co-immobilized CCMNPs. The fermenter was maintained at 50 °C and 200 rpm with 1 vvm aeration for 192 h. The medium was fed aseptically with 10 g/L of filter-sterilized xylan. Samples were collected every 24 h and analysed for xylose estimation on Shimadzu HPLC.

5.2.4.2 Repeated batch production of xylose

The repeated-batch fermentation was carried out in 250 mL Erlenmeyer flasks containing 50 mL sterile medium at 52.31°C and 200 rpm. After every 48 h (based on RSM), the fermentation broth was drained aseptically, harvested CCMNP, with citrate buffer and the new run was started in the same buffer solution. Samples were taken every 48 h for determination of xylose in HPLC. The co-immobilized enzymes before the first cycle were assigned the relative activity of 100%.

5.2.5. Total xylan in sugarcane bagasse

Total xylan content was estimated using a modified method as per NREL (Sluiter *et al*., 2008; Gao *et al*., 2014). Briefly, samples were regularly withdrawn after every 1 h and 13 ml of sample was reacted with 87 mL of 4% H_2SO_4 at 121 °C, 10 atm. for an hour. Thereafter the solutions were neutralised with 6 M NaOH and the final volume was noted. The hydrolysates were then analysed on the HPLC Aminex-87H column using a refractive index detector. The column oven was set at 80 °C while the detector was at 60 °C. The xylose peak was compared to a xylose standard solution peak of 0.5mg/ml to quantify the xylose content in the hydrolysate. The amount of xylose released was calculated based on each gram of xylan can produce a maximum of 0.88g on complete hydrolysis as stated in sec (Temelli 2020) The tests were done in triplicates. The 0.88 factor describes the possible maximum xylan to xylose used during the hydrolysis used.

5.2.6. Fermentation of xylose to bioethanol and xylitol by *S. stipites*

5.2.6.1. Preparation of yeast inoculum

The yeast seed culture of *S. stipitis* was prepared by inoculating two loops full of overnight grown organisms in a 50 mL YPDX medium containing 10 g/L yeast extract, 20 g/L peptone, 10 g/L glucose and 10 g/L xylose in 250 mL shake flasks. Inoculated flasks were incubated at 30 °C and 200 rpm for 16 h. For future usage, the microorganism was preserved on glycerol stocks at -80 °C. Produced xylose from a batch of co-immobilized CCMNPs was supplemented with 5 g/L KH_2PO_4, 2 g/L $(NH_4)_2SO_4$, 0.2 g /L $MgSO_4 \cdot 7H_2O$, 1 g/L peptone, 5 g/L yeast extract, was used as the fermentation medium. This was followed by subsequently inoculating 5% (v/v) yeast seed culture into the fermentation medium in a 5 L laboratory bioreactor (Minifors) at 30 °C, 200 rpm for 50 h and 1 vvm aeration.

5.2.7. Ethanol estimation using Gas Chromatography (GC)

GC analyses were performed to estimate ethanol using a Varian 3800 chromatograph using a flame ionisation detector (FID) and CP-wax column (30 m × 0.15 mm, Varian). The working parameters were as follows: injector temperature 200 °C; detector temperature 250 °C; carrier gas H, 300 KPa, N 400 KPa and O_2; FID oven temperature 300 °C and 1µl injection volume.

5.2.8. Estimation of xylitol and xylose using liquid chromatography

LCMS-2020 liquid chromatography system (Shimadzu) was used to estimate xylose and xylitol concentrations using Aminex HPX 87-H column (Bio-Rad) and an ELSD-LT II detector (Shimadzu). Water was used as at a flow rate of 0.5 ml/min as a mobile phase and samples on the column were eluted at 50 °C (Zhang *et al*. 2019).

5.3 RESULTS

5.3.1 Xylose production in shake flasks of varied volumes and 5 L bioreactor

Table 5.1 shows xylose production in varying volumes of shake flasks and a 5 L laboratory bioreactor under previously optimized conditions. No significant increase in xylose production was observed during the enzymatic saccharification on shake flasks and a 5 L laboratory bioreactor.

Table 5 1 Xylose production after 48 h in varied volumes of shake flasks and laboratory fermenter at 52.31 °C at a pH of 6.18

Volume (mL)	Volume of medium (mL)	Xylose production (g/L)
Shake flasks		
250	50	7.62 ± 0.19
500	100	7.83 ± 0.20
1000	200	8.02 ± 0.20
2000	400	7.80 ± 0.17
Fermenters		
5000	3000	8.21 ± 0.23

5.3.2 Batch production of xylose: validation of RSM

Following co-immobilization of TlxylA and Tlxyn1 on CCMNPs, their effectiveness on xylan hydrolysis to xylose was compared to that of free enzymes. As shown in Fig.5.1, xylose yield for co-immobilized enzymes was 4-times higher than free enzymes during the first 6 h. At 48 h, there was 32% conversion on free enzymes and there was 76.3% conversion on co-immobilized enzymes

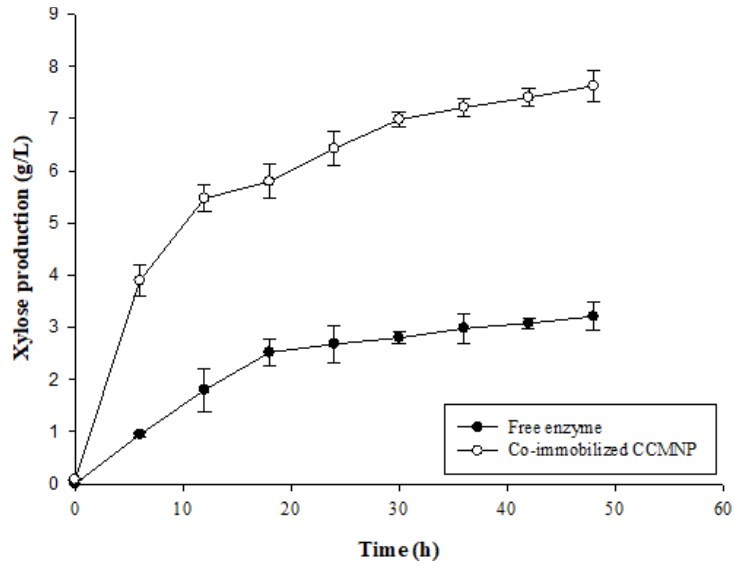

Figure 5. 1 Xylose batch production profile using 1% xylan extracted from SCB and RSM optimized enzyme doses (60 U/ml TlxylA,30 U/ml Tlxyn1) as by on free and co-immobilized CCMNPs at 50 °C for 48 h. Each point represents the mean of triplicate experiments ± SD

5.3.3 Preliminary optimization for fed-batch fermentation

5.3.3.1 Selection of time of feed

Maximum xylose production (g/L) was observed at 48 h. While xylose production also reached 8.87 g/L when feeded at 36 h (Fig.5.2), the production did not improve any further. However, as shown in Fig 5.2. Continuous increase in xylose procution was observed after 48 h feeding and the production continued to increase even after 78 h.

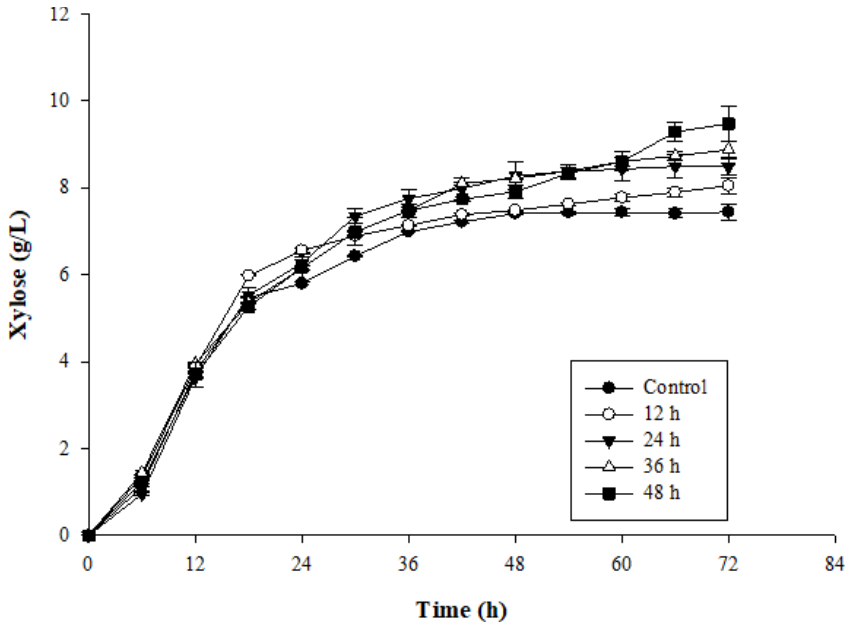

Figure 5. 2: Effect of time of feed on xylose production using 10 mL of 100 g/L xylan in a 5 L fermenter after different intervals of time in separate experiments at 50 °C for 48 h. Each point represents the mean triplicate of experiments ± SD

5.3.3.2 Optimization of xylan concentration

While investigating the effect of different concentrations of xylan on xylose production, 2 g/L xylan feed at 48 h produced 8.49 g/L xylose after 72 h. However, 9.46 g/L xylose was produced when supplemented with 15 g/L xylan (Fig.5.4). Maximum xylose was produced using 10 g/L xylan.

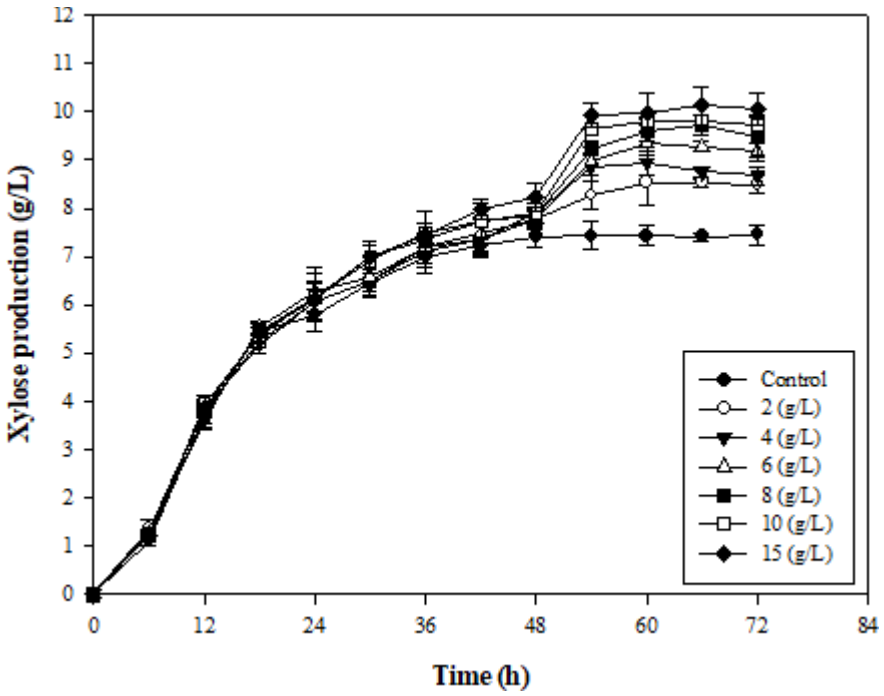

Figure 5. 3: Effect of feeding different concentrations of xylan at 50 °C after 72 h on xylose production by co-immobilized CCMNPs in a 5 L fermenter in separate experiments. Each point represents the mean triplicate of experiments ± SD

5.3.4 Repeated batch production of xylose from 1% xylan

Six cycles of xylose production using co-immobilized CCMNPs was examined to determine the reusability of CCMNPs (Fig.5.4). After the 6th cycle, CCMNPs produced 39.68% of initial production at 48 h while only 19.30% of the initial production could be achieved after the 6th cycle at 24 h. These results suggest that co-immobilized CCMNPs are stable and can be used over repeated cycles.

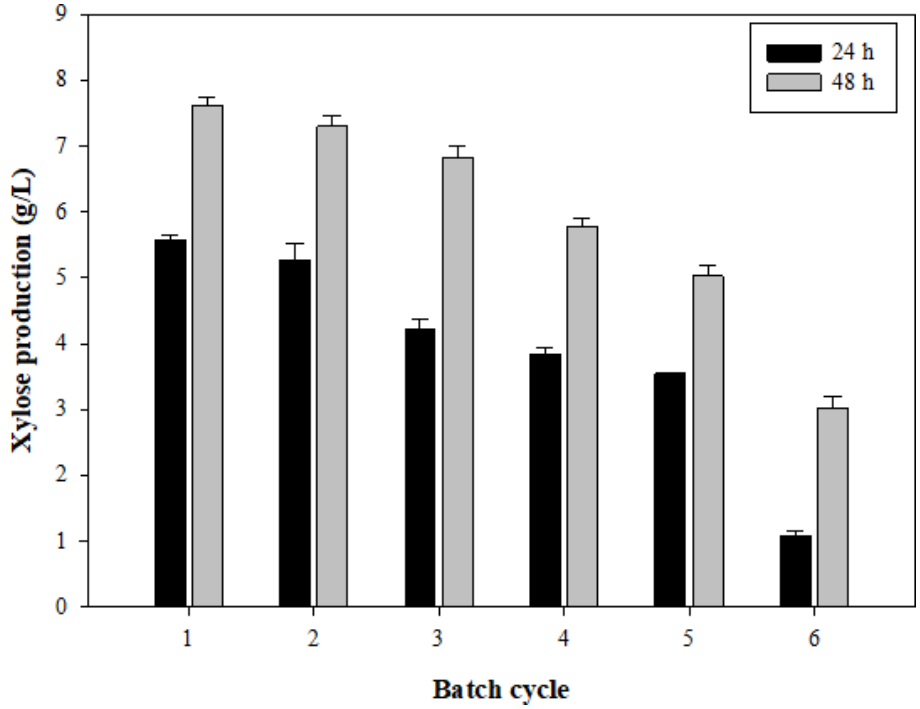

Figure 5. 4: Repeated batch profile of xylose from co-immobilized TlxylA and Tlxyn1 on CCMNPs at for 6 cycles. Each point represents the mean triplicate of experiments ± SD

5.3.5 Fed-batch production of xylose

The time course profile of xylose production during fed-batch is shown in Fig.5.5. Based on optimized time and xylan concentration, 10 g/L xylan was fed every 48 h until 192 h. Xylan was hydrolyzed fast during the first 12 h. After 196 h, xylose reached 16.48 g/L. There was an average of 69% convension efficiency of xylan to xylose.

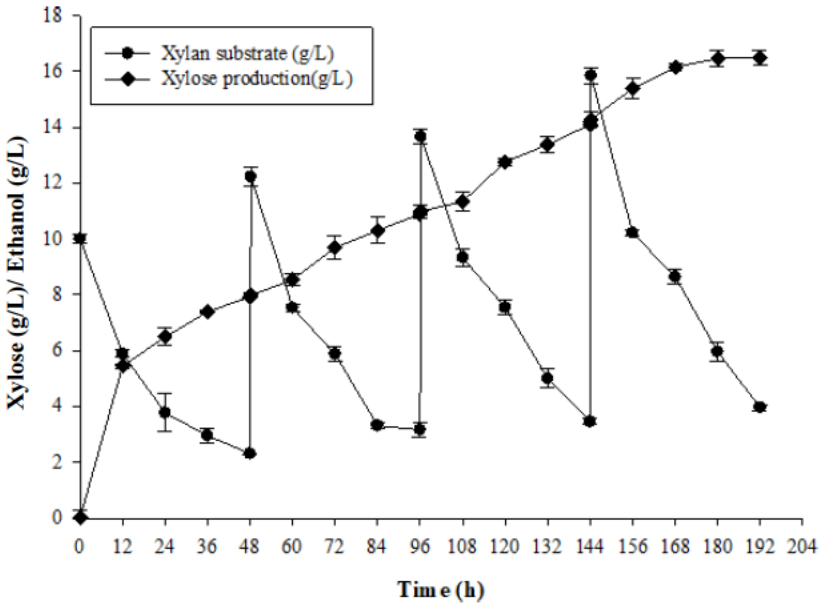

Figure 5. 5 Fedbatch production of xylose in a 5 L fermenter with an optimized xylan feed of 10 g/L every 48 h. Each point represents the mean triplicate of experiments ± SD

5.3.6 Ethanol and xylitol production from fermentation by *S. stipitis*

Bioethanol and xylitol were by-products of xylose fermentation by *S. stipitis*. The fermentation process took 50 h. As seen in Fig.5.6, xylose was reduced from 8.10 g/L to 0.14 g/L after 50 h. Results yielded 3.96 g/L bioethanol and 0.52 mg/mL xylitol. Based on the ethanol stoichiometry in section 5.4.2 above, there was 71.87% conversion.

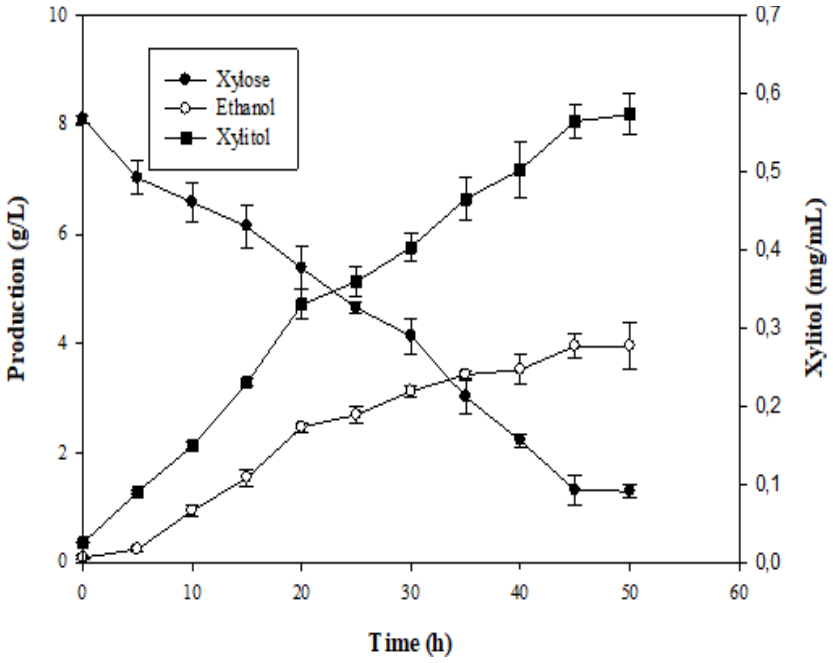

Figure 5. 6 Simultaneous hydrolysis and fermentation of CCMNP-produced xylose using S. stipitis (5% (v/v)) for the production of ethanol and xylitol in a 5 L laboratory bioreactor (Minifors) at 30 °C, 200 rpm for 50 h and 1 vvm aeration. Each point represents the mean triplicate of experiments ± SD

5.4 DISCUSSION

D-xylose accounts for about ⅓ of the total carbohydrates from lignocellulosic biomass. This paves the path for large-scale ethanol production from lignocellulose biomass, requiring efficient xylose fermentation. Achieving effective high xylose yield and its fermentation to bioethanol requires pentose utilizing yeast strains. Over the past years, there has been increased interest in *S.stipitis* as a pentose fermenting yeast. This chapter focuses on different fermentation strategies for improved xylose yield using co-immobilized CCMNPs with TlxylA and Tlxyn1 on 1% xylan.

In the present chapter, statistically optimized parameters of xylose production were validated on varying volumes of shake flasks and 5 L laboratory reactors. Maximum xylose production was observed on a 5 L bioreactor (Table 5.1). Slightly reduced production in shake flasks could be attributed to uncontrolled parameters (Barbuto Ferraiuolo *et al*. 2021). Upscaling xylose

production in a 5 L bioreactor eliminated/reduced possible inhibitors such as dissolved oxygen for maximum production. Maximum production of xylose was 8.21 g/L. Similar reports on xylose production from SCB xylan of 74% were obtained by Khaire *et al*. (2021). It is presumed that co-immobilized enzyme systems improve product yield due to improved stability on support matrices and minimized distance between the enzymes. This closeness may contribute to the fast utilization of substrate during early periods of fermentation (You *et al*. 2012). Batch, fed-batch and repeated batch fermentations were performed to study the release of xylose from 1% xylan. During batch fermentation (Fig 5.1), maximum xylose production for both free and co-immobilized CCMNPs was obtained at 48 h and the fermentation was terminated because there was no significant growth in production. Co-immobilized system had higher xylose production compared to the free enzyme system due to better stability during fermentation. A decrease in xylose production was noticed due to depletion of xylan in the medium over time.

Therefore, further attempts were made to improve xylose production using fed-batch fermentations. Preliminary studies were conducted to optimize the time of feed and the concentration of xylan. However, as shown in Fig 5.2, continuous increase in xylose procution was observed after 48 h. The substrate was kept at 10 g/L throughout feeding times producing 9.27 g/L after 72 h. Another feeding strategy after 48 h was not attempted due to high cost associated with prolonged running of bioreactor. Therefore, 48 h was selected for fed-batch production of xylose using 10 g/L xylan.

In this study, the reusability of co-immobilized enzymes was evaluated over six cycles for xylose production. Although continued production of xylose was noticed, the production decreased as the number of cycles increased (Fig.5.3). This was due to the decrease of enzyme activity over cycles when decanting old media with the fresh media. During the study, investigations were done at two different cycle time intervals (24 and 48 h) and each interval with six repeated batch cycles. As shown in Fig.5.4, 68.57% of initial xylose was produced in the 4^{th} cycle of 24 h, while the 48 h batch retained 75.85% of initial production in the 4^{th} cycle. After 6 cycles of 48 h, 39.69% of initial xylose production was retained. These results indicate that immobilized enzymes showed efficient stability and reusability. Reduced xylose production upon repeated use could be attributed to a change in the stereochemical structure of immobilized enzymes and the leaching of enzymes during the recycling of NPs. In addition, frequent interaction of the substrate with the active site of immobilized enzymes could lead to distortion of the active site, resulting in loss of enzyme

activity (Defaei *et al*. 2018) and this is why the activity of the co-immmobilized system gradually decreases ovee time. Perwez, Ahmad and Sardar (2017) reused MNPs for 7 cycles at 30 °Cwith a short cycle time of 10 min per cycle. These results differ from those obtained by Dalal, Sharma and Gupta (2007) where immobilized cellulase on naked MNPs was recycled 5 times at the operational conditions of 30 °C and 30 min per cycle time. Operational stability for hydrolysisand the covalent bonding of enzymes on MNPs enhanced conformational stability.

Fed-batch enzymatic hydrolysis from alkali pre-treated SCB was investigated in the study to increase the production of xylose and reduce production-related costs. Fed-batch production resulted in sustained levels of xylose using a 5 L laboratory bioreactor. During this study, the optimal initial feeding time and feed concentration were examined. The hydrolysis was initiated with 1% (w/v) solid substrate, after 196 h, xylose reached its maximum production of 8.10 g/L. The rate and extent of enzymatic hydrolysis of lignocellulosic biomass are highly dependent on solids loading, enzyme loading hydrolysis time and structural features of the substrate site (Zhu *et al*. 2008). From figure 5.5, it could be observed that the hydrolysis rate was high in the first 48 h, which can be explained by a reduction in crystallinity and an increase in exposed availability of catalytic sites. Whereas Gao *et al*. (2014) started with 12% (w/v) of solids and obtained a high rate during the 12 h. As time progresses, there was a decrease in enzyme accessibility sites and the product inhibition resulted in a decreased rate of hydrolysis during the final hydrolysis stage (Zhu *et al*. 2008). Yang *et al*. (2010) suggested early fed fresh solids to shorten the total hydrolysis time.

During the study, fed-batch mode was found to be better than all modes that were tested, providing sustained levels of xylose. However, Brethauer and Wyman (2010) concluded that continuous mode provided more production compared to batch mode as it enhances volumetric productivity and consequently smaller bioreactor volumes. Additionally, this lowers the investment and operational costs.

An attempt was made to study the simultaneous saccharification of xylan by co-immobilized CCMNPs and pentose-fermenting *S.stipitis*. During this study, 1.05 g/L of xylose was quickly produced before the actual incubation, which is primarily due to the highly active xylanolytic

enzymes. The highest xylose production of 6.8 g/L was obtained at 24 h. There was a drastic decrease in xylose and it was believed that *S.stipitis* was actively fermenting xylose to ethanol (data not shown). Upon feeding the fermentation system, the viscosity increased with no significant improvement in the production of either xylose or ethanol.

Figure 5.6 shows fermentation of xylose over 50 h yielding ethanol and xylitol. Xylose drastically dropped at 45 – 50 h where maximum ethanol was produced. Ethanol production of 3.96 g/L was observed after 50 h and a maximum of 0.52 mg/mL xylitol. Only 16.05% xylose was not converted to ethanol. The conversion of xylose to ethanol by *S.stipitis* was still good. This is evidenced in a study by Germec *et al*. (2016), who reported ethanol production of 2.85 g/L and 2.84 g/L and a sugar utilization of 73.68% and 63.27% when using *S.stipitis* ATCC58784 and *S.stipitis* ATCC58785, respectively. Bader, Germec and Turhan (2021) obtained ethanol production of 3.80% from 25% xylose which is slightly higher than this study. During xylose fermentation by *S.stipitis*, xylose is first reduced to xylitol by xylose reductase (XR), which then oxidizes it to xylulose by xylitol dehydrogenase (XDH). It should be noted that another hexose fermenting yeast *S.cerevisiae* is unable to metabolize xylose due lack of XR and XDH activity (Patiño *et al*. 2019). Xylitol is used in soft drinks, candies, ice cream, chewing gum and various pharmaceutical products. Xylitol has a key role in sweetened food products and is used as a natural sweetener in toothpaste (Basit *et al*. 2020). During ethanol production, excess yeast is removed in the process and yeast extract can be produced as a by-product with fed-batch methods.

5.4 **Conclusions**

The fed-batch strategy was selected for maximum production of xylose from xylan. In this study, *S.stipitis* yeast was used to successfully ferment xylose from xylan and produced bioethanol. Xylose presents the second most abundant monosaccharide in lignocellulosic biomass. Bioethanol has proved to be an alternative fuel; however, more substrates need to be investigated for bioethanol production to avoid raw material shortage.

CHAPTER 6: GENERAL DISCUSSION

The use of enzymes from the environment has been practiced for a long time. To date, there has been tremendous growth in the production and utilization of microbial enzymes. They are used as biocatalysts for many reactions including hydrolysis of agricultural biomass. Over the past decades, Aalam and Saravanan (2015) have reported the production of xylanolytic enzymes, xylanase and xylosidase from *Aspergillus tamarrii* using wheat bran, corn cob and SCB as substrates. Xylanoltic enzymes have gained massive attention due to their ability to hydrolyze lignocellulosic biomass such as sugar cane bagasse to fermentable sugar such as xylose which can be fermented to bioethanol. Guerfali, Maalej-Achouri and Belghith (2013) isolated *Talaromyces thermophilus*, a producer of broad-spectrum polysaccharide-hydrolyzing enzymes which are mostly endo-β-1,4-xylanase, β-xylosidase, γ-L-arabiofuranosidase and β-D-mannosidase. The fungus was further immobilized on chitosan and used for continuous hydrolysis of wheat bran for xylose (18.6mg/g) production after 6 h. Xylose was then hydrolyzed by crude *Thermus thermophilus* into xylitol for further production.

Another filamentous fungus, *Aspergillus terreus* RWY has the spectacular ability to produce not only xylanolytic but also cellulolytic enzymes. An incredible producer for cellulase, β-glucosidase (BGL), endoglucanase (EG), cellulase, cellobiohydrolase (CBH), xylanase, γ-L-arabiofuranosidase and β-xylosidase (Sharma *et al*. 2014). These enzymes perform an enormous role in lignocellulose hydrolysis. Similarly, Singh, Madlala and Prior (2003) isolated *T. lanuginosus* SSBP which is a hyper producer of β-D-xylanase and a source of many other enzymes like; β-D-xylosidase, α-D-xylosidase, α-glucuronidase, acetylxylan esterase, α-galactose, α-L-arabinofuranosidase, endo-β-1,4-mannase, β-D-glucosidase, pectinases, lipases, phytases, chitinases, cynate hydratase and L-glutaminase.

The major bottleneck in the economical practical production of second-generation bioethanol is low stability low efficiency and high costs of hydrolytic enzymes. One of the means to reduce enzyme cost is by exploiting microorganisms that have the ability to produce hemicellulases in significant yields while using inexpensive substrates through solid-state fermentation (SSF). Solid-state fermentation for enzyme production provides lower capital costs and, low operating costs.

Some required features for commercial production of second-generation ethanol include anenzyme that can operate at a wide pH range and the ability for efficient hydrolysis at higher substrate loading.

The United States of America are considers developing and putting in place sustainable biofuels a priority. The lack of good adequate energy services is a major impediment to development in Africa, and biofuels in particular can play a crucial role in this project (Biswas, Bryce and Diesendorf 2001). Out of five forms of biofuels (biogas, bioethanol, biohydrogen, biodiesel and biomethanol) only bioethanol and biogas are operational on the continent as purely car fuel or by blending with petroleum fuels. Presently, South African energy is highly dependent on non-renewable energy resources such as coal. Over the past 15 years, the Energy Policy Document of South Africa strived to attain 15% of renewable energy contributing to the national energy mix which has not been a success (Bugaje 2006). The African continent has 54 countries and out of them, only four (Algeria, Nigeria, Libya and Egypt) are energy exporters while the remaining countries including South Africa, are extremely dependent on imports (Amigun, Musango and Stafford 2011). Above all, South Africa has massive potential to solve the energy crisis with proper infrastructural support to harness its abundant renewable resources.

In this study, previously isolated and reported enzymes β-xylanase and β-xylosidase from the Institute's Enzyme Technology Research Group were co-immobilized on chitosan-coated magnetic nanoparticles for bioethanol production from 1% xylan produced from SCB. Sugarcane bagasse is rich in hemicellulose and cellulose and therefore ideal for bioethanol production (Sindhu *et al*. 2016). The first part of this project was to produce two xylanolytic enzymes, TlxylA and Tlxyn1 on shake flasks and upscaled their production in a 5 L laboratory bioreactor. TlxylA was produced from a coarse corn cob medium using *T.lanuginosus* SSBP and Tlxyn1 was produced from a YPD medium using a cloned *P. pastoris* G115. Both enzymes were partially purified by ammonium sulphate purification of 25 – 50%, and 75 – 90% for TlxylA and Tlxyn1, respectively. TlxylA from *T.lanuginosus* SSBP was purified to 4.51-fold with 47.64% yield using 3 steps, ammonium sulphate precipitation (25 – 50%), ion-exchange (DEAEFF) and gel-filtration. Similarly, *T.lanuginosus* PC7S1T xylanase was purified to homogeneity in four chromatographic steps and demonstrated an 11- fold and 36% yield (Della Torre *et al*. 2021). Tlxyn1 from *P. pastoris* G115 was purified to 7.89-fold and a yield of 14.67% using 3 steps, ammonium sulphate

precipitation (75 – 90%), ion-exchange (Resource Q) and gel-filtration. The molecular weights for TlxylA and Tlxyn1 were 23 and 55 kDa, respectively using a molecular protein marker. The single band on each SDS-PAGE confirmed the purity of the enzymes. Seemakram *et al*. (2020a) previously reported 25 kDa molecular weight by *SDS–PAGE* purified xylanase from *T. dupontii* KKU–CLD–E2–3, which is similar to that from *T.lanuginosus* SSBP. An almost doubled molecular weight of 45 kDa with a 5.3 purification fold and 21% yield was obtained from *Bacillus velezensis* AG20 compared to that of *T.lanuginosus* SSBP (Ghosh *et al*. 2021). Purified β-xylosidase, reported by Jin *et al*. (2020), exhibited an apparent molecular mass of 74.5 kDa from *Aspergillus fumigatus.* The difference in molecular weight may be explained based on different species.

The second part of the project was to prepare, functionalize and characterize chitosan-coated magnetic nanoparticles without enzymes followed by the extraction of xylan from SCB by alkali pretreatment. Synthesized MNPs were able to be separated with an external magnet and were coated with chitosan. The agglomeration observed on SEM (Fig.3.4) and HRTEM (Fig.3.5) was reduced by functionalization with APTES (Fig.3.6). HRTEM confirmed 1.73 – 17 nm sized spherical shaped nanoparticles. These results are in good agreement with that reported by Piosik *et al*. (2021) with an average of 11.8 nm from CCMNP using GA as a cross-linker. The obtained shape differs and the size is more than 150-times smaller than the size reported by Ghorbani-Vaghei *et al*. (2021), who reported a cubical shaped Fe_3O_4 NPs with a size around 150 – 250 nm using alginate as a coating agent. The thin film layer surrounding NPs demonstrates chitosan coating.

Desired bonds of characteristic peaks on NPs are observed across the FTIR spectrum. The spectra of uncoated MNPs depict an absorption band of Fe–O of Fe_3O_4 at 563 cm^{-1} which is one of the most important key characteristics of MNPs. Other key observed bands include 1637, 1653 and 1386 which were for amine, GA cross-linkage in the vicinity, and C–H vibration of CH_2, respectively. The broad-band peak around 3200 cm^{-1} was assigned to O–H stretching and H–O–H bending modes of water absorbed on MNPs (Irfan *et al*. 2021). FTIR made it possible to characterize CCMNPs. The 1386 cm^{-1} band that appeared on presented MNPs is also present on CCMNPs. A stretching vibrating band around 1547 cm^{-1} is assigned to GA, this band did not appear on the MNPs serving as confirmation of the presence of chitosan on the surface of MNPs.

The wave numbers confirming presence of chitosan NPs were also reported by González-Martínez *et al*. (2021). However, there was a shift on the 3200 cm^{-1} peak to around 3500 cm^{-1}, linked to absorbed water molecules on samples. There were four common absorption peaks (563, 3200–3500, 1653, 1386 cm^{-1}) for MNPS and CCMNPs.

Additionally, the thermostability of MNPs and CCMNPs was confirmed by TGA–DSC by monitoring changes in weight due increase in heating temperature. The TGA curve of MNPs shows weight loss with an increase in temperature until 150 °C. This may be attributed to the removal of OA and other organic layers present. DSC shows large exothermic peaks at 125 °C while Zeng *et al*. (2021) obtained large exothermic peaks between 200 and 400 °C, corresponding to oxidation and decomposition of OA. The small endothermic peak at 350 °C resulted from Fe_3O_4 to Fe_2O_3 transition. It can be observed that CCMNPs were stable up to 250 °C, weight loss at 75 °C could be water adsorbed on NPs. Uncoated MNPs and CCMNPs show a significant change in weight at 600 °C, CCMNPs retaining very less weight due to chitosan susceptibility to extremely high temperatures. This means that the working temperature of CCMNPs and corresponding composites cannot be higher than 85 °C. Therefore, when working with CCMNPs, the temperature must not exceed 85 °C for desired results.

Highly positive or negatively charged zeta potential is required for various biological applications (Santos *et al*. 2018) to avoid aggregation of NPs. zeta potential 26 – 30 mV upwards and zeta potential less than −30 mV are highly stable (Nallamuthu, Devi and Khanum 2015). In the present study, the positive zeta potential of CCMNPs was almost half that of MNPs due to the presence of chitosan. Ahmadifard *et al*. (2020) reported a similar observation but negatively charged on zeta potential for uncoated MNPs and CCMNPs of -42.5 and -20.2, respectively. Based on the obtained zeta potential, it is concluded that MNPs and CCMNPs are stable in dispersed water. The difference in charge between uncoated and coated MNPs indicates that chitosan layer has successfully covered the NPs thus providing them with protection from corrosion, resulting in improvement in retinol stability and solubility.

The next part of the investigation was to collect the fluffy remains of SCB and pretreat them to liberate xylan. The highest xylan extraction yield from SCB was an average of 75.1% and was

achieved using optimized RSM parameters. Silva *et al*. (2021) reported the highest xylan extraction yield from SCB of 59% after working with 15% solids and a xylanase dosage of 500 IU/g. The prominent absorption band at 3440 cm^{-1} was attributed to O-H stretching vibrations that are present at the SCB xylan and water involved in the hydrogen bonds (Sun et al. 2013). A sharp absorption band at 1620 cm^{-1} was due to bending made by water because hemicellulose usually has a strong affinity for water (Ayoub *et al*. 2013). Brienzo, Siqueira and Milagres (2009) and Peng *et al*. (2009)**,** implied that the absence of a band around 1730 cm^{-1} confirms that the application of NaOH completely cleaved ester bonds on SCB. Additionally, Kačuráková *et al*. (1999) also emphasized the absence of pectin in the extracted xylan by the absence of a band at 1520 cm^{-1}. The glycosidic linkage between sugar units was characterized by a sharp band at 900 cm^{-1} (Sabiha-Hanim, Noor and Rosma 2015). Jayapal *et al*. (2013), concluded that overall absorbance bands at 3440, 1400,1020 and 900 cm^{-1} were associated with xylan molecule, therefore the current study has successfully extracted xylan from sugarcane bagasse.

Preliminary studies evaluating the action of TlxylA and Tlxyn1 on extracted xylan from SCB was monitored by TLC. The end-product xylose from hydrolysis action on xylan was confirmed by dark spots from TLC. Results reveal successful synergistic action of TlxylA and Tlxyn1 on xylan to liberate xylose. Purified xylanase acted on β-1,4-glycosydic bonds to release xylooligosaccharides; therefore, xylosidase preferably cleaved on XOS releasing xylose as the final product. From the results, it is concluded that TlxylA and Tlxyn1 are synergistic with each other, which is also evidenced in a reported study by Della Torre *et al.* (2021) where only XOS were liberated from beech wood xylan from purified xylanase of *T.lanuginosus* PC7S1T with no xylose being produced. The importance of xylan to xylose hydrolysis has motivated Lee, Jin and Cha (2022) to engineer *Sulfolobus acidocaldarius* to utilize xylan by introducing xylanase and xylosidase. The synergetic action of xylanase and xylosidase on 5% xylan was visualized by dark spots on TLC. In another report, xylan-to-xylose conversion was achieved by two step saccharification. The first step involved saccharification by xylanase (CtXyn11A) and α-1-arabinofuranosidase (PsGH43_12) and the second step of saccharification was by xylosidase (BoGH43), xylose was evident from TLC resulting to 69.6% xylan-to-xylose conversion for SCB (Thakur *et al.* 2021).

Different enzyme systems were employed to select the best enzyme system for better xylose production. From the three enzyme systems, the free enzyme showed better yield followed by co-immobilized TlxylA and Tlxyn1 on CCMNPs. However, the co-immobilized system was selected for further studies due to its stability for prolonged use during fermentation/application processes. The difference between free and co-immobilized systems on xylose production was less than 8%, whereas the mixture of solely immobilized enzymes only had about 15% xylose yield after 36 h. It is impossible to immobilise 100% of enzymes on nanoparticles, especially if it is more than one enzyme. Synthesis and drying methods of MNPs play a significant role in effectiveness binding of enzymes on NPs. Lyophilized dried NPs account for up to 200% higher enzyme immobilization than the same NPs dried in a vacuum oven. The binding efficiency of proteins to MNPs is dependent on the availability of the carboxyl and amino groups on the NP (Ziegler-Borowska *et al*. 2019). Anything above 60% binding efficiency is considered after enzyme immobilization for effective application on the substrate. An average of 82.5% binding efficiency was observed after co-immobilization of TlxylA and Tlxyn1 on CCMNPs while unbound protein was below 20%. Kaur *et al*. (2021a) reported 79.44% binding efficiency on single immobilization of ellagic acid on Tween 80-coated chitosan nanoparticles while Deng *et al*. (2021) obtained 87.5% immobilization efficiency of β-glucosidase from *Agrocybe aegerit* on magnetic nanoparticles. The binding efficiency of the obtained immobilized system is effective for application on substrate.

Co-immobilized CCMNPs showed aggregated spherical shapes. Less aggregation was observed on HRTEM. Using image J, the average size of co-immobilized CCMNPs was 21.34 nm, HRTEM accurately demonstrates chitosan covering co-immobilized CCMNP with a thin layer surrounding NPs. Covalent attachment of co-immobilized TlxylA and Tlxyn1 on CCMNPs was further confirmed by FTIR (Fig 3.8). In all cases of synthesized NPs, 563, 3000 – 3600 cm^{-1} are associated with Fe –O and hydroxyl group from absorbed water on NPs. Sharp and broad peak at 3440 cm^{-1} regions in all samples corresponds with the OH bond stretching (Altun *et al*. 2015; González-Martínez *et al*. 2021). In this experiment, the hypothesis was that GA would act as a cross-linker to link amine of amino on MNPs to amine groups of enzymes during immobilization. While direct functionalization by covering Fe_3O_4 nanoparticles with APTES was used to eliminate the loss of magnetism Ghazanfari *et al*. 2016). From FTIR results, it is conclusive that GA has linked enzymes to the NPs while APTES evenly dispersed MNPs reducing aggression of NPs.

Sharp peaks at 1637 and around 1400 cm^{-1} were associated with covalently bonded enzymes with glutaraldehyde, indicating successful co-immobilization of enzymes on CCMNPs. These peaks have slightly shifted to those reported by Sukprasert *et al*. (2021)**,** which were 1722 and 1459. Alam et *al*. (2021), associated asparaginase protein structure on MNPs with 1750 and 1260 cm^{-1} peaks, -C=O and -C-O stretching, respectively. The peak corresponding to Si–O–Si of APTES is observed at 1020 cm^{-1}, confirming coverage of saline with the free amine group of APTES on MNPs. Karade *et al*. (2021) reported a peak corresponding to APTES at 1015 cm^{-1}. It is important to maintain an average of 10% GA, low GA is sufficient for enzyme binding while high/excess GA causes an enzyme to lose versatility due to unwanted binding enzyme active sites. This results in excessive binding of enzyme molecules, thus decreased enzyme activity (Sheldon and biotechnology 2011). GA does not only provide crosslinking but also improves enzyme rigidity resulting in improved enzyme stability (Barbosa *et al*. 2013). Zhang *et al*. (2020) associated 1394 cm^{-1}absorption peaks to laccase immobilized on chitosan of Fe_3O_4 nanoparticles. All these FTIR spectra indicate that enzymes were successfully co-immobilized on CCMNPs, and chitosan was attached to the surface of Fe_3O_4 nanoparticles. They can therefore be applied in various biotechnology applications.

The zeta potential of +29.057 and +28.87 mV on produced CCMNPs in the present study indicate that they are stable. Melo *et al*. (2020) reported zeta potential values between +20.1 and +28.4 mV after immobilization of peroxidase into chitosan nanoparticles. TGA thermogram of co-immobilized CCMNPs shows two gentle decomposition processes. The first decomposition is exhibited in the range of 25 – 200 °C related to the elimination of water. The next decomposition step range of 200 – 400 °C may be related to the decomposition of amine groups of co-immobilized enzymes and chitosan. Gawali *et al*. (2021) reported four major decompositions on Fe_3O_4 nanoparticles with proteins at about 25, 200 and 350 and 500 °C. A broad endothermic peak was caused by the reduction of amine on chitosan of co-immobilized CCMNPs (Naicker, Nombona and van Zyl 2020) from the DSC profile of co-immobilized CCMNPs. The broad endothermic peak is caused by oxidation. When comparing the TGA-DSC profile of CCMNP without enzymes, it was noted that very less weight was retained after 600 °C. Coupling with enzyme has improved thermal stability, this was noted by improved weight retained after 600 °C, improving mechanical properties at elevated temperatures than its optimum making them suitable for applications at slightly higher temperatures.

Free, solely immobilized, and co-immobilized TlxylA showed high activity in a pH range of 5–7.0, with optimal pH 6.0, 5.50 and 6.0, respectively. A thermophilic fungal xylanase from *T. dupontii* KKU−CLD−E2−3 showed maximum activity at high alkaline pH of 8.0 (Seemakram *et al*. 2020b). However, Liu *et al*. (2014) reported high activity in the pH range of 4.0–7.0 with optimal pH at 5.5 and 5.0 for free and immobilized *Aspergillus niger* xylanase on CCMNPs. Nanoparticles provide a buffering effect on enzymes to bear enhanced alkaline or acidic environments. The highest activity for free, solely immobilized, and co-immobilized Tlxyn1 was 5.50, 5.0 and 5.50, respectively. Both enzymes exhibited the same pH optimum range for free and co-immobilized. Cheng *et al*. (2019) reported a forward shift from pH 7.0 to 7.50 after immobilizing α-glucosidase on APTES functionalized Fe_3O_4 nanoparticles. The shift in pH optimum is attributed to the binding of enzymes on the support matrix via a Schiff base reaction, changing the enzymes' conformation and increasing its relative activity at a broader pH range (Feng *et al*. 2016).

The lack of pH and temperature stability of free enzyme together with solely immobilized and co-immobilized enzyme system provoked the research group to commence the study. Enzyme stability is the product of equilibrium between stabilizing and destabilizing forces associated with linkages (de Castro *et al*. 2015). pH stability results indicated that free TlxylA showed maximum activity at pH 6.5, with 56,21% residual activity after 4 h. Xylanase from *T.lanuginosus* VAPS-24 was most stable at pH 7.0 (Kumar, Chhabra and Shukla 2017). Solely immobilized TlxylA on CCMNPs showed improved pH stability compared to free TlxylA at pH 6.0 with a 10.07% improvement. A maximum of 1.97 and 3.57 U/mg were reported at pH 6.0 and 4.0 for free and immobilized xylanase respectively on CCMNPs to evaluate its biochemical properties and reuse capacity (Amaro-Reyes *et al*. 2019). There was no significant difference in the retained residual activity between free and co-immobilized TlxylA. Co-immobilized TlxylA retained 56.51% residual activity after 4 h incubation at pH 6.0. Ladole *et al*. (2021) reported maximum activity at pH 5.5 for pectinase and naringinase on CCMNPs for clarification and debittering of grapefruit juice. Moreover, co-immobilized TlxylA on CCMNPs was chosen for prolonged application due to the stability provided by the NPs

Free Tlxyn1 was poorly stable in most pH ranges, retaining only 36.39% residual activity at pH 5.5 after 4 h. Generally, yeast xylosidases have pH stability of 5.0 (Tong *et al*. 2021) and 5.5 (Souto

et al. 2021). Tlxyn1 was solely immobilized on CCMNPs to enhance pH stability. Immobilized Tlxyn1 improved pH stability at pH 6, with 2.45-fold over 4 h from free Tlxyn1. Surprisingly, Liao *et al*. (2020) reported slightly lower pH stability than that of free HpaB and HpaC separately immobilized on MNPs. Co-immobilized Tlxyn1on CCMNPs were stable at pH 6.0. The co-immobilized Tlxyn1 retained a slightly lower residual activity than solely immobilized TlxylA. Improvement and stability of both solely and co-immobilized enzymes in acid and alkaline environments may be due to the covalent bond between enzymes and CCMNPs (Guo *et al*. 2021) resulting in a stable molecular structure.

Temperature is another important factor for enzyme characterization over a wide temperature range. Moreover, immobilized enzymes usually display better temperature stability and activity than free enzymes. Thermal behavior for free, solely immobilized, and co-immobilized TlxylA on CCMNPs was carefully studied. Free TlxylA showed fair stability at 60 and 70 °C with the optimal temperature at 50 °C. Lower thermal stability on free TlxylA may be attributed to the sensitive environment the enzyme was exposed to, hindering efficient delivery and supplementation of enzymes (Pavlovic, Rouster and Szilagyi 2017). Following immobilization of TlxylA on CCMNPs, thermal stability improved from that of free TlxylA. Functionalization of CCMNP increased electrostatic attraction between CCMNPs and TlxylA, resulting in improved substantial thermal stability of NPs. Co-immobilized TlxylA showed better thermal stability amongst all enzyme systems. In another report, bi-enzyme immobilization of cellulase and lysozyme onto amino-functionalized magnetitic nanoparticles showed improved thermal and pH stability for application in the extraction of lipids from microalgae (Chen *et al*. 2018).

Free Tlxyn1 was fairly stable between 30 and 40 °C, relative activity decreased drastically with increased temperature. Increasing temperature from 60 to 80 °C indicated no residual activity during 4 h. A case where free enzyme isocitrate dehydrogenase rapidly loses activity at a temperature above 30 °C was also discovered by Farhan *et al*. (2021) for the determination of magnesium in water. The decrease in activity at elevated temperatures may cause partial enzyme denaturation. Immobilizing Tlxyn1 on CCMNPs indicated better thermal stability due to covalent bonding between Tlxyn1 and GA of CCMNPs (Amin et al. 2018). Solely immobilized Tlxyn1 showed activity at 60, 70 and 80 °C after 4 h and improved stability at lower temperatures of the study. Co-immobilized Tlxyn1 showed similar thermal stability behaviour to that of solely

immobilized Tlxyn1 with slight thermal stability. Projected thermal stability made it ideal for its application in biomass degradation. Co-immobilized Tlxyn1 had the highest thermal activity at 30 °C, retaining 60.26% activity after 4 h. Stability improved in increased temperature, however, results revealed that Tlxyn1 prefers lower temperatures.

Overall, the stability of immobilized TlxylA and Tlxyn1 was largely preserved as compared to free enzymes. Enzyme stability could have been enhanced by a substrate (You *et al*. 2010). These results show that immobilized enzymes can be used at a wider pH and temperature range providing significant advantageous biotechnology applications. Similarly, Bilal *et al*. (2021), reported broader pH and temperature stability for co-immobilized lysozyme and cellulase on amino-functionalized MNPs for the degradation of Nannochloropsis sp. cell wall compared to free enzymes. Immobilization may have enhanced enzyme structural stability providing long-term stabilization and preventing inactivation during harsh environments (Sáringer *et al*. 2021). Zhang *et al*. (2011), reported superior functional stability and efficiency from tri-immobilized α-amylase, β-amylase, and glucosidase on polydopamine microcapsule for bioconversion of starch to isomaltooligosaccharide. The resulting co-immobilized TlxylA and Tlxyn1 on CCMNPs were used to hydrolyze xylan from SCB for xylose production.

Long-term storage stability offers preservation of enzymes and saves enzyme costs, this is one of important properties for industrial applications (DiCosimo *et al*. 2013). Generally, immobilized, and co-immobilized enzymes improve stability including storage for future use. Immobilized enzymes showed improved storage stability compared to free enzymes. In all cases of free, solely immobilized, mixed solely enzymes and co-immobilized TlxylA and Tlxyn1; solely immobilized enzymes showed slightly higher stability than co-immobilized enzymes with a difference less than 10%. Immobilized lipase storage stability on MNPs for biodiesel production did not decrease appreciably for 60 days (Shalini *et al*. 2021), the noticeable decrease was noted from days 70 and 80. In another storage stability, immobilized α-amylase showed improved stability compared to free α-amylase, retaining 60% of its initial activity after 6 weeks storage at 4 °C (Defaei *et al*. 2018). There are very few studies on storage stability for co-immobilized enzymes. Liao et al. (2020) reported 76,6% retained stability activity for 12 days on co-immobilized two-component hydroxylase monooxygenase on magnetic nanoparticles while free enzymes decreased at a fast rate retaining 29.2% of activity.

For upscaled production of products, scientists have performed RSM for optimizing production parameters. Response surface methodology designs experiments to minimise time and resources and minimizes several experiments (Chelladurai *et al*. 2021). Appropriate optimization of xylose sugars from lignocellulosic biomass warrants multiple products under biorefinery. During the present study, RSM provided by Design-Expert software version 6.0 was effective in obtaining optimal conditions for xylan hydrolysis by TlxylA and Tlxyn1 co-immobilized on CCMNPs to produce xylose. All parameters displayed a positive effect on xylose production. On optimized conditions, 70.62% xylan was converted to xylosidase. The production was carried out by considering significantly influencing factors such as TlxylA and Tlxyn1 load on CCMNPs, temperature, and pH. According to our knowledge and intensive reading, this is the first study that optimized xylose production from SCB using RSM on co-immobilized TlxylA and Tlxyn1 on CCMNPs. There are few reports on the immobilization of xylanase and xylosidase on CCMNPs for hydrolysis of xylan to yield xylose. Synthesis of silver nanoparticles from *Bacillus cereus* was optimized with other parameters using RSM to study their characterization, antimicrobial, antioxidant, and catalytic potential (Ibrahim *et al*. 2021). For future studies and the application of our research, it is mandatory to optimize CCMNPs on RSM for immobilization of any enzyme. This may have a significant effect on the absorption of enzymes thus better action of application. In another study, Shahedi *et al*. (2019), used RSM to optimize fatty acid methyl esters yield using co-immobilized lipase from *Candida antarctica* B and *Rhizomucor miehei* on epoxy functionalized silica gel. This study is like that of Shahedi et al. (2021), enhanced biodiesel production by transesterification of palm oil using bi-enzymes lipase from Candida antarctica B and *T. lanuginose* immobilized on epoxy functionalized silica gel. In both literature studies and any other study, no one has attempted to optimize enzyme co-immobilized dose on RSM with other factors for improved production.

After validating optimum conditions for co-immobilization of TlxylA and Tlxyn1 on CCMNPs to hydrolyze xylanase to xylose. It was mandatory to upscale xylose production from shake flasks to laboratory bioreactors to enable fermentation by *S. stipitis* to yield bioethanol. The results showed no significant xylose concentration but greater production on a large scale. Xylose as a substrate for bioethanol production, batch, fed-batch and repeated batch fermentation processes were investigated to increase yield. During batch fermentation, minimum medium assisted in highlighting the metabolism of xylan to xylose using free and co-immobilized TlxylA and Tlxyn1

on CCMNPs, offering quick identification of any metabolites present and easy interpretation of the production trend.

Limitations associated with batch fermentation such as the inability to control fermentation conditions (Pérez-Burillo *et al*. 2021), and not being able to provide data for the prolonged time effect of the substrate during fermentation (Liu, Segato and Wilkins 2021) restrict it from being used. Therefore, xylose production was studied using fed-batch strategies by first optimizing the time of feed and concentration of the feed. Xylan feeding (10 g/L) at 24 h intervals was best for maximum xylose production against other xylan concentrations. Increasing substrate for 2 g/L to 10 g/L induced xylose production. Decreased xylose production at a concentration higher than 10 g/L may be attributed to inhibition influenced by excessive substrate concentration on xylose production (Lu *et al*. 2020). It is important to note that too less substrate can result in low product yield (Tasminto, Bachruddin and Kurniawati 2021). Based on our intense reading, we have found no reports on fed-batch strategies of xylan for xylose production. Instead, researchers like Schneider *et al*. (2001); Prasad Uday *et al*. (2017) have used xylan on fed-batch strategies as a carbon source to enhance xylanase production by *Bacillus* strain and *Aspergillus niger* KP874102.1, respectively. Overall, optimization for feeding concentration resulted to 9.47 g/L xylose.

The results showed that co-immobilized TlxylA and Tlxyn1 on CCMNPs retained 66% of activity and 39.68% conversion after 6 cycles of 48 h while there was 60% of activity and 19.30% conversion after 6 cycles of 24 h. This suggests that co-immobilized TlxylA and Tlxyn1 that were stable on the surface of CCMNPs, had high efficacy and reusability, and an external magnet efficiently recovered immobilized enzymes. Alnadari *et al*. (2021) reported 40.44% activity and converted a maximum of 28.67% galactooligosaccharides after six repeated 12 h cycles from immobilized β–glucosidase on MNPs. In another report, 52.67% conversion efficiency of rice straw was obtained from immobilized cellulase on MNPs with retention of 50.43% activity after 4 cycles (Kaur *et al*. 2021b). Results from fermentation systems suggested that fed-batch is a greater option to enhance the production of xylose from xylan.

Xylose is one of the most abundant sugars present in lignocellulosic biomass, its efficiency and rapid utilization is a prerequisite for sustainable and economical production of bioethanol. The final stage of the present study aimed at the fermentation of xylose sugar bioethanol by *S.stipitis*

from a 5 L bioreactor. The study obtained multi-products which is ethanol and xylitol. There was an over 80% xylose-to-ethanol conversion, implying that *S.stipitis* is the most efficient yeast strain for xylose fermentation to ethanol. In a similar study, 2.6 g/L ethanol was produced from 5.95 g/L xylose by *Pichia kudriavzevii* yeast, with 88.8% fermentation efficiency (Hebbale, Mishra and Ramachandra 2021). Ethanol production through fed-batch from 300.0 g/L resulted in 135.0 g/L ethanol after 30 h (Cruz *et al*. 2021); from these results, it is possible to vacuum concentrate xylose for a maximum substrate to enhance bioethanol production.

In the present study, xylitol was produced as a byproduct of ethanol having many health benefits. Xylitol is a sugar alcohol naturally occurring in small amounts in fibrous birchwood, fruits and vegetables. It is widely used in oral products for whitening and removing plaque formation; low glycemic index making it ideal for diabetics. *Kluveromyces marxianus* II PE453 mtcc 5314 was designed for lignocellulosic bioethanol and xylitol production by Dasgupta *et al*. (2017) using the multiproduct biorefinery concept. Xylitol can also be used as raw material for plastics and directly utilized as a plasticizer for polymer interactions (Chaudhary 2010). Most xylitol is produced chemically on catalytic reduction of pure xylose under high pressure and temperature utilizing expensive catalysts and intense costs and energy consumption.

Ethanol obtained in the present study has significant amount of conversion for its application in the motor industry and many more. Ethanol production is projected to reach 131 billion L by 2027, most of this increment is expected to take place in developing countries (Aarti, Khusro and Agastian 2021). Twenty and thirty percent of fuel containing ethanol was found to be the best blend by volume; engine performance and pollutant emission of an SI engine using ethanol-gasoline fuels (He *et al*. 2003). Ethanol-gasoline blending also contributes to increased brake power, brake thermal efficiency, volumetric efficiency and fuel consumption (Al-Hasan 2003). However, an increase in ethanol blends results in tail pipe unburned ethanol and acetaldehyde emission increase; its inhalation can alter breathing by narrowing airway openings, irritating the eyes and nose, damaging cell lining, prompting white blood cells to enter the lungs and causing global warming.

Conclusively, the present study reports on the co-immobilization of xylanolytic enzymes on CCMNPs for hydrolysis of lignocellulosic biomass for application in bioethanol production. Many thanks to the recovery of magnetic nanoparticles which allowed recycling and repeatable use of

CCMNPs. It is important to note that Brazil is in first place in bioethanol production as their monthly sugarcane is equivalent to that of South Africa annually. Their SCB is waste from first-generation (1G) ethanol which is then used for second-generation (2G) bioethanol from sugarcane mills. To be competitive on the costs associated with bioethanol production, our next investigation will consider complete hydrolysis of xylan incorporating other synergistic enzymes like arabinofuranosidase, β-glucuronidase, acetylxylan esterase, ferulic acid esterase and p-coumaric acid esterase. Future perspectives should focus on the oxidation of bioethanol to acetaldehyde, which may become a better and green choice for preparation from ethylene. To further reduce energy-demanding costs of anhydrous bioethanol, bioethanol can be converted to other valuable chemicals that are insensitive to water reactions such as H_2 through catalytic steam reforming, acetaldehyde, acetic acid or ethyl acetate. The synthesis of NP's using plants and microorganisms has immense potential as it is eco-friendly and cost effective, uses minimal harsh chemicals and requires little energy. Bacteria (actinomycetes), fungi and yeasts have been previously studied for intra and extracellularly synthesis of metal nanoparticles.

REFERENCES

Aalam, C. S. and Saravanan, C. 2015. Effects of nano metal oxide blended Mahua biodiesel on CRDI diesel engine. Ain Shams Engineering Journal,

Aarti, C., Khusro, A. and Agastian, P. J. W. N. o. N. S. 2021. Lignocellulosic biomass as potent feedstock resource for bioethanol production: Recent updates. 37: 164-181.

Abdel-Rahman, M. A., Tashiro, Y. and Sonomoto, K. J. J. o. b. 2011. Lactic acid production from lignocellulose-derived sugars using lactic acid bacteria: overview and limits. 156 (4): 286-301.

Abraham, R. E., Verma, M. L., Barrow, C. J. and Puri, M. 2014. Suitability of magnetic nanoparticle immobilised cellulases in enhancing enzymatic saccharification of pretreated hemp biomass. *Biotechnology for biofuels, 7 (1): 1-12*.

Abdeshahian, P., Samat, N. and Wan Yusoff, W. 2010. Production of β-xylosidase by Aspergillus niger FTCC 5003 using palm kernel cake in a packed-bed bioreactor. *Journal of Applied Sciences, 10 (5): 419-424*.

Ahmad, M. S., Ali, M. S. and Abd Rahim, N. 2021. Hydrogen energy vision 2060: Hydrogen as energy Carrier in Malaysian primary energy mix–Developing P2G case. *Energy Strategy Reviews, 35: 100632*.

Ahmadi, S., Fazilati, M., Nazem, H. and Mousavi, S. M. J. B. R. I. 2021. Green synthesis of magnetic nanoparticles using Satureja hortensis essential oil toward superior antibacterial/fungal and anticancer performance. 2021

Ahmadifard, Z., Ahmeda, A., Rasekhian, M., Moradi, S., Arkan, E. J. J. o. D. D. S. and Technology. 2020. Chitosan-coated magnetic solid lipid nanoparticles for controlled release of letrozole. 57: 101621.

Akinboade, O. A., Ziramba, E. and Kumo, W. L. 2008. The demand for gasoline in South Africa: An empirical analysis using co-integration techniques. *Energy Economics, 30 (6): 3222-3229.*

Al-Hasan, M. 2003. Effect of ethanol unleaded gasoline blends on engine performance and exhaust emission. *Energy conversion and management, 44 (9): 1547-1561*.

Al-Najada, A. R., Almulaiky, Y. Q., Aldhahri, M., El-Shishtawy, R. M., Mohamed, S. A., Baeshen, M., Ammar, A.-F., Abdulaal, W. H. and Al-Harbi, S. A. J. S. r. 2019. Immobilisation of α-amylase on activated amidrazone acrylic fabric: a new approach for the enhancement of enzyme stability and reusability. 9 (1): 1-9.

Alam, S., Nagpal, T., Singhal, R. and Khare, S. K. J. B. T. 2021. Immobilization of L-asparaginase on magnetic nanoparticles: Kinetics and functional characterization and applications. 125599.

Alnadari, F., Xue, Y., Almakas, A., Mohedein, A., Samie, A., Abdel‐Shafi, M. and Abdin, M. J. J. o. F. B. 2021. Large batch production of Galactooligosaccharides using β–glucosidase immobilized on chitosan–functionalized magnetic nanoparticle. 45 (2): e13589.

Altun, S., Çakıroğlu, B., Özacar, M., Özacar, M. J. C. and Biointerfaces, S. B. 2015. A facile and effective immobilization of glucose oxidase on tannic acid modified CoFe2O4 magnetic nanoparticles. 136: 963-970.

Alzaidi, J., Alzahrani, E. and El-Mouhty, N. 2016. Chemical studies on the preparation of magnetic nanoparticles coated with glycine and its application for removal of heavy metals. *Oriental Journal of Chemistry, 32 (3): 1503-1513*.

Amaro-Reyes, A., Díaz-Hernández, A., Gracida, J., García-Almendárez, B. E., Escamilla-García, M., Arredondo-Ochoa, T. and Regalado, C. J. C. 2019. Enhanced Performance of Immobilized Xylanase/Filter Paper-ase on a Magnetic Chitosan Support. 9 (11): 966.

Amigun, B., Musango, J. K. and Stafford, W. 2011. Biofuels and sustainability in Africa. Renewable and Sustainable Energy Reviews, 15 (2): 1360-1372.

Amin, R., Khorshidi, A., Shojaei, A. F., Rezaei, S. and Faramarzi, M. A. J. I. j. o. b. m. 2018. Immobilization of laccase on modified Fe3O4@ SiO2@ Kit-6 magnetite nanoparticles for enhanced delignification of olive pomace bio-waste. 114: 106-113.

An, J., Li, G., Zhang, Y., Zhang, T., Liu, X., Gao, F., Peng, M., He, Y. and Fan, H. J. C. 2020. Recent advances in enzyme-nanostructure biocatalysts with enhanced activity. 10 (3): 338.

Ansari, S. A. and Husain, Q. 2012. Potential applications of enzymes immobilized on/in nano materials: A review. *Biotechnology Advances, 30 (3): 512-523.*

Arana-Peña, S., Carballares, D., Berenguer-Murcia, Á., Alcántara, A. R., Rodrigues, R. C. and Fernandez-Lafuente, R. J. C. 2020. One pot use of combilipases for full modification of oils and fats: Multifunctional and heterogeneous substrates. 10 (6): 605.

Arévalo-Cid, P., Isasi, J., Caballero, A. C., Martín-Hernández, F. and González-Rubio, R. J. B. d. l. S. E. d. C. y. V. 2021. Effects of shell-thickness on the powder morphology, magnetic behavior and stability of the chitosan-coated Fe_3O_4 nanoparticles.

Arıca, M. Y., Altıntas, B. and Bayramoğlu, G. 2009. Immobilization of laccase onto spacer-arm attached non-porous poly (GMA/EGDMA) beads: application for textile dye degradation. *Bioresource Technology, 100 (2): 665-669.*

Arumugam, N., Biely, P., Puchart, V., Singh, S. and Pillai, S. 2018. Structure of peanut shell xylan and its conversion to oligosaccharides. *Process Biochemistry, 72: 124-129.*

Asgher, M., Shahid, M., Kamal, S. and Iqbal, H. M. N. 2014. Recent trends and valorization of immobilization strategies and ligninolytic enzymes by industrial biotechnology. *Journal of Molecular Catalysis B: Enzymatic, 101: 56-66.*

Ávila, P. F., Cairo, J. P. L. F., Damasio, A., Forte, M. B. and Goldbeck, R. 2020. Xylooligosaccharides production from a sugarcane biomass mixture: Effects of commercial enzyme combinations on bagasse/straw hydrolysis pretreated using different strategies. *Food research international, 128: 108702.*

Ayoub, A., Venditti, R. A., Pawlak, J. J., Sadeghifar, H. and Salam, A. 2013. Development of an acetylation reaction of switchgrass hemicellulose in ionic liquid without catalyst. *Industrial Crops and Products, 44: 306-314.*

Azzolini, S. S. A., Sasaki, S. D., Torquato, R. J. S., Andreotti, R., Andreotti, E. and Tanaka, A. S. 2003. Rhipicephalus sanguineus trypsin inhibitors present in the tick larvae: isolation, characterization, and partial primary structure determination. *Archives of Biochemistry and Biophysics, 417 (2): 176-182.*

Bacovsky, D., Dallos, M., Wörgetter, M. and Task, I. B. 2010. Status of 2nd generation biofuels demonstration facilities in June 2010. *IEA Bioenergy Task 39: Commercializing 1st and 2nd generation liquid biofuels from biomass, 39: 1-126.*

Bader, N. B., Germec, M. and Turhan, I. J. P. B. 2021. Ethanol production from different medium compositions of rice husk hydrolysate by using *Scheffersomyces stipitis* in a repeated-batch biofilm reactor and its modeling. 100: 26-38.

Balasubramanian, R. and Chowdhury, S. 2021. Graphene-based 3D Macrostructures for Clean Energy and Environmental Applications. Royal Society of Chemistry.

Barbosa, O., Torres, R., Ortiz, C., Berenguer-Murcia, Á., Rodrigues, R. C. and Fernandez-Lafuente, R. J. B. 2013. Heterofunctional supports in enzyme immobilization: from traditional immobilization protocols to opportunities in tuning enzyme properties. 14 (8): 2433-2462.

Barbuto Ferraiuolo, S., Restaino, O. F., Gutiérrez-del-Río, I., Ventriglia, R., Cammarota, M., Villar, C. J., Lombó, F. and Schiraldi, C. J. F. 2021. Optimization of Pre-Inoculum, Fermentation Process Parameters and Precursor Supplementation Conditions to Enhance Apigenin Production by a Recombinant *Streptomyces albus* Strain. 7 (3): 161.

Basaran, P. and Ozcan, M. 2008. Characterization of β-xylosidase enzyme from a *Pichia stipitis* mutant. *Bioresource technology, 99 (1): 38-43.*

Basit, A., Jiang, W. and Rahim, K. 2020. Xylanase and its industrial applications. In: Biomass. IntechOpen.

Bastawde, K. 1992. Xylan structure, microbial xylanases, and their mode of action. *World Journal of Microbiology and Biotechnology, 8 (4): 353-368.*

Becker, C. L., Duffy, R. J., Gandarilla, J. and Richter, S. M. 2020. Purification of ADCs by Hydrophobic Interaction Chromatography. In: Antibody-Drug Conjugates. Springer, 273-290.

Berg, J. M., Tymoczko, J. L. and Stryer, L. 2012. Biochemistry/Jeremy M. Berg, John L. Tymoczko, Lubert Stryer; with Gregory J. Gatto, Jr: New York: WH Freeman.

Berry, C. C. and Curtis, A. S. 2003. Functionalisation of magnetic nanoparticles for applications in biomedicine. *Journal of physics D: Applied physics, 36 (13): R198.*

Bezuidenhout, C. and Singels, A. 2007. Operational forecasting of South African sugarcane production: Part 1–System description. Agricultural Systems, 92 (1-3): 23-38.

Bhattacharya, A., Pletschke, B. I. J. E. and technology, m. 2014. Magnetic cross-linked enzyme aggregates (CLEAs): a novel concept towards carrier free immobilization of lignocellulolytic enzymes. 61: 17-27.

Bian, J., Peng, F., Peng, P., Xu, F. and Sun, R.-C. 2010. Isolation and fractionation of hemicelluloses by graded ethanol precipitation from *Caragana korshinskii*. Carbohydrate research, 345 (6): 802-809.

Bilal, M., Asgher, M., Iqbal, H. M. N., Hu, H. and Zhang, X. 2017. Biotransformation of lignocellulosic materials into value-added products—A review. *International Journal of Biological Macromolecules, 98: 447-458.*

Bilal, M., Hussain, N., Américo-Pinheiro, J. H. P., Almulaiky, Y. Q. and Iqbal, H. M. J. I. J. o. B. M. 2021. Multi-enzyme co-immobilized nano-assemblies: Bringing enzymes together for expanding bio-catalysis scope to meet biotechnological challenges.

Bilal, M., Rasheed, T., Zhao, Y., Iqbal, H. M. and Cui, J. J. I. j. o. b. m. 2018a. "Smart" chemistry and its application in peroxidase immobilization using different support materials.

Bilal, M., Zhao, Y., Rasheed, T. and Iqbal, H. M. J. I. j. o. b. m. 2018b. Magnetic nanoparticles as versatile carriers for enzymes immobilization: A review.

Biswas, W. K., Bryce, P. and Diesendorf, M. 2001. Model for empowering rural poor through renewable energy technologies in Bangladesh. *Environmental Science & Policy, 4 (6): 333-344.*

Boddu, V. M., Abburi, K., Talbott, J. L., Smith, E. D. and Haasch, R. 2008. Removal of arsenic (III) and arsenic (V) from aqueous medium using chitosan-coated biosorbent. *Water research, 42 (3): 633-642.*

Bokhari, S. A. I., Latif, F. and Rajoka, M. I. 2009. Purification and characterization of xylanases from *Thermomyces lanuginosus* and its mutant derivative possessing novel kinetic and thermodynamic properties. *World Journal of Microbiology and Biotechnology*, 25 (3): 493-502.

Bonzom, C., Hüttner, S., Mirgorodskaya, E., Chong, S.-L., Uthoff, S., Steinbüchel, A., Verhaert, R. M. and Olsson, L. 2019. Glycosylation influences activity, stability and immobilization of the feruloyl esterase 1a from *Myceliophthora thermophila*. *AMB Express, 9 (1): 126.*

Bosetto, A., Justo, P. I., Zanardi, B., Venzon, S. S., Graciano, L., Dos Santos, E. L. and Simão, R. d. C. G. 2016. Research progress concerning fungal and bacterial β-xylosidases. *Applied Biochemistry and Biotechnology, 178 (4): 766-795.*

Bradford, M. M. 1976. A rapid and sensitive method for the quantitation of microgram quantities of protein utilizing the principle of protein-dye binding. *Analytical biochemistry, 72 (1-2): 248-254.*

Brethauer, S. and Wyman, C. E. 2010. Continuous hydrolysis and fermentation for cellulosic ethanol production. *Bioresource technology, 101 (13): 4862-4874.*

Breuil, C. and Saddler, J. 1985. Comparison of the 3, 5-dinitrosalicylic acid and Nelson-Somogyi methods of assaying for reducing sugars and determining cellulase activity. *Enzyme and Microbial Technology, 7 (7): 327-332*.

Brienzo, M., Carvalho, W. and Milagres, A. F. 2010. Xylooligosaccharides Production from Alkali-Pretreated Sugarcane Bagasse Using Xylanases from Thermoascus aurantiacus. *Appl Biochem Biotechnol, 162 (4): 1195-1205*.

Brienzo, M., Siqueira, A. and Milagres, A. M. 2009. Search for optimum conditions of sugarcane bagasse hemicellulose extraction. *Biochemical Engineering Journal, 46 (2): 199-204*.

Bugaje, I. 2006. Renewable energy for sustainable development in Africa: a review. *Renewable and Sustainable Energy Reviews, 10 (6): 603-612*.

Bui, N. T., Duong, L. T., Nguyen, T. T. and Tran, N. T. J. I. J. o. N. 2021. Heavy metal removal from polluted water by Nopal cactus biopolymer-based magnetic nanocomposites. 13 (1): 42-61.

Cao, P., Liu, H., Wu, D. and Wang, X. 2021. Immobilization of laccase on phase-change microcapsules as self-thermoregulatory enzyme carrier for biocatalytic enhancement. *Chemical Engineering Journal, 405: 126695*.

Cekmecelioglu, D. and Demirci, A. 2020. Production of Cellulase and Xylanase Enzymes Using Distillers Dried Grains with Solubles (DDGS) by Trichoderma reesei at Shake-Flask Scale and the Validation in the Benchtop Scale Bioreactor. *Waste and Biomass Valorization: 1-10*.

Celińska, E. and Nicaud, J.-M. 2019. Filamentous fungi-like secretory pathway strayed in a yeast system: peculiarities of Yarrowia lipolytica secretory pathway underlying its extraordinary performance. *Applied microbiology and biotechnology, 103 (1): 39-52*.

Chaichi, M. J. and Ehsani, M. 2016. A novel glucose sensor based on immobilization of glucose oxidase on the chitosan-coated Fe_3O_4 nanoparticles and the luminol–H_2O_2–gold nanoparticle chemiluminescence detection system. *Sensors and Actuators B: Chemical, 223: 713-722*.

Chapla, D., Pandit, P. and Shah, A. 2012. Production of xylooligosaccharides from corncob xylan by fungal xylanase and their utilization by probiotics. *Bioresource Technology, 115: 215-221*.

Chaudhary, D. S. J. J. o. a. p. s. 2010. Competitive plasticization in ternary plasticized starch biopolymer system. 118 (1): 486-495.

Chaudhary, R., Kuthiala, T., Singh, G., Rarotra, S., Kaur, A., Arya, S. K. and Kumar, P. 2021. Current status of xylanase for biofuel production: a review on classification and characterization. *Biomass Conversion and Biorefinery: 1-19*.

Chelladurai, S. J. S., Murugan, K., Ray, A. P., Upadhyaya, M., Narasimharaj, V. and Gnanasekaran, S. J. M. T. P. 2021. Optimization of process parameters using response surface methodology: *A review. 37: 1301-1304*.

Chen, J.-P., Yang, P.-C., Ma, Y.-H. and Wu, T. 2011. Characterization of chitosan magnetic nanoparticles for in situ delivery of tissue plasminogen activator. Carbohydrate polymers, 84 (1): 364-372.

Chen, Q., Liu, D., Wu, C., Yao, K., Li, Z., Shi, N., Wen, F. and Gates, I. D. J. B. t. 2018. Co-immobilization of cellulase and lysozyme on amino-functionalized magnetic nanoparticles: an activity-tunable biocatalyst for extraction of lipids from microalgae. 263: 317-324.

Cheng, G., Xing, J., Pi, Z., Liu, S., Liu, Z. and Song, F. J. C. C. L. 2019. α-Glucosidase immobilization on functionalized Fe_3O_4 magnetic nanoparticles for screening of enzyme inhibitors. 30 (3): 656-659.

Corrales, R. C. N. R., Mendes, F. M. T., Perrone, C. C., Sant'Anna, C., de Souza, W., Abud, Y., Bon, E. P. P. d. S. and Ferreira-Leitão, V. 2012. Structural evaluation of sugar cane bagasse steam pretreated in the presence of CO_2 and SO_2. *Biotechnology for biofuels, 5 (1): 1-8*.

Cipolatti, E. P., Silva, M. J. A., Klein, M., Feddern, V., Feltes, M. M. C., Oliveira, J. V., Ninow, J. L. and de Oliveira, D. 2014. Current status and trends in enzymatic nanoimmobilization. *Journal of Molecular Catalysis B: Enzymatic, 99: 56-67*.

Compeán, R. G. and Polenske, K. R. 2011. Antagonistic bioenergies: Technological divergence of the ethanol industry in Brazil. *Energy Policy, 39 (11): 6951-6961*.

Conde, J., Dias, J. T., Grazú, V., Moros, M., Baptista, P. V. and de la Fuente, J. M. 2014. Revisiting 30 years of biofunctionalization and surface chemistry of inorganic nanoparticles for nanomedicine. *Frontiers in chemistry, 2: 48*.

Cruz, M. L., de Resende, M. M., Ribeiro, E. J. J. B. and Engineering, B. 2021. Improvement of ethanol production in fed-batch fermentation using a mixture of sugarcane juice and molasse under very high-gravity conditions. 44 (3): 617-625.

Dalal, S., Sharma, A. and Gupta, M. N. J. C. C. J. 2007. A multipurpose immobilized biocatalyst with pectinase, xylanase and cellulase activities. 1 (1): 16.

Darwesh, O. M., Ali, S. S., Matter, I. A., Elsamahy, T. and Mahmoud, Y. A. J. M. i. e. 2020. Enzymes immobilization onto magnetic nanoparticles to improve industrial and environmental applications. 630: 481-502.

Dasgupta, D., Ghosh, D., Bandhu, S. and Adhikari, D. K. J. M. r. 2017. Lignocellulosic sugar management for xylitol and ethanol fermentation with multiple cell recycling by *Kluyveromyces marxianus* IIPE453. 200: 64-72.

De Castro, R. J. S., Ohara, A., Nishide, T. G., Albernaz, J. R. M., Soares, M. H., Sato, H. H. J. B. and Biotechnology, A. 2015. A new approach for proteases production by *Aspergillus niger* based on the kinetic and thermodynamic parameters of the enzymes obtained. 4 (2): 199-207.

Defaei, M., Taheri-Kafrani, A., Miroliaei, M. and Yaghmaei, P. J. I. j. o. b. m. 2018. Improvement of stability and reusability of α-amylase immobilized on naringin functionalized magnetic nanoparticles: A robust nanobiocatalyst. 113: 354-360.

Dehnavi, E., Siadat, S. O. R., Roudsari, M. F. and Khajeh, K. 2016. Cloning and high-level expression of β-xylosidase from Selenomonas ruminantium in *Pichia pastoris* by optimizing of pH, methanol concentration and temperature conditions. Protein expression and purification, 124: 55-61.

Della Torre, C. L., Silva-Lucca, R. A., Ferreira, R. d. S., Andrade Luz, L., Oliva, M. L. V., Kadowaki, M. K. J. B. and Biotransformation. 2021. Correlation of the conformational structure and catalytic activity of the highly thermostable xylanase of *Thermomyces lanuginosus* PC7S1T. 1-12.

Deng, Y., Ouyang, J., Wang, H., Yang, C., Zhu, Y., Wang, J., Li, D., Ma, K. J. B. and Biotransformation. 2021. Magnetic nanoparticles prepared in natural deep eutectic solvent for enzyme immobilisation. 1-11.

Dhiraj, N., Rutuja, N., Kalpesh, S., Sunil, K. J. A. J. o. P. R. and Development. 2020. Synthesis of Schiff's Bases With Simple Synthetic Approach. 8 (5): 72-74.

Dhoble, R. M., Lunge, S., Bhole, A. and Rayalu, S. 2011. Magnetic binary oxide particles (MBOP): a promising adsorbent for removal of As (III) in water. *Water research, 45 (16): 4769-4781*.

DiCosimo, R., McAuliffe, J., Poulose, A. J. and Bohlmann, G. J. C. S. R. 2013. Industrial use of immobilized enzymes. 42 (15): 6437-6474.

Digigow, R. G., Dechézelles, J.-F., Dietsch, H., Geissbühler, I., Vanhecke, D., Geers, C., Hirt, A. M., Rothen-Rutishauser, B. and Petri-Fink, A. 2014. Preparation and characterization of functional silica hybrid magnetic nanoparticles. *Journal of Magnetism and Magnetic Materials, 362: 72-79*.

Dincer, I. 2000. Renewable energy and sustainable development: a crucial review. Renewable and Sustainable Energy Reviews, 4 (2): 157-175.

Doner, L. W. and Hicks, K. B. 1997. Isolation of hemicellulose from corn fiber by alkaline hydrogen peroxide extraction. *Cereal Chemistry, 74 (2): 176-181*.

Dongre, R. S. J. H. o. C. 2019. Chitosan formulations: chemistry, characteristics and contextual adsorption in unambiguous modernization of S&T. 147.

Doria, G., Conde, J., Veigas, B., Giestas, L., Almeida, C., Assunção, M., Rosa, J. and Baptista, P. V. 2012. Noble metal nanoparticles for biosensing applications. *Sensors, 12 (2): 1657-1687.*

Du, X., He, J., Zhu, J., Sun, L. and An, S. J. A. S. S. 2012. Ag-deposited silica-coated Fe3O4 magnetic nanoparticles catalyzed reduction of p-nitrophenol. 258 (7): 2717-2723.

Dyal, A., Loos, K., Noto, M., Chang, S. W., Spagnoli, C., Shafi, K. V., Ulman, A., Cowman, M. and Gross, R. A. 2003. Activity of Candida rugosa lipase immobilized on γ-Fe_2O_3 magnetic nanoparticles. *Journal of the American Chemical Society, 125 (7): 1684-1685.*

Emamdadi, N., Gholizadeh, M. and Housaindokht, M. R. J. I. J. o. B. M. 2021. Investigation of static magnetic field effect on horseradish peroxidase enzyme activity and stability in enzymatic oxidation process. 170: 189-195.

Fanzo, J., Rudie, C., Sigman, I., Grinspoon, S., Benton, T. G., Brown, M. E., Covic, N., Fitch, K., Golden, C. D. and Grace, D. 2022. Sustainable food systems and nutrition in the 21st century: a report from the 22nd annual Harvard Nutrition Obesity Symposium. *The American Journal of Clinical Nutrition, 115 (1): 18-33.*

Farhan, L. O., Mehdi, W. A., Taha, E. M., Farhan, A. M., Mehde, A. A. and Özacar, M. J. I. J. o. B. M. 2021. Various type immobilizations of Isocitrate dehydrogenases enzyme on hyaluronic acid modified magnetic nanoparticles as stable biocatalysts. 182: 217-227.

Feng, J., Yu, S., Li, J., Mo, T. and Li, P. J. C. E. J. 2016. Enhancement of the catalytic activity and stability of immobilized aminoacylase using modified magnetic Fe_3O_4 nanoparticles. 286: 216-222.

Fernández-Fernández, M., Sanromán, M. Á. and Moldes, D. 2013. Recent developments and applications of immobilized laccase. *Biotechnology Advances, 31 (8): 1808-1825.*

Ferreira-Leitão, V. S., Soccol, C. R., Vandenberghe, L. P. d. S., Medeiros, A. B. P., Karp, S. G., Buckeridge, M., Ramos, L. P., Pitarelo, A. P., Gottschalk, L. M. F. and Ferrara, M. A. 2011. Bioethanol from lignocelluloses-status and perspectives in Brazil.

Gao, Y., Xu, J., Yuan, Z., Zhang, Y., Liu, Y. and Liang, C. 2014. Optimization of fed-batch enzymatic hydrolysis from alkali-pretreated sugarcane bagasse for high-concentration sugar production. *Bioresource technology, 167: 41-45.*

Gao, Y., Xu, Z., Chen, S., Gu, W., Chen, L. and Li, Y. 2008. Arginine-chitosan/DNA self-assemble nanoparticles for gene delivery: In vitro characteristics and transfection efficiency. *International journal of pharmaceutics, 359 (1-2): 241-246.*

Gao, X., Kumar, R. and Wyman, C.E., 2014. Fast hemicellulose quantification via a simple one-step acid hydrolysis. *Biotechnology and bioengineering*, *111*(6), pp.1088-1096.

Gashtasbi, F., Ahmadian, G., Noghabi, K. A. J. E. and Technology, M. 2014. New insights into the effectiveness of alpha-amylase enzyme presentation on the *Bacillus subtilis* spore surface by adsorption and covalent immobilization. 64: 17-23.

Gawali, S. L., Shelar, S. B., Gupta, J., Barick, K. and Hassan, P. J. I. J. o. B. M. 2021. Immobilization of protein on Fe3O4 nanoparticles for magnetic hyperthermia application. 166: 851-860.

Georgieva, S., Godjevargova, T., Portaccio, M., Lepore, M. and Mita, D. 2008. Advantages in using non-isothermal bioreactors in bioremediation of water polluted by phenol by means of immobilized laccase from *Rhus vernicifera*. *Journal of Molecular Catalysis B: Enzymatic, 55 (3-4): 177-184*.

Germec, M., Demirci, A., Turhan, I. J. B. and Biotechnology, A. 2020. Biofilm reactors for value-added products production: An in-depth review. 27: 101662.

Germec, M., Kartal, F. K., Bilgic, M., Ilgin, M., Ilhan, E., Güldali, H., Isci, A. and Turhan, I. J. B. p. 2016. Ethanol production from rice hull using *Pichia stipitis* and optimization of acid pretreatment and detoxification processes. 32 (4): 872-882.

Ghaeidamini, M., Kharat, A. N., Haertlé, T., Ahmad, F. and Saboury, A. A. J. T. J. o. P. C. B. 2018. β-Cyclodextrin-Modified Magnetic Nanoparticles Immobilized on Sepharose Surface Provide an Effective Matrix for Protein Refolding. 122 (43): 9907-9919.

Ghazanfari, M. R., Kashefi, M., Shams, S. F. and Jaafari, M. R. J. B. r. i. 2016. Perspective of Fe_3O_4 nanoparticles role in biomedical applications. 2016

Ghorbani-Vaghei, R., Veisi, H., Aliani, M. H., Mohammadi, P. and Karmakar, B. J. J. o. M. L. 2021. Alginate modified magnetic nanoparticles to immobilization of gold nanoparticles as an efficient magnetic nanocatalyst for reduction of 4-nitrophenol in water. 327: 114868.

Ghosh, A., Chandra, A., Dhar, A., Shukla, P. and Baishya, D. J. P. B. 2021. Multi-efficient thermostable endoxylanase from Bacillus velezensis AG20 and its production of xylooligosaccharides as efficient prebiotics with anticancer activity.

Ghosh, R., Pradhan, L., Devi, Y. P., Meena, S., Tewari, R., Kumar, A., Sharma, S., Gajbhiye, N., Vatsa, R. and Pandey, B. N. 2011. Induction heating studies of Fe_3O_4 magnetic nanoparticles capped with oleic acid and polyethylene glycol for hyperthermia. *Journal of Materials Chemistry, 21 (35): 13388-13398*.

Ghoshal, G., Banerjee, U. and Shivhare, U. 2014. Xylanase production by *Penicillium citrinum* in laboratory-scale stirred tank reactor. *Chemical and biochemical engineering quarterly, 28 (3): 399-408*.

González-Martínez, E., Pérez, A. G., González-Martínez, D. A., Águila, C. R. D., Urbina, E. C., Ramírez, D. U., Yee-Madeira, H. J. I. and Chemistry, N.-M. 2021. Chitosan-coated magnetic nanoparticles; exploring their potentialities for DNA and Cu (II) recovery. 51 (8): 1098-1107.

Gou, Z., Ma, N. L., Zhang, W., Lei, Z., Su, Y., Sun, C., Wang, G., Chen, H., Zhang, S. and Chen, G. 2020. Innovative hydrolysis of corn stover biowaste by modified magnetite laccase immobilized nanoparticles. *Environmental research, 188: 109829*.

Gramany, V., Khan, F. I., Govender, A., Bisetty, K., Singh, S. and Permaul, K. 2016. Cloning, expression, and molecular dynamics simulations of a xylosidase obtained from *Thermomyces lanuginosus*. *Journal of Biomolecular Structure and Dynamics, 34 (8): 1681-1692.*

Guerfali, M., Maalej-Achouri, I. and Belghith, H. 2013. Hydrolytic potential of Talaromyces thermophilus β-xylosidase and its use for continuous xylose production. *Food Technology and Biotechnology, 51 (4): 479-487*.

Gullón, P., González-Muñoz, M. J., Gool, M. P. v., Schols, H. A., Hirsch, J., Ebringerová, A. and Parajó, J. C. 2011a. Structural features and properties of soluble products derived from Eucalyptus globulus hemicelluloses. *Food Chemistry, 127 (4): 1798-1807*.

Gullón, P., Salazar, N., Muñoz, M. J. G., Gueimonde, M., Ruas-Madiedo, P., Clara, G. and Parajó, J. C. 2011b. Assessment on the fermentability of xylooligosaccharides from rice husks. *BioResources, 6 (3): 3096-3114.*

Guo, H., Lei, B., Yu, J., Chen, Y. and Qian, J. J. I. J. o. B. M. 2021. Immobilization of lipase by dialdehyde cellulose crosslinked magnetic nanoparticles.

Gupta, M. N., Kaloti, M., Kapoor, M. and Solanki, K. 2011. Nanomaterials as matrices for enzyme immobilization. *Artificial Cells, Blood Substitutes, and Biotechnology, 39 (2): 98-109*.

Hahn-Hägerdal, B., Galbe, M., Gorwa-Grauslund, M. F., Lidén, G. and Zacchi, G. 2006. Bio-ethanol – the fuel of tomorrow from the residues of today. *Trends in Biotechnology, 24 (12): 549-556*.

Han, J., Wang, L., Wang, Y., Dong, J., Tang, X., Ni, L. and Wang, L. 2018. Preparation and characterization of Fe_3O_4-NH_2@4-arm-PEG-NH_2, a novel magnetic four-arm polymer-nanoparticle composite for cellulase immobilization. *Biochemical Engineering Journal, 130: 90-98*.

Haq, Z. and Easterly, J. L. 2006. Agricultural residue availability in the United States. *Applied biochemistry and biotechnology, 129 (1-3): 3-21*.

Harris, A. D. and Ramalingam, C. 2010. Xylanases and its application in food industry: a review. *Journal of Experimental Sciences*

He, B.-Q., Wang, J.-X., Hao, J.-M., Yan, X.-G. and Xiao, J.-H. J. A. E. 2003. A study on emission characteristics of an EFI engine with ethanol blended gasoline fuels. 37 (7): 949-957.

Hebbale, D., Mishra, R. S. and Ramachandra, T. J. B. R. 2021. Prioritizing Wild Yeast Strains for Macroalgal Bioethanol Production. 1-16.

Hebraud, M. and Fevre, M. 1990. Purification and characterization of an extracellular β-xylosidase from the rumen anaerobic fungus *Neocallimastix frontalis*. *FEMS microbiology letters, 72 (1-2): 11-16*.

Heinen, P., Bauermeister, A., Ribeiro, L., Messias, J., Almeida, P., Moraes, L., Vargas-Rechia, C., De Oliveira, A., Ward, R. and Kadowaki, M. 2018. GH11 xylanase from *Aspergillus tamarii Kita*: Purification by one-step chromatography and xylooligosaccharides hydrolysis monitored in real-time by mass spectrometry. *International journal of biological macromolecules, 108: 291-299*.

Hema, S., Krishnan, A., Akther, A., Suresh, A., Sambhudevan, S. and Shankar, B. J. M. T. P. 2021. Green nanocomposites based on natural rubber latex containing xylan from sugarcane bagasse–Synthesis, characterization and dye absorption studies.

Hirsch, R. L., Bezdek, R. and Wendling, R. 2005. Peaking of world oil production: impacts, mitigation, & risk management. National Energy Technology Laboratory (NETL), Pittsburgh, PA, Morgantown, WV

Hess, T. M., Sumberg, J., Biggs, T., Georgescu, M., Haro-Monteagudo, D., Jewitt, G., Ozdogan, M., Marshall, M., Thenkabail, P. and Daccache, A. 2016. A sweet deal? Sugarcane, water and agricultural transformation in Sub-Saharan Africa. *Global environmental change, 39: 181-194*.

Hojnik Podrepšek, G., Knez, Ž. and Leitgeb, M. 2013. Different preparation methods and characterization of magnetic maghemite coated with chitosan. *Journal of Nanoparticle Research, 15 (6): 1751*.

Hola, K., Markova, Z., Zoppellaro, G., Tucek, J. and Zboril, R. 2015. Tailored functionalization of iron oxide nanoparticles for MRI, drug delivery, magnetic separation and immobilization of biosubstances. *Biotechnology Advances, 33 (6): 1162-1176*.

Hong, S., Chang, Y. and Rhee, I. 2010. Chitosan-coated ferrite (Fe3O4) nanoparticles as a T2 contrast agent for magnetic resonance imaging. *J. Korean Phys. Soc, 56 (3): 868-873*.

Hosseini, F., Seyedsadjadi, M. and Farhadyar, N. 2014. Fe3O4 nanoparticles modified with APTES as the carrier for (+)-(S)-2-(6-methoxynaphthalen-2-yl) propanoic acid (Naproxen) and (RS) 2-(3-benzoylphenyl)-propionic acid (Ketoprofen) drug. *Oriental Journal of Chemistry, 30 (4): 1609-1618*.

Huang, J., Zhao, R., Wang, H., Zhao, W. and Ding, L. 2010. Immobilization of glucose oxidase on Fe_3O_4/SiO_2 magnetic nanoparticles. *Biotechnology letters, 32 (6): 817-821*.

Huang, Y., Zheng, X., Pilgaard, B., Holck, J., Muschiol, J., Li, S. and Lange, L. 2019. Identification and characterization of GH11 xylanase and GH43 xylosidase from the chytridiomycetous fungus, *Rhizophlyctis rosea*. *Applied microbiology and biotechnology, 103 (2): 777-791*.

Huisman, G. W. and Collier, S. J. 2013. On the development of new biocatalytic processes for practical pharmaceutical synthesis. *Current Opinion in Chemical Biology, 17 (2): 284-292*.

Husain, Q. and Jan, U. 2000. Detoxification of phenols and aromatic amines from polluted wastewater by using phenol oxidases.

Ibrahim, S., Ahmad, Z., Manzoor, M. Z., Mujahid, M., Faheem, Z. and Adnan, A. J. S. R. 2021. Optimization for biogenic microbial synthesis of silver nanoparticles through response surface methodology, characterization, their antimicrobial, antioxidant, and catalytic potential. 11 (1): 1-18.

Irfan, M., Dogan, N., Bingolbali, A., Aliew, F. J. J. o. M. and Materials, M. 2021. Synthesis and characterization of $NiFe_2O_4$ magnetic nanoparticles with different coating materials for magnetic particle imaging (MPI). 537: 168150.

Jacobs, A. and Dahlman, O. 2001. Characterization of the molar masses of hemicelluloses from wood and pulps employing size exclusion chromatography and matrix-assisted laser desorption ionization time-of-flight mass spectrometry. *Biomacromolecules, 2 (3): 894-905*.

Jadhav, S., Nikam, D., Khot, V., Thorat, N., Phadatare, M., Ningthoujam, R., Salunkhe, A. and Pawar, S. 2013. Studies on colloidal stability of PVP-coated LSMO nanoparticles for magnetic fluid hyperthermia. *New Journal of Chemistry, 37 (10): 3121-3130*.

Jadhav, S. A. and Bongiovanni, R. 2012. Synthesis and organic functionalization approaches for magnetite (Fe_3O_4) nanoparticles. *Adv Mat Lett, 3 (5): 356-361*.

Jain, M., Sebatini, M., Sharmila, G., Muthukumaran, C., Baskar, G. and Tamilarasan, K. 2015. Fabrication of a Chitosan-Coated Magnetic Nanobiocatalyst for Starch Hydrolysis. *Chemical Engineering & Technology, 38 (8): 1444-1451*.

Jayapal, N., Samanta, A., Kolte, A. P., Senani, S., Sridhar, M., Suresh, K. and Sampath, K. 2013. Value addition to sugarcane bagasse: xylan extraction and its process optimization for xylooligosaccharides production. *Industrial Crops and Products, 42: 14-24*.

Jia, H., Zhu, G. and Wang, P. 2003. Catalytic behaviors of enzymes attached to nanoparticles: the effect of particle mobility. *Biotechnology and bioengineering, 84 (4): 406-414*.

Jin, X., Song, J., Ma, J. and Liu, G.-Q. 2020. Thermostable β-xylosidase from *Aspergillus fumigatus*: Purification, characterization and potential application in lignocellulose bioethanol production.

Jordan, D. B. and Wagschal, K. 2010. Properties and applications of microbial β-D-xylosidases featuring the catalytically efficient enzyme from *Selenodonts ruminantium*. *Applied Microbiology and Biotechnology, 86 (6): 1647-1658.*

Kačuráková, M., Belton, P. S., Wilson, R. H., Hirsch, J. and Ebringerová, A. 1998. Hydration properties of xylan‐type structures: an FTIR study of xylooligosaccharides. *Journal of the Science of Food and Agriculture, 77 (1): 38-44*.

Kačuráková, M., Ebringerova, A., Hirsch, J. and Hromadkova, Z. 1994. Infrared study of arabinoxylans. *Journal of the Science of Food and Agriculture, 66 (3): 423-427*.

Kačuráková, M., Wellner, N., Ebringerová, A., Hromádková, Z., Wilson, R. and Belton, P. 1999. Characterisation of xylan-type polysaccharides and associated cell wall components by FT-IR and FT-Raman spectroscopies. *Food hydrocolloids, 13 (1): 35-41*.

Lama, L., Calandrelli, V., Gambacorta, A. and Nicolaus, B. 2004. Purification and characterization of thermostable xylanase and β-xylosidase by the thermophilic bacterium *Bacillus thermantarcticus*. *Research in Microbiology, 155 (4): 283-289*.

Kambourova, M., Mandeva, R., Fiume, I., Maurelli, L., Rossi, M. and Morana, A. 2007. Hydrolysis of xylan at high temperature by co-action of the xylanase from *Anoxybacillus flavithermus* BC and the β‐xylosidase/α‐arabinosidase from *Sulfolobus solfataricus*. *Journal of applied microbiology, 102 (6): 1586-1593*.

Kanna, M., Yano, S., Inoue, H., Fujii, T. and Sawayama, S. 2011. Enhancement of β-xylosidase productivity in cellulase producing fungus *Acremonium cellulolyticus*. *AMB Express, 1 (1): 15*.

Karade, V., Sharma, A., Dhavale, R., Shingte, S., Patil, P., Kim, J., Zahn, D., Chougale, A., Salvan, G. and Patil, P. J. S. r. 2021. APTES monolayer coverage on self-assembled magnetic nanospheres for controlled release of anticancer drug Nintedanib. 11 (1): 1-12.

Katapodis, P., Nerinckx, W., Claeyssens, M. and Christakopoulos, P. 2006. Purification and characterization of a thermostable intracellular β-xylosidase from the thermophilic fungus *Sporotrichum thermophile*. *Process Biochemistry, 41 (12): 2402-2409.*

Kaur, H., Ghosh, S., Kumar, P., Basu, B. and Nagpal, K. J. L. S. 2021a. Ellagic acid-loaded, tween 80-coated, chitosan nanoparticles as a promising therapeutic approach against breast cancer: In-vitro and in-vivo study. 119927.

Kaur, P., Taggar, M. S., Kalia, A. J. B. C. and Biorefinery. 2021b. Characterization of magnetic nanoparticle–immobilized cellulases for enzymatic saccharification of rice straw. 11 (3): 955-969.

Kaur, P., Taggar, M. S. and Kalia, A. 2021. Characterization of magnetic nanoparticle–immobilized cellulases for enzymatic saccharification of rice straw. *Biomass Conversion and Biorefinery, 11 (3): 955-969.*

Khaire, K. C., Sharma, K., Thakur, A., Moholkar, V. S., Goyal, A. J. J. o. B. and Bioengineering. 2021. Extraction and characterization of xylan from sugarcane tops as a potential commercial substrate. 131 (6): 647-654.

Khaleghipour, L., Linares-Pastén, J. A., Rashedi, H., Ranaei Siadat, S. O., Jasilionis, A., Al-Hamimi, S., Sardari, R. R. and Karlsson, E. N. 2021. Extraction of sugarcane bagasse arabinoxylan, integrated with enzymatic production of xylo-oligosaccharides and separation of cellulose. *Biotechnology for biofuels, 14 (1): 1-19.*

Khanahmadi, M., Arezi, I., Amiri, M.-s. and Miranzadeh, M. 2018. Bioprocessing of agro-industrial residues for optimization of xylanase production by solid- state fermentation in flask and tray bioreactor. *Biocatalysis and Agricultural Biotechnology, 13: 272-282.*

Khoshkho, S. M., Mahdavian, M., Karimi, F., Karimi-Maleh, H. and Razaghi, P. 2022. Production of bioethanol from carrot pulp in the presence of *Saccharomyces cerevisiae* and beet molasses inoculum; A biomass based investigation. *Chemosphere, 286: 131688.*

Khoshnevisan, K., Bordbar, A.-K., Zare, D., Davoodi, D., Noruzi, M., Barkhi, M. and Tabatabaei, M. 2011. Immobilization of cellulase enzyme on superparamagnetic nanoparticles and determination of its activity and stability. *Chemical Engineering Journal, 171 (2): 669-673.*

Khucharoenphaisan, K., Tokuyama, S. and Kitpreechavanich, V. 2010. Purification and characterization of a high-thermostable β-xylanase from newly isolated *Thermomyces lanuginosus* THKU-49. *Mycoscience, 51: 405-410.*

Khucharoenphaisan, K., Tokuyama, S., Ratanakhanokchai, K. and Kitpreechavanich, V. 2010. Induction and repression of beta-xylanase of *Thermomyces lanuginosus* TISTR 3465. *Pakistan journal of biological sciences: PJBS, 13 (5): 209-215*.

Kim, E. H., Lee, H. S., Kwak, B. K. and Kim, B.-K. 2005. Synthesis of ferrofluid with magnetic nanoparticles by sonochemical method for MRI contrast agent. *Journal of Magnetism and Magnetic Materials, 289: 328-330.*

Kim, S.-J., Sim, H.-J., Kim, J.-W., Lee, Y.-G., Park, Y.-C. and Seo, J.-H. J. B. t. 2017. Enhanced production of 2, 3-butanediol from xylose by combinatorial engineering of xylose metabolic pathway and cofactor regeneration in pyruvate decarboxylase-deficient *Saccharomyces cerevisiae*. 245: 1551-1557.

Kim, S. and Dale, B. E. 2004. Global potential bioethanol production from wasted crops and crop residues. *Biomass and bioenergy, 26 (4): 361-375*.

Kim, S. and Dale, B. E. 2005. Life cycle assessment of various cropping systems utilized for producing biofuels: Bioethanol and biodiesel. *Biomass and Bioenergy, 29 (6): 426-439*.

Kim, Y.-K. and Lee, H. 2016. Use of magnetic nanoparticles to enhance bioethanol production in syngas fermentation. *Bioresource technology, 204: 139-144*.

Kim, Y.-K., Park, S. E., Lee, H. and Yun, J. Y. 2014. Enhancement of bioethanol production in syngas fermentation with Clostridium ljungdahlii using nanoparticles. *Bioresource technology, 159: 446-450.*

Kim, Y. A. and Yoon, K.-H. 2010. Characterization of a Paenibacillus woosongensis β-xylosidase/α-arabinofuranosidase produced by recombinant *Escherichia coli*. *J Microbiol Biotechnol, 20 (12): 1711-1716.*

Knob, A., Terrasan, C. and Carmona, E. 2010. β-Xylosidases from filamentous fungi: an overview. *World Journal of Microbiology and Biotechnology, 26 (3): 389-407.*

Kocabaş, D. S., Güder, S. and Özben, N. 2015. Purification strategies and properties of a low-molecular weight xylanase and its application in agricultural waste biomass hydrolysis. *Journal of Molecular Catalysis B: Enzymatic, 115: 66-75.*

Konde, K. S., Nagarajan, S., Kumar, V., Patil, S. V. and Ranade, V. V. 2021. Sugarcane bagasse based biorefineries in India: potential and challenges. *Sustainable Energy & Fuels, 5 (1): 52-78.*

Kootstra, A. M. J., Mosier, N. S., Scott, E. L., Beeftink, H. H. and Sanders, J. P. 2009. Differential effects of mineral and organic acids on the kinetics of arabinose degradation under lignocellulose pretreatment conditions. *Biochemical Engineering Journal, 43 (1): 92-97.*

Kumar, K. S., Manimaran, A., Permaul, K. and Singh, S. 2009. Production of β-xylanase by a *Thermomyces lanuginosus* MC 134 mutant on corn cobs and its application in biobleaching of bagasse pulp. *Journal of bioscience and bioengineering, 107 (5): 494-498.*

Kumar, R., Singh, S., Singh, O. V. J. J. o. i. m. and biotechnology. 2008. Bioconversion of lignocellulosic biomass: biochemical and molecular perspectives. 35 (5): 377-391.

Kumar, V., Chhabra, D. and Shukla, P. J. B. t. 2017. Xylanase production from *Thermomyces lanuginosus* VAPS-24 using low cost agro-industrial residues via hybrid optimization tools and its potential use for saccharification. 243: 1009-1019.

Kumar, V., Dangi, A. K. and Shukla, P. 2018. Engineering thermostable microbial xylanases toward its industrial applications. *Molecular biotechnology, 60 (3): 226-235*.

Kumar, V., Marin-Navarro, J. and Shukla, P. 2016. Thermostable microbial xylanases for pulp and paper industries: trends, applications and further perspectives. *World Journal of Microbiology and Biotechnology, 32 (2): 34*.

Kumari, S. and Das, D. 2015. Improvement of gaseous energy recovery from sugarcane bagasse by dark fermentation followed by biomethanation process. *Bioresource Technology, 194: 354-363*.

Kurian, J. K., Ashok, M. K., Banerjee, A. and Kishore, V. J. B. 2010. Bioconversion of hemicellulose hydrolysate of sweet sorghum bagasse to ethanol by using *Pichia stipitis* NCIM 3497 and *Debaryomyces hansenii* sp. 5 (4): 2404-2416.

Ladole, M. R., Pokale, P. B., Varude, V. R., Belokar, P. G. and Pandit, A. B. J. I. J. o. B. M. 2021. One pot clarification and debittering of grapefruit juice using co-immobilized enzymes@ chitosan MNPs. 167: 1297-1307.

Laemmli, U. K. 1970. Cleavage of structural proteins during the assembly of the head of bacteriophage T4. *Nature, 227 (5259): 680-685*.

Lama, L., Calandrelli, V., Gambacorta, A. and Nicolaus, B. 2004. Purification and characterization of thermostable xylanase and β-xylosidase by the thermophilic bacterium *Bacillus thermantarcticus*. *Research in Microbiology, 155 (4): 283-289*.

Lapeña, D., Olsen, P. M., Arntzen, M. Ø., Kosa, G., Passoth, V., Eijsink, V. G., Horn, S. J. J. B. and engineering, b. 2020. Spruce sugars and poultry hydrolysate as growth medium in repeated fed-batch fermentation processes for production of yeast biomass. 43 (4): 723-736.

Lee, A., Jin, H. and Cha, J. 2022. Engineering of *Sulfolobus acidocaldarius* for Hemicellulosic Biomass Utilization.

Lee, C., Teng, Q., Zhong, R. and Ye, Z.-H. 2011. Molecular dissection of xylan biosynthesis during wood formation in poplar. *Molecular plant, 4 (4): 730-747*.

Lee, S.-M., Jin, L. H., Kim, J. H., Han, S. O., Na, H. B., Hyeon, T., Koo, Y.-M., Kim, J. and Lee, J.-H. 2010. β-Glucosidase coating on polymer nanofibers for improved cellulosic ethanol production. *Bioprocess and biosystems engineering, 33 (1): 141*.

Lee, S.-Y., Chen, F. and Lee, T. Y. J. A. 2021. Tryptamine-functionalized magnetic nanoparticles for highly sensitive detection of *Salmonella typhimurium*. 146 (8): 2559-2566.

Leridon, H. 2020. World population outlook: Explosion or implosion? Population Societies, (1): 1-4

Li, Q., Wu, T., Qi, Z., Zhao, L., Pei, J. and Tang, F. 2018. Characterization of a novel thermostable and xylose-tolerant GH 39 β-xylosidase from *Dictyoglomus thermophilum*. BMC biotechnology, 18 (1): 29.

Li, T., Yu, Z., Yang, T., Xu, G., Guan, Y., Guo, C. J. E. T. and Innovation. 2021. Modified Fe3O4 magnetic nanoparticles for COD removal in oil field produced water and regeneration. 23: 101630.

Li, X., She, Y., Sun, B., Song, H., Zhu, Y., Lv, Y. and Song, H. 2010. Purification and characterization of a cellulase-free, thermostable xylanase from *Streptomyces rameus* L2001 and its biobleaching effect on wheat straw pulp. *Biochemical Engineering Journal, 52 (1): 71-78.*

Li, X. T., Jiang, Z. Q., Li, L. T., Yang, S. Q., Feng, W. Y., Fan, J. Y. and Kusakabe, I. 2005a. Characterization of a cellulase-free, neutral xylanase from *Thermomyces lanuginosus* CBS 288.54 and its biobleaching effect on wheat straw pulp. Bioresource Technology, 96 (12): 1370-1379.

Li, Z., Wei, L., Gao, M. and Lei, H. 2005b. One‐Pot Reaction to Synthesize Biocompatible Magnetite Nanoparticles. *Advanced Materials, 17 (8): 1001-1005*.

Liang, H., Jiang, S., Yuan, Q., Li, G., Wang, F., Zhang, Z. and Liu, J. 2016. Co-immobilization of multiple enzymes by metal coordinated nucleotide hydrogel nanofibers: improved stability and an enzyme cascade for glucose detection. *Nanoscale, 8 (11): 6071-6078*.

Liao, J., Han, S., Li, X., He, J., Secundo, F. and Liang, H. J. I. J. o. B. M. 2020. Co-immobilization of two-component hydroxylase monooxygenase by functionalized magnetic nanoparticles for preserving high catalytic activity and enhancing enzyme stability. 164: 3163-3170.

Liao, M.-H. and Chen, D.-H. 2001. Immobilization of yeast alcohol dehydrogenase on magnetic nanoparticles for improving its stability. *Biotechnology letters, 23 (20): 1723-1727.*

Lin, J., Ndlovu, L. M., Singh, S. and Pillay, B. 1999. Purification and biochemical characteristics of β‐D‐xylanase from a thermophilic fungus, *Thermomyces lanuginosus*‐SSBP. *Biotechnology and Applied Biochemistry, 30 (1): 73-79*.

Liu, E., Segato, F. and Wilkins, M. R. J. B. T. 2021. Fed-batch production of *Thermothelomyces thermophilus* lignin peroxidase using a recombinant *Aspergillus nidulans* strain in stirred-tank bioreactor. 325: 124700.

Liu, M.-q., Dai, X.-j., Guan, R.-f. and Xu, X. J. C. C. 2014. Immobilization of *Aspergillus niger* xylanase A on Fe3O4-coated chitosan magnetic nanoparticles for xylooligosaccharide preparation. 55: 6-10.

Liu, Q., Fan, H., Mou, H., Liu, J., Huang, J., Dong, X., Song, H. J. I. C. and Products. 2021a. Preparation and characterization of xylan by an efficient approach with mechanical pretreatments. 165: 113420.

Liu, X., Jiang, Z., Liu, Y., You, X., Yang, S. and Yan, Q. J. B. f. b. 2019. Biochemical characterization of a novel exo-oligoxylanase from *Paenibacillus barengoltzii* suitable for monosaccharification from corncobs. 12 (1): 1-14.

Liu, Z., Shi, E., Ma, F. and Jiang, K. 2021b. An integrated biorefinery process for co-production of xylose and glucose using maleic acid as efficient catalyst. *Bioresource technology, 325: 124698*.

Long, J., Pan, T., Xie, Z., Xu, X. and Jin, Z. J. L. 2020. Co-immobilization of β-fructofuranosidase and glucose oxidase improves the stability of Bi-enzymes and the production of lactosucrose. 128: 109460.

López, M. C., Mateo, J. J. and Maicas, S. 2015. Screening of β - Glucosidase and β - Xylosidase Activities in Four Non - *Saccharomyces* Yeast Isolates. *Journal of food science, 80 (8): C1696-C1704*.

Lu, A. H., Salabas, E. e. L. and Schüth, F. 2007. Magnetic nanoparticles: synthesis, protection, functionalization, and application. *Angewandte Chemie International Edition, 46 (8): 1222-1244*.

Lu, C., Jing, Y., Zhang, H., Lee, D.-J., Tahir, N., Zhang, Q., Li, W., Wang, Y., Liang, X. and Wang, J. J. B. t. 2020. Biohydrogen production through active saccharification and photo-fermentation from alfalfa. 304: 123007.

Ma, W., Ya, F.-Q., Han, M. and Wang, R. 2007. Characteristics of equilibrium, kinetics studies for adsorption of fluoride on magnetic-chitosan particle. *Journal of Hazardous Materials, 143 (1-2): 296-302*.

Ma, Y., Luo, M., Xu, Y., Liu, Y., Liu, X., Bi, X., Yuan, Y., Su, F. and Yin, X. 2020. Purification and characterization of a thaumatin-like protein-1 with polyphenol oxidase activity found in Prunus mume. *RSC Advances, 10 (48): 28746-28754*.

Machida, M., Asai, K., Sano, M., Tanaka, T., Kumagai, T., Terai, G., Kusumoto, K.-I., Arima, T., Akita, O. and Kashiwagi, Y. 2005. Genome sequencing and analysis of *Aspergillus oryzae*. *Nature, 438 (7071): 1157*.

Mah, M. H., Lam, M. Q., Tokiman, L., Kamaroddin, M. F., Ibrahim, Z., Shahir, S. and Chong, C. S. 2021. Revealing the Potential of Xylanase from a New Halophilic *Microbulbifer* sp. CL37 with Paper De-Inking Ability. *Arabian Journal for Science and Engineering: 1-11*.

Maier-Hauff, K., Ulrich, F., Nestler, D., Niehoff, H., Wust, P., Thiesen, B., Orawa, H., Budach, V. and Jordan, A. 2011. Efficacy and safety of intratumoral thermotherapy using magnetic iron-oxide nanoparticles combined with external beam radiotherapy on patients with recurrent glioblastoma multiforme. *Journal of neuro-oncology, 103 (2): 317-324*.

Martín, C., Galbe, M., Wahlbom, C. F., Hahn-Hägerdal, B. and Jönsson, L. J. 2002. Ethanol production from enzymatic hydrolysates of sugarcane bagasse using recombinant xylose-utilising *Saccharomyces cerevisiae*. *Enzyme and Microbial Technology, 31 (3): 274-282*.

Matkawala, F., Nighojkar, S., Kumar, A. and Nighojkar, A. 2019. A novel thiol-dependent serine protease from *Neocosmospora* sp. N1. *Heliyon, 5 (8): e02246.*

Matsuzawa, T., Kameyama, A. and Yaoi, K. 2020. Identification and characterization of α-xylosidase involved in xyloglucan degradation in Aspergillus oryzae. *Applied Microbiology and Biotechnology, 104 (1): 201-210.*

Mattos, C. and Ringe, D. 2001. Proteins in organic solvents. *Current opinion in structural biology, 11 (6): 761-764.*

Maziero, P., de Oliveira Neto, M., Machado, D., Batista, T., Cavalheiro, C. C. S., Neumann, M. G., Craievich, A. F., de Moraes Rocha, G. J., Polikarpov, I. and Gonçalves, A. R. 2012. Structural features of lignin obtained at different alkaline oxidation conditions from sugarcane bagasse. *Industrial Crops and Products, 35 (1): 61-69.*

McGrath, T. 1977. Substrate stabilization of lysozyme to thermal and guanidine hydrochloride denaturation. Texas A&M University.

Mchunu, N. P., Permaul, K., Abdul Rahman, A. Y., Saito, J. A., Singh, S. and Alam, M. 2013. Xylanase superproducer: genome sequence of a compost-loving thermophilic fungus, *Thermomyces lanuginosus* strain SSBP. *Genome announcements, 1 (3): e00388-00313.*

Melo, M. N., Pereira, F. M., Rocha, M. A., Ribeiro, J. G., Diz, F. M., Monteiro, W. F., Ligabue, R. A., Severino, P. and Fricks, A. T. J. P. B. 2020. Immobilization and characterization of Horseradish Peroxidase into Chitosan and Chitosan/PEG nanoparticles: A comparative study. 98: 160-171.

Mhetras, N., Liddell, S. and Gokhale, D. 2016. Purification and characterization of an extracellular β-xylosidase from Pseudozyma hubeiensis NCIM 3574 (PhXyl), an unexplored yeast. *Amb Express, 6 (1): 73.*

Micheal, A. and Moussa, R. R. 2021. Investigating the Economic and Environmental Effect of Integrating Sugarcane Bagasse (SCB) Fibers in Cement Bricks. *Ain Shams Engineering Journal*

Michelin, M., Maria de Lourdes, T., Ruzene, D. S., Silva, D. P., Ruiz, H. A., Vicente, A. A., Jorge, J. A., Terenzi, H. F. and Teixeira, J. A. 2012. Production of xylanase and β-xylosidase from autohydrolysis liquor of corncob using two fungal strains. *Bioprocess and biosystems engineering, 35 (7): 1185-1192.*

Miller, G. L., Blum, R., Glennon, W. E. and Burton, A. L. 1960. Measurement of carboxymethyl cellulase activity. *Analytical Biochemistry, 1 (2): 127-132.*

Mirkin, C. A., Letsinger, R. L., Mucic, R. C. and Storhoff, J. J. 1996. A DNA-based method for rationally assembling nanoparticles into macroscopic materials. *Nature, 382 (6592): 607-609.*

Mohammadi, H. and Shaterian, H. R. J. A. O. C. 2019. (3 ‐ Oxo ‐ [1, 2, 4] triazolidin ‐ 1 ‐ yl) bis (butane ‐ 1 ‐ sulfonic acid) functionalized magnetic γ ‐ Fe_2O_3 nanoparticles: A novel and heterogeneous nanocatalyst for one ‐ pot and efficient four ‐ component synthesis of novel spiro [indeno [1, 2 ‐ b] quinoxaline derivatives. 33 (6): e4901.

Mohammadi, M., Mokarram, R. R., Ghorbani, M. and Hamishehkar, H. J. I. j. o. b. m. 2019. Inulinase immobilized gold-magnetic nanoparticles as a magnetically recyclable biocatalyst for facial and efficient inulin biotransformation to high fructose syrup. 123: 846-855.

Mohammed, A. J. and Shaker, A. H. 2020. Purification of Urokinase Enzyme from Serum Blood of Patients with Pneumonia. Female Patient, 28 (158.1): 9.59.

Mohapatra, B. R. 2021. Characterization of β-mannanase extracted from a novel *Streptomyces* species Alg-S25 immobilized on chitosan nanoparticles. *Biotechnology & Biotechnological Equipment, 35 (1): 150-161.*

Moodley, P., Sewsynker-Sukai, Y. and Kana, E. G. 2020. Progress in the development of alkali and metal salt catalysed lignocellulosic pretreatment regimes: Potential for bioethanol production. *Bioresource technology, 310: 123372.*

Morais, C. G., Cadete, R. M., Uetanabaro, A. P. T., Rosa, L. H., Lachance, M.-A. and Rosa, C. A. 2013a. D-xylose-fermenting and xylanase-producing yeast species from rotting wood of two Atlantic Rainforest habitats in Brazil. Fungal genetics and biology, 60: 19-28.

Morais, C. G., Lara, C. A., Marques, S., Fonseca, C., Lachance, M.-A. and Rosa, C. A. 2013b. *Sugiyamaella xylanicola* sp. nov., a xylan-degrading yeast species isolated from rotting wood. International journal of systematic and evolutionary microbiology, 63 (6): 2356-2360.

Motta, F., Andrade, C. and Santana, M. 2013. A review of xylanase production by the fermentation of xylan: classification, characterization and applications. Sustainable degradation of lignocellulosic biomass-techniques, applications and commercialization, 1

Mou, X., Ali, Z., Li, S., He, N. J. J. o. n. and nanotechnology. 2015. Applications of magnetic nanoparticles in targeted drug delivery system. 15 (1): 54-62.

Moutta, R. D. O., Ferreira-Leitão, V. S. and Bon, E. P. D. S. 2014. Enzymatic hydrolysis of sugarcane bagasse and straw mixtures pretreated with diluted acid. *Biocatalysis and Biotransformation, 32 (1): 93-100.*

Murray, C. B., Kagan, C. and Bawendi, M. 2000. Synthesis and characterization of monodisperse nanocrystals and close-packed nanocrystal assemblies. Annual Review of Materials Science, 30 (1): 545-610.

Mustafa, G., Kousar, S., Rajoka, M. I. and Jamil, A. 2016. Molecular cloning and comparative sequence analysis of fungal β-Xylosidases. *AMB Express, 6 (1): 30*.

Naicker, C., Nombona, N. and van Zyl, W. E. J. C. P. 2020. Fabrication of novel magnetic chitosan/graphene-oxide/metal oxide nanocomposite beads for Cr (VI) adsorption. 74 (2): 529-541.

Nallamuthu, I., Devi, A. and Khanum, F. J. a. j. o. p. s. 2015. Chlorogenic acid loaded chitosan nanoparticles with sustained release property, retained antioxidant activity and enhanced bioavailability. 10 (3): 203-211.

Naskar, S., Sharma, S. and Kuotsu, K. 2019. Chitosan-based nanoparticles: An overview of biomedical applications and its preparation. *Journal of Drug Delivery Science and Technology, 49: 66-81*.

Neamţu, B., Isnard, O., Chicinaş, I., Vagner, C., Jumate, N., Plaindoux, P. J. M. C. and Physics. 2011. Influence of benzene on the Ni_3Fe nanocrystalline compound formation by wet mechanical alloying: An investigation combining DSC, X-ray diffraction, mass and IR spectrometries. 125 (3): 364-369.

Nel, W. P. and Cooper, C. J. 2009. Implications of fossil fuel constraints on economic growth and global warming. *Energy Policy, 37 (1): 166-180*.

Neto, M., Hassuani, S., Leal, M. and Macedo, I. 2005. Characterization of sugarcane trash and bagasse. *Biomass Power Generation. Sugarcane Bagasse and Trash: 24*.

Nordin, A. H., Wong, S., Ngadi, N., Zainol, M. M., Abd Latif, N. A. F. and Nabgan, W. J. J. o. E. C. E. 2021. Surface functionalization of cellulose with polyethyleneimine and magnetic nanoparticles for efficient removal of anionic dye in wastewater. 9 (1): 104639.

Okamoto, K., Goda, T., Yamada, T. and Nagoshi, M. J. F. 2021. Direct Ethanol Production from Xylan and Acorn Using the Starch-Fermenting Basidiomycete Fungus *Phlebia acerina*. 7 (3): 116.

Olguin-Maciel, E., Singh, A., Chable-Villacis, R., Tapia-Tussell, R. and Ruiz, H. A. 2020. Consolidated bioprocessing, an innovative strategy towards sustainability for biofuels production from crop residues: an overview. *Agronomy, 10 (11): 1834*.

Olsson, L. and Hahn-Hägerdal, B. 1996. Fermentation of lignocellulosic hydrolysates for ethanol production. *Enzyme and Microbial Technology, 18 (5): 312-331*.

Panchuk, M., Kryshtopa, S., Sładkowski, A. and Panchuk, A. 2020. Environmental aspects of the production and use of biofuels in transport. Ecology in Transport: Problems and Solutions. Lecture Notes in Networks and Systems (LNNS, volume 124). Springer Nature: 115-168.

Patel, H., Divecha, J. and Shah, A. 2018. Enhanced production of β-xylosidase from *Aspergillus niger* ADH-11 and development of synergistic enzyme cocktail for saccharification of sugarcane bagasse. *Current Biotechnology, 7 (4): 273-287*.

Pathak, P., Bhardwaj, N. K. and Singh, A. K. 2014. Production of crude cellulase and xylanase from *Trichoderma harzianum* PPDDN10 NFCCI-2925 and its application in photocopier wastepaper recycling. *Applied Biochemistry and Biotechnology, 172 (8): 3776-3797*.

Patiño, M. A., Ortiz, J. P., Velásquez, M. and Stambuk, B. U. 2019. D‐Xylose consumption by nonrecombinant *Saccharomyces cerevisiae*: a review. Yeast, 36 (9): 541-556.

Pavlovic, M., Rouster, P. and Szilagyi, I. J. N. 2017. Synthesis and formulation of functional bionanomaterials with superoxide dismutase activity. 9 (1): 369-379.

Pečová, M., Šebela, M., Markova, Z., Polakova, K., Čuda, J., Šafářová, K. and Zbořil, R. 2013. Thermostable trypsin conjugates immobilized to biogenic magnetite show a high operational stability and remarkable reusability for protein digestion. *Nanotechnology, 24 (12): 125102*.

Peng, F., Ren, J.-L., Xu, F., Bian, J., Peng, P. and Sun, R.-C. 2009. Comparative study of hemicelluloses obtained by graded ethanol precipitation from sugarcane bagasse. *Journal of Agricultural and Food Chemistry, 57 (14): 6305-6317*.

Peng, H.-P., Liang, R.-P. and Qiu, J.-D. 2011. Facile synthesis of Fe_3O_4@ Al_2O_3 core–shell nanoparticles and their application to the highly specific capture of heme proteins for direct electrochemistry. Biosensors and Bioelectronics, 26 (6): 3005-3011.

Pérez-Burillo, S., Molino, S., Navajas-Porras, B., Valverde-Moya, Á. J., Hinojosa-Nogueira, D., López-Maldonado, A., Pastoriza, S. and Rufián-Henares, J. Á. J. N. P. 2021. An in vitro batch fermentation protocol for studying the contribution of food to gut microbiota composition and functionality. 1-24.

Perwez, M., Ahmad, R. and Sardar, M. J. I. j. o. b. m. 2017. A reusable multipurpose magnetic nanobiocatalyst for industrial applications. 103: 16-24.

Piosik, E., Ziegler-Borowska, M., Chełminiak-Dudkiewicz, D. and Martyński, T. J. I. J. o. M. S. 2021. Effect of Aminated Chitosan-Coated Fe_3O_4 Nanoparticles with Applicational Potential in Nanomedicine on DPPG, DSPC, and POPC Langmuir Monolayers as Cell Membrane Models. 22 (5): 2467.

Polizeli, M., Rizzatti, A., Monti, R., Terenzi, H., Jorge, J. A. and Amorim, D. 2005. Xylanases from fungi: properties and industrial applications. *Applied Microbiology and Biotechnology, 67 (5): 577-591*.

Polizzi, K. M., Bommarius, A. S., Broering, J. M. and Chaparro-Riggers, J. F. 2007. Stability of biocatalysts. *Current Opinion in Chemical Biology, 11 (2): 220-225.*

Poorakbar, E., Shafiee, A., Saboury, A. A., Rad, B. L., Khoshnevisan, K., Ma'mani, L., Derakhshankhah, H., Ganjali, M. R. and Hosseini, M. J. P. b. 2018. Synthesis of magnetic gold mesoporous silica nanoparticles core shell for cellulase enzyme immobilization: improvement of enzymatic activity and thermal stability. 71: 92-100.

Prajapati, B. P., Jana, U. K., Suryawanshi, R. K. and Kango, N. 2020. Sugarcane bagasse saccharification using *Aspergillus tubingensis* enzymatic cocktail for 2G bio-ethanol production. *Renewable Energy, 152: 653-663.*

Prasad Uday, U. S., Bandyopadhyay, T. K., Goswami, S. and Bhunia, B. J. B. 2017. Optimization of physical and morphological regime for improved cellulase free xylanase production by fed batch fermentation using *Aspergillus niger* (KP874102. 1) and its application in bio-bleaching. 8 (2): 137-146.

Prasoulas, G., Gentikis, A., Konti, A., Kalantzi, S., Kekos, D. and Mamma, D. 2020. Bioethanol production from food waste applying the multienzyme system produced on-site by *Fusarium oxysporum* F3 and mixed microbial cultures. *Fermentation, 6 (2): 39.*

Price, N. and Stevens, L. 1999. Enzyme technology, fundamentals of enzymology: The cell and molecular biology of catalytic proteins: Oxford University Press, UK.

Qing, Q., Yang, B. and Wyman, C. E. 2010. Xylooligomers are strong inhibitors of cellulose hydrolysis by enzymes. *Bioresource technology, 101 (24): 9624-9630.*

Qiu, X., Wang, S., Miao, S., Suo, H., Xu, H. and Hu, Y. J. J. o. H. M. 2021. Co-immobilization of laccase and ABTS onto amino-functionalized ionic liquid-modified magnetic chitosan nanoparticles for pollutants removal. 401: 123353.

Ramírez, N., Ubilla, C., Campos, J., Valencia, F., Aburto, C., Vera, C., Illanes, A. and Guerrero, C. J. B. T. 2021. Enzymatic production of lactulose by fed-batch and repeated fed-batch reactor. 125769.

Ranjbakhsh, E., Bordbar, A., Abbasi, M., Khosropour, A. and Shams, E. 2012. Enhancement of stability and catalytic activity of immobilized lipase on silica-coated modified magnetite nanoparticles. *Chemical Engineering Journal, 179: 272-276.*

Ravindran, R. and Jaiswal, A. K. 2016. A comprehensive review on pre-treatment strategy for lignocellulosic food industry waste: challenges and opportunities. *Bioresource Technology, 199: 92-102.*

Rawoof, S. A. A., Kumar, P. S., Vo, D.-V. N., Devaraj, K., Mani, Y., Devaraj, T. and Subramanian, S. J. E. C. L. 2021. Production of optically pure lactic acid by microbial fermentation: a review. 19 (1): 539-556.

Reddy, S. S. and Krishnan, C. 2016. Production of high-pure xylooligosaccharides from sugarcane bagasse using crude β-xylosidase-free xylanase of *Bacillus subtilis* KCX006 and their bifidogenic function. *LWT-Food Science and Technology, 65: 237-245*.

Repo, A., Tuomi, M. and Liski, J. 2011. Indirect carbon dioxide emissions from producing bioenergy from forest harvest residues. *Gcb Bioenergy, 3 (2): 107-115*.

Robert, P., Marquis, M., Barron, C., Guillon, F. and Saulnier, L. 2005. FT-IR investigation of cell wall polysaccharides from cereal grains. Arabinoxylan infrared assignment. *Journal of Agricultural and Food Chemistry, 53 (18): 7014-7018.*

Romero, A., Mateo, J. and Maicas, S. 2012. Characterization of an ethanol‐tolerant 1, 4‐β‐xylosidase produced by *Pichia membranifaciens*. *Letters in applied microbiology, 55 (5): 354-361*.

Sabiha-Hanim, S., Noor, M. A. M. and Rosma, A. 2015. Fractionation of oil palm frond hemicelluloses by water or alkaline impregnation and steam explosion. *Carbohydrate polymers, 115: 533-539.*

Saleem, A., Waris, S., Ahmed, T. and Tabassum, R. J. I. J. o. B. M. 2021. Biochemical characterization and molecular docking of cloned xylanase gene from Bacillus subtilis RTS expressed in E. coli. 168: 310-321.

Salem, K., Jabalera, Y., Puentes-Pardo, J. D., Vilchez-Garcia, J., Sayari, A., Hmida-Sayari, A., Jimenez-Lopez, C., Perduca, M. J. A. S. C. and Engineering. 2021. Enzyme Storage and Recycling: Nano assemblies of α-Amylase and Xylanase Immobilized on Biomimetic Magnetic Nanoparticles. 9 (11): 4054-4063.

Samanta, A., Jayapal, N., Kolte, A., Senani, S., Sridhar, M., Suresh, K. and Sampath, K. 2012. Enzymatic production of xylooligosaccharides from alkali solubilized xylan of natural grass (Sehima nervosum). *Bioresource Technology, 112: 199-205.*

Sánchez-Ramírez, J., Martínez-Hernández, J. L., Segura-Ceniceros, P., López, G., Saade, H., Medina-Morales, M. A., Ramos-González, R., Aguilar, C. N. and Ilyina, A. 2017. Cellulases immobilization on chitosan-coated magnetic nanoparticles: application for Agave Atrovirens lignocellulosic biomass hydrolysis. *Bioprocess and biosystems engineering, 40 (1): 9-22*.

Sanchez, O. J. and Cardona, C. A. 2008. Trends in biotechnological production of fuel ethanol from different feedstocks. *Bioresource technology, 99 (13): 5270-5295*.

Sanjuan, R., Anzaldo, J., Vargas, J., Turrado, J. and Patt, R. 2001. Morphological and chemical composition of pith and fibers from Mexican sugarcane bagasse. Holz als Roh-und Werkstoff, 59 (6): 447-450.

Santos, E. C. d. S., Watanabe, A., Vargas, M. D., Tanaka, M. N., Garcia, F. and Ronconi, C. M. J. N. J. o. C. 2018. AMF-responsive doxorubicin loaded β-cyclodextrin-decorated superparamagnetic nanoparticles. 42 (1): 671-680.

Sáringer, S., Rouster, P., Szilagyi, I. J. J. o. C. and Science, I. 2021. Co-immobilization of antioxidant enzymes on titania nanosheets for reduction of oxidative stress in colloid systems. 590: 28-37.

Saroj, P., Manasa, P. and Narasimhulu, K. 2018. Characterization of thermophilic fungi producing extracellular lignocellulolytic enzymes for lignocellulosic hydrolysis under solid-state fermentation. *Bioresources and Bioprocessing, 5 (1): 31*.

Schneider, G., Strehaiano, P., Taillandier, P. J. J. o. C. T., *Biotechnology: International Research in Process, E. and Technology, C. 2001*. Improvement of a fed ‐ batch process for high level xylanase production by a Bacillus strain. 76 (5): 456-460.

Seemakram, W., Boonrung, S., Aimi, T., Ekprasert, J., Lumyong, S. and Boonlue, S. J. S. R. 2020a. Purification, characterization and partial amino acid sequences of thermo-alkali-stable and mercury ion-tolerant xylanase from *Thermomyces dupontii* KKU–CLD–E2 ‐ 3. 10 (1): 1-10.

Seemakram, W., Boonrung, S., Kokaew, U., Aimi, T. and Boonlue, S. J. C. M. J. S. 2020b. Optimization of culture conditions for xylanase production from cellulase-free xylanase-producing thermophilic fungus, *Thermomyces dupontii* KKU− CLD− E2− 3. 47: 391-402.

Seetaha, S., Ratanabanyong, S. and Choowongkomon, K. 2019. Expression, purification, and characterization of the native intracellular domain of human epidermal growth factor receptors 1 and 2 in *Escherichia coli*. *Applied microbiology and biotechnology, 103 (20): 8427-8438*.

Selden, C. and Fuller, B. 2018. Role of bioreactor technology in tissue engineering for clinical use and therapeutic target design. *Bioengineering, 5 (2): 32*.

Shah, A. R. and Madamwar, D. 2005. Xylanase production by a newly isolated *Aspergillus foetidus* strain and its characterization. Process *Biochemistry, 40 (5): 1763-1771*.

Shah, M. I., Javed, M. F., Aslam, F. and Alabduljabbar, H. 2022. Machine learning modeling integrating experimental analysis for predicting the properties of sugarcane bagasse ash concrete. *Construction and Building Materials, 314: 125634*.

Shahedi, M., Habibi, Z., Yousefi, M., Brask, J. and Mohammadi, M. J. I. J. o. B. M. 2021. Improvement of biodiesel production from palm oil by co-immobilization of *Thermomyces*

lanuginosas lipase and *Candida antarctica* lipase B: Optimization using response surface methodology. 170: 490-502.

Shahedi, M., Yousefi, M., Habibi, Z., Mohammadi, M. and As' habi, M. A. J. R. E. 2019. Co-immobilization of *Rhizomucor miehei* lipase and Candida antarctica lipase B and optimization of biocatalytic biodiesel production from palm oil using response surface methodology. 141: 847-857.

Shalini, P., Deepanraj, B., Vijayalakshmi, S. and Ranjitha, J. 2021a. Synthesis and characterisation of lipase immobilised magnetic nanoparticles and its role as a catalyst in biodiesel production. Materials Today: Proceedings.

Shalini, P., Deepanraj, B., Vijayalakshmi, S. and Ranjitha, J. J. M. T. P. 2021b. Synthesis and characterisation of lipase immobilised magnetic nanoparticles and its role as a catalyst in biodiesel production.

Shao, W., Xue, Y., Wu, A., Kataeva, I., Pei, J., Wu, H. and Wiegel, J. 2011. Characterization of a novel β-xylosidase, XylC, from Thermoanaerobacterium saccharolyticum JW/SL-YS485. Applied and environmental microbiology, 77 (3): 719-726.

Sharma, A. and Aggarwal, N. K. 2020. Strategies for Saccharification of Lignocellulosic Substrate. In: Water Hyacinth: A Potential Lignocellulosic Biomass for Bioethanol. Springer, 73-89.

Sharma, C., Bhardwaj, N. K. and Pathak, P. J. J. o. C. P. 2021. Static intermittent fed-batch production of bacterial nanocellulose from black tea and its modification using chitosan to develop antibacterial green packaging material. 279: 123608.

Sharma, H. K., Xu, C., Qin, W. J. W. and valorization, b. 2019. Biological pretreatment of lignocellulosic biomass for biofuels and bioproducts: an overview. 10 (2): 235-251.

Sharma, K., Morla, S., Khaire, K. C., Thakur, A., Moholkar, V. S., Kumar, S. and Goyal, A. J. I. J. o. B. M. 2020. Extraction, characterization of xylan from *Azadirachta indica* (neem) sawdust and production of antiproliferative xylooligosaccharides. 163: 1897-1907.

Sharma, M. and Kumar, A. 2013. Xylanases: an overview. *British Biotechnology Journal, 3 (1): 1*.

Sharma, R., Kocher, G. S., Bhogal, R. S. and Oberoi, H. S. 2014. Cellulolytic and xylanolytic enzymes from thermophilic *Aspergillus terreus* RWY. *Journal of basic microbiology, 54 (12): 1367-1377*.

Sharma, S., Vaid, S., Bajaj, B. J. C. R. i. M. and Biotechnology. 2015. Screening of thermo-alkali stable fungal xylanases for potential industrial applications. 3 (1): 536-541.

Shaw, S.-Y., Chen, Y.-J., Ou, J.-J. and Ho, L. 2006. Preparation and characterization of *Pseudomonas putida* esterase immobilized on magnetic nanoparticles. *Enzyme and microbial technology, 39 (5): 1089-1095.*

Sheldon, R. A. J. A. m. and biotechnology. 2011. Characteristic features and biotechnological applications of cross-linked enzyme aggregates (CLEAs). 92 (3): 467-477.

Shete, P. B., Patil, R. M., Thorat, N. D., Prasad, A., Ningthoujam, R. S., Ghosh, S. J. and Pawar, S. H. 2014b. Magnetic chitosan nanocomposite for hyperthermia therapy application: Preparation, characterization and in vitro experiments. *Applied Surface Science, 288: 149-157.*

Shikwambana, L., Ncipha, X., Sangeetha, S. K., Sivakumar, V. and Mhangara, P. 2021. Qualitative Study on the Observations of Emissions, Transport and the Influence of Climatic Factors from Sugarcane Burning: A South African Perspective. *International Journal of Environmental Research and Public Health, 18 (14): 7672.*

Sluiter, A., Hames, B., Ruiz, R., Scarlata, C., Sluiter, J., Templeton, D. and Crocker, D.L.A.P., 2010. Determination of structural carbohydrates and lignin in biomass. *Laboratory analytical procedure*, (TP-510-42618).

Shvedova, A. A., Kagan, V. E. and Fadeel, B. 2010. Close encounters of the small kind: adverse effects of man-made materials interfacing with the nano-cosmos of biological systems. Annual review of pharmacology and toxicology, 50: 63-88.

Silva, V. T., Quintero, L. P., Milagres, A. M. J. B. and Biotechnology, A. 2021. Characteristics of sugarcane bagasse fibers after xylan extraction and their high-solid hydrolysis cellulase-catalyzed. 102123.

Sims, R. E., Mabee, W., Saddler, J. N. and Taylor, M. 2010. An overview of second-generation biofuel technologies. *Bioresource Technology, 101 (6): 1570-1580.*

Sindhu, R., Gnansounou, E., Binod, P. and Pandey, A. 2016. Bioconversion of sugarcane crop residue for value added products–An overview. *Renewable Energy, 98: 203-215.*

Singh, A. K., Singh, M. and Verma, N. 2017. Extraction, purification, kinetic characterization and immobilization of urease from *Bacillus sphaericus* MTCC 5100. *Biocatalysis and Agricultural Biotechnology, 12: 341-347.*

Singh, R. D., Banerjee, J. and Arora, A. 2015. Prebiotic potential of oligosaccharides: A focus on xylan derived oligosaccharides. *Bioactive Carbohydrates and Dietary Fibre, 5 (1): 19-30.*

Singh, S., Madlala, A. M. and Prior, B. A. J. F. M. R. 2003. *Thermomyces lanuginosus*: properties of strains and their hemicellulases. 27 (1): 3-16.

Singh, S., Pillay, B. and Prior, B. A. 2000. Thermal stability of β-xylanases produced by different *Thermomyces lanuginosus* strains. *Enzyme and microbial technology, 26 (7): 502-508.*

Singh, S., Reddy, P., Haarhoff, J., Biely, P., Janse, B., Pillay, B., Pillay, D. and Prior, B. A. 2000. Relatedness of *Thermomyces lanuginosus* strains producing a thermostable xylanase. *Journal of biotechnology, 81 (2-3): 119-128.*

Singh, V. and Ahmed, S. 2012. Silver nanoparticle (AgNPs) doped gum acacia–gelatin–silica nanohybrid: An effective support for diastase immobilization. *International journal of biological macromolecules, 50 (2): 353-361.*

Solomon, K. V., Haitjema, C. H., Henske, J. K., Gilmore, S. P., Borges-Rivera, D., Lipzen, A., Brewer, H. M., Purvine, S. O., Wright, A. T. and Theodorou, M. K. J. S. 2016. Early-branching gut fungi possess a large, comprehensive array of biomass-degrading enzymes. 351 (6278): 1192-1195.

Souto, B. d. M., de Araújo, A. C. B., Hamann, P. R. V., Bastos, A. d. R., Cunha, I. d. S., Peixoto, J., Kruger, R. H., Noronha, E. F. and Quirino, B. F. J. P. o. 2021. Functional screening of a Caatinga goat (Capra hircus) rumen metagenomic library reveals a novel GH3 β-xylosidase. 16 (1): e0245118.

Souza, A., Henriques, R. O., Moreno-Pérez, S., de Morais Junior, W. G., Chioma, A. O. and Manuel, J. 2016. Immobilization of Plant Cell Wall Degrading Enzymes. Mycology: Current and Future Developments: Fungal Biotechnology for Biofuel Production, 1: 276.

Sperling, R. A. and Parak, W. 2010. Surface modification, functionalization and bioconjugation of colloidal inorganic nanoparticles. Philosophical Transactions of the Royal Society of London A: *Mathematical, Physical and Engineering Sciences, 368 (1915): 1333-1383.*

Srinivasan, A., Aruldhas, J., Perumal, S. S. and Ekambaram, S. P. J. J. o. F. B. 2021. Phenolic acid bound arabinoxylans extracted from Little and Kodo millets modulate immune system mediators and pathways in RAW 264.7 cells. 45 (1): e13563.

Subramaniyan, S. 2012. Isolation, purification and characterisation of low molecular weight xylanase from *Bacillus pumilus* SSP-34. *Applied biochemistry and biotechnology, 166 (7): 1831-1842.*

Sui, Y., Cui, Y., Nie, Y., Xia, G.-M., Sun, G.-X. and Han, J.-T. 2012. Surface modification of magnetite nanoparticles using gluconic acid and their application in immobilized lipase. *Colloids and Surfaces B: Biointerfaces, 93: 24-28.*

Sukprasert, J., Thumanu, K., Phung-on, I., Jirarungsatean, C., Chaisalee, P., Tuitemwong, P., Tuitemwong, K. J. J. o. S. and Technology. 2021. Characterization of Amino-Functionalized Ferromagnetic Nanoparticles with Glutaraldehyde Cross-linking. 13 (1): 38-46.

Sun, J., Xu, B., Shi, Y., Yang, L. and Ma, H.-l. 2017. Activity and stability of trypsin immobilized onto chitosan magnetic nanoparticles. *Advances in Materials Science and Engineering, 2017*

Sun, S.-L., Wen, J.-L., Ma, M.-G. and Sun, R.-C. 2013. Successive alkali extraction and structural characterization of hemicelluloses from sweet sorghum stem. *Carbohydrate polymers, 92 (2): 2224-2231.*

Sunna, A. and Antranikian, G. 1997. Xylanolytic enzymes from fungi and bacteria. *Critical reviews in biotechnology, 17 (1): 39-67.*

Sutay Kocabaş, D., Güder, S. and Özben, N. 2015. Purification strategies and properties of a low-molecular weight xylanase and its application in agricultural waste biomass hydrolysis. *Journal of Molecular Catalysis B: Enzymatic, 115: 66-75.*

Swietalski, P., Hetzel, F., Seitl, I. and Fischer, L. 2020. Secretion of a low and high molecular weight β-glycosidase by *Yarrowia lipolytica*. *Microbial Cell Factories, 19: 1-13.*

Tahmasebi, E., Yamini, Y., Mehdinia, A. and Rouhi, F. J. J. o. s. s. 2012. Polyaniline ‐ coated F e_3O_4 nanoparticles: An anion exchange magnetic sorbent for solid ‐ phase extraction. 35 (17): 2256-2265.

Tai, Y., Wang, L., Yan, G., Gao, J. m., Yu, H. and Zhang, L. 2011. Recent research progress on the preparation and application of magnetic nanospheres. *Polymer International, 60 (7): 976-994.*

Talbert, J. N. and Goddard, J. M. 2013. Characterization of lactase-conjugated magnetic nanoparticles. *Process Biochemistry, 48 (4): 656-662.*

Tasminto, D., Bachruddin, Z. and Kurniawati, A. 2021. Effect of purple sweet potato levels (Ipomoea batatas L.) carbohydrate sources on fermentation kinetics and lactic acid production by *Lactobacillus paracasei*. In: Proceedings of IOP Conference Series: Earth and Environmental Science. IOP Publishing, 012048.

Teixeira, R. S. S., Siqueira, F. G., de Souza, M. V., Ferreira Filho, E. X. and da Silva Bon, E. P. 2010. Purification and characterization studies of a thermostable β-xylanase from *Aspergillus awamori*. *Journal of industrial microbiology & biotechnology, 37 (10): 1041-1051.*

Temelli, N. 2020. Organosolv treatment for prebiotic oligosaccharide production from agro-food waste. *Izmir Institute of Technology (Turkey).*

Terrasan, C. R. F., Guisan, J. M. and Carmona, E. C. 2016. Xylanase and β-xylosidase from *Penicillium janczewskii*: Purification, characterization and hydrolysis of substrates. *Electronic Journal of Biotechnology, 23: 54-62.*

Thakur, A., Sharma, A., Khaire, K. C., Moholkar, V. S., Pathak, P., Bhardwaj, N. K. and Goyal, A. 2021a. Two-step saccharification of the xylan portion of sugarcane waste by recombinant xylanolytic enzymes for enhanced xylose production. ACS omega, 6 (17): 11772-11782.

Thakur, A., Sharma, A., Khaire, K. C., Moholkar, V. S., Pathak, P., Bhardwaj, N. K. and Goyal, A. J. A. o. 2021b. Two-Step Saccharification of the Xylan Portion of Sugarcane Waste by Recombinant Xylanolytic Enzymes for Enhanced Xylose Production. 6 (17): 11772-11782.

Tian, F., Guo, Y., Lin, F., Zhang, Y., Yuan, Q. and Liang, H. 2016. Rational surface silane modification for immobilizing glucose oxidase. *International Journal of Biological Macromolecules, 87: 191-194.*

Timell, T. 1967. Recent progress in the chemistry of wood hemicelluloses. *Wood Science and Technology, 1 (1): 45-70.*

Todan, L., Andronescu, C., Vuluga, D. M., Culita, D. C., Zaharescu, M. J. J. o. t. a. and calorimetry. 2013. Thermal behavior of silicophosphate gels obtained from different precursors. 114 (1): 91-99.

Tong, X., Qi, Z., Zheng, D., Pei, J., Li, Q. and Zhao, L. J. B. C. 2021. High-level expression of a novel multifunctional GH3 family β-xylosidase/α-arabinosidase/β-glucosidase from Dictyoglomus turgidum in *Escherichia coli*. 111: 104906.

Triana, O., Leonard, M., Saavedra, F., Acan, I., Garcia, O. and Abril, A. 1990. Atlas of sugarcane bagasse. Geplacea and ICIDCA, México,

Uday, U. S. P., Choudhury, P., Bandyopadhyay, T. K. and Bhunia, B. 2016. Classification, mode of action and production strategy of xylanase and its application for biofuel production from water hyacinth. *International journal of biological macromolecules, 82: 1041-1054.*

Vadivel, M., Babu, R. R., Arivanandhan, M., Ramamurthi, K. and Hayakawa, Y. J. R. A. 2015. Role of SDS surfactant concentrations on the structural, morphological, dielectric and magnetic properties of $CoFe_2O_4$ nanoparticles. 5 (34): 27060-27068.

van den Brink, J. and de Vries, R. P. 2011. Fungal enzyme sets for plant polysaccharide degradation. *Applied Microbiology and Biotechnology, 91 (6): 1477.*

Vidya, B., Palaniswamy, M., Angayarkanni, J., Nawaz, K. A., Thandeeswaran, M., Chaithanya, K. K., Tekluu, B., Muthusamy, K. and Gopalakrishnan, V. 2020. Purification and characterization of β-galactosidase from newly isolated *Aspergillus terreus* (KUBCF1306) and evaluating its efficacy on breast cancer cell line (MCF-7). *Bioorganic Chemistry, 94: 103442.*

Wang, F., Chi, C.-y., Wang, L.-y., Qiao, Y., Jin, X.-x. and Ding, G.-h. 2014. Gene cloning and expression of MAP30 in *Pichia pastoris*. *Biotechnology & Biotechnological Equipment, 28 (1): 136-139.*

Wang, S., Ru, B., Lin, H. and Sun, W. 2015. Pyrolysis behaviors of four O-acetyl-preserved hemicelluloses isolated from hardwoods and softwoods. Fuel, 150: 243-251.

Winters, D., Tran, M., Yoo, D. and Walker, K. W. 2020. Development of BioRad NGC and GE ÄKTA pure systems for highly automated three column protein purification employing tandem affinity, buffer exchange and size exclusion chromatography. Protein expression and purification, 165: 105497.

Wongwisansri, S., Promdonkoy, P., Matetaviparee, P., Roongsawang, N., Eurwilaichitr, L. and Tanapongpipat, S. 2013. High-level production of thermotolerant β-xylosidase of *Aspergillus* sp. BCC125 in *Pichia pastoris*: Characterization and its application in ethanol production. *Bioresource Technology, 132: 410-413.*

Wu, T., Hua, M.-Y., Chen, J.-p., Wei, K.-C., Jung, S.-M., Chang, Y.-J., Jou, M.-J. and Ma, Y.-H. 2007. Effects of external magnetic field on biodistribution of nanoparticles: A histological study. *Journal of Magnetism and Magnetic Materials, 311 (1): 372-375.*

Xiao, A., Xu, C., Lin, Y., Ni, H., Zhu, Y. and Cai, H. 2016. Preparation and characterization of κ-carrageenase immobilized onto magnetic iron oxide nanoparticles. *Electronic Journal of Biotechnology, 19 (1): 1-7.*

Xu, J.-K., Zhang, F.-F., Sun, J.-J., Sheng, J., Wang, F. and Sun, M. 2014. Bio and nanomaterials based on Fe_3O_4. Molecules, 19 (12): 21506-21528.

Yan, J., Su, T., Cheng, F., Cao, J., Zhang, H. and He, B. 2017. Multifunctional nanoparticles self-assembled from polyethylenimine-based graft polymers as efficient anticancer drug delivery. *Colloids and Surfaces B: Biointerfaces, 155: 118-127.*

Yan, Q., Wang, L., Jiang, Z., Yang, S., Zhu, H. and Li, L. 2008. A xylose-tolerant β-xylosidase from *Paecilomyces thermophila*: characterization and its co-action with the endogenous xylanase. Bioresource Technology, 99 (13): 5402-5410.

Yang, C., Liu, Z., Yu, M. and Bian, X. J. S. M. 2021. Magnetic nanofluid based on amorphous Fe-Ni-B@ OA particles applied in the treatment of oil slick. 19 (2): 159-167.

Yao, G., Wang, X., Yang, M., Chen, F., Ling, Y., Liu, T., Xing, S., Yao, M. and Zhang, F. J. L. 2020a. Co-immobilization of bi-lipases on magnetic nanoparticles as an efficient catalyst for synthesis of functional oil rich in diacylglycerols, phytosterol esters and α-linolenic acid. 129: 109522.

Yao, J., He, Y., Su, N., Bharath, S. R., Tao, Y., Jin, J.-M., Chen, W., Song, H. and Tang, S.-Y. J. N. c. 2020b. Developing a highly efficient hydroxytyrosol whole-cell catalyst by de-bottlenecking rate-limiting steps. 11 (1): 1-12.

You, C., Myung, S. and Zhang, Y. H. P. J. A. C. I. E. 2012. Facilitated substrate channeling in a self‐assembled trifunctional enzyme complex. 51 (35): 8787-8790.

You, C., Yuan, H., Huang, Q. and Lu, H. J. A. J. o. B. 2010. Substrate molecule enhances the thermostability of a mutant of a family 11 xylanase from *Neocallimastix patriciarum*. 9 (9)

Yang, M., Li, W., Liu, B., Li, Q. and Xing, J. 2010. High-concentration sugars production from corn stover based on combined pretreatments and fed-batch process. *Bioresource technology, 101 (13): 4884-4888.*

Yuwei, C. and Jianlong, W. 2011. Preparation and characterization of magnetic chitosan nanoparticles and its application for Cu (II) removal. *Chemical Engineering Journal, 168 (1): 286-292.*

Zeng, Y., Zhou, N., Xiong, C., Huang, Z., Du, G., Fan, Z. and Chen, N. J. J. o. A. P. S. 2021. Highly stretchable silicone rubber nanocomposites incorporated with oleic acid‐modified Fe3O4 nanoparticles. 51476.

Zhang, K., Yang, W., Liu, Y., Zhang, K., Chen, Y. and Yin, X. J. J. o. M. S. 2020. Laccase immobilized on chitosan-coated Fe_3O_4 nanoparticles as reusable biocatalyst for degradation of chlorophenol. 1220: 128769.

Zhang, L., Shi, J., Jiang, Z., Jiang, Y., Qiao, S., Li, J., Wang, R., Meng, R., Zhu, Y. and Zheng, Y. J. G. C. 2011a. Bioinspired preparation of polydopamine microcapsule for multienzyme system construction. 13 (2): 300-306.

Zhang, M., Puri, A. K., Wang, Z., Singh, S. and Permaul, K. 2019. A unique xylose reductase from *Thermomyces lanuginosus*: Effect of lignocellulosic substrates and inhibitors and applicability in lignocellulosic bioconversion. *Bioresource technology*, 281: 374-381.

Zhang, W., Qiu, J., Feng, H., Zang, L. and Sakai, E. 2015. Increase in stability of cellulase immobilized on functionalized magnetic nanospheres. *Journal of Magnetism and Magnetic Materials, 375: 117-123.*

Zhang, Y., Chen, B., Zhang, L., Huang, J., Chen, F., Yang, Z., Yao, J. and Zhang, Z. 2011b. Controlled assembly of Fe_3O_4 magnetic nanoparticles on graphene oxide. Nanoscale, 3 (4): 1446-1450.

Zhao, X., Zhang, L. and Liu, D. 2012. Biomass recalcitrance. Part I: the chemical compositions and physical structures affecting the enzymatic hydrolysis of lignocellulose. *Biofuels, Bioproducts and Biorefining, 6 (4): 465-482*.

Zhongming, Z., Linong, L., Wangqiang, Z. and Wei, L. 2020. EIA expects US crude oil production to remain relatively flat through 2021.

Zhou, Y.-T., Su, S.-N., Song, M.-M., Nie, H.-L., Zhu, L.-M. and Branford-White, C. 2009. Improving the stability of cellulase by immobilization on chitosan-coated magnetic nanoparticles modified alpha-ketoglutaric acid. In: Proceedings of Bioinformatics and Biomedical Engineering, 2009. ICBBE 2009. 3rd International Conference on. IEEE, 1-4.

Zhu, J., Wang, G., Pan, X. and Gleisner, R. 2008. The status of and key barriers in lignocellulosic ethanol production: A technological perspective. In: Proceedings of International Conference on Biomass Energy Technologies: Guangzhou, China, December 3-5, 2008: Volume 1. [Guangzhou, China]: Guangzhou Institute of Energy Conversion, The Chinese Academy of Science, 2008: Pages 1-12.

Zhu, X., Wang, J., Zhang, X., Chang, Y. and Chen, Y. 2010. Trophic transfer of TiO_2 nanoparticles from daphnia to zebrafish in a simplified freshwater food chain. *Chemosphere, 79 (9): 928-933*.

Ziegler-Borowska, M., Mylkie, K., Kozlowska, M., Nowak, P., Chelminiak-Dudkiewicz, D., Kozakiewicz, A., Ilnicka, A. and Kaczmarek-Kedziera, A. J. M. 2019. Effect of geometrical structure, drying, and synthetic method on aminated chitosan-coated magnetic nanoparticles utility for HSA effective immobilization. 24 (10): 1925.

APPENDIX

1. Characteristic IR Absorptions

Key: w=weak, m=medium, n=narrow, b=broad, sh=sharp, s=strong
Frequency of functional group bond measured in cm^{-1}

690-515(m) C-Br stretch alkyl halides
700-610(b, s)-C≡C-H:C-H bend alkynes
725-720(m) C-H rock alkanes
850-550(m) C-Cl stretch alkyl halides
900-675(s) C-H "oop" aromatics
910-665(s,b)N-H wag 1°, 2° amines
950-910(m) O-H bend carboxylic acids
1000-650(s)=C-H bend alkenes
1250-1020(m)C-N stretch aliphatic amines
1300-115(m)C-H wag(-CH2X) alkylhalides
1320-1000 (s) C-O stretch alcohols, carboxylic acids, esters, ethers.
1335-1250 (s) C-N stretch aromatics amines
1360-1290 (m) N-O symmetric stretch nitro compounds
1370-1350 (m) C-H rock alkanes
1470-1450 (m) C-H bend alkanes
1500-1400 (m) C-C stretch (in-ring) aromatics
1550-1475(s) N-O asymmetric stretch nitro compounds
1600-1585(m) C-C stretch (in-ring) aromatics
1650-1580(m) N-H bend 1° amines
1680-1640(m) -C=C-stretch alkenes
1760-1665 (s) C=O stretch carbonyls (general)
1710-1665 (s) C=O stretch α, β-unsaturated aldehydes, ketones
1715(s) C=O stretch ketones, saturated aliphatic
1730-1715(s) C=O stretch α, β-unsaturated esters
1740-1720(s) C=O stretch aldehydes, saturated aliphatic
1750-1735(s) C=O stretch esters, saturated aliphatic
1760-1690(s) C=O stretch carboxylic acids
2830-2695(m) H-C=O:C-H stretch aldehydes
3100-3000(m) =C-H stretch alkenes
2260-2210(v) C≡N stretch nitriles
3100-3000 (s) C-H stretch aromatics
2260-2100(w) -C≡C-stretch alkynes
3300-2500 (m) O-H stretch carboxylic acids
3400-3250 (m) N-H stretch 1°,2° amines, amides
3500-3200 (s,b) O-H stretch, H-bonded alcohols,phenols
3600-3610 (s,sh) O-H stretch, free hydroxyl alcohols, phenols